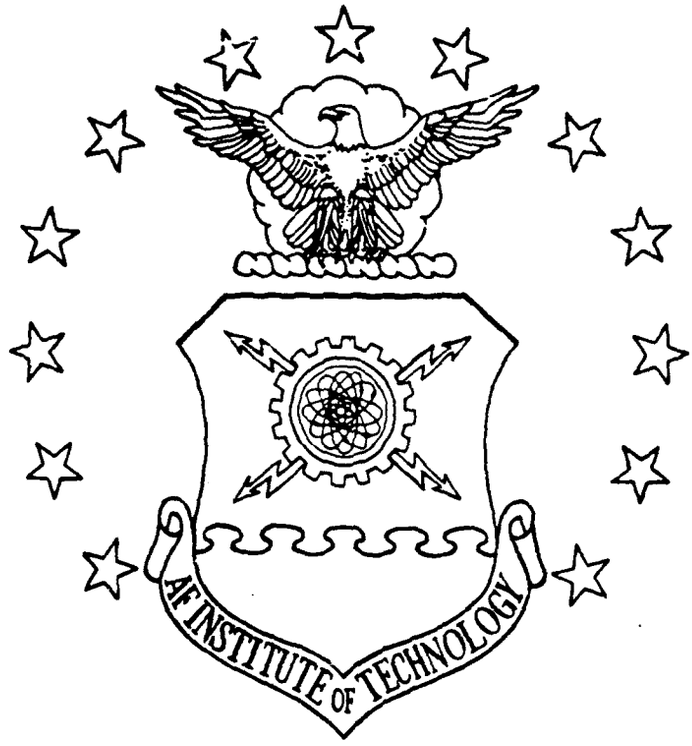

DEPARTMENT OF THE AIR FORCE

AIR UNIVERSITY

AIR FORCE INSTITUTE OF TECHNOLOGY

Wright-Patterson Air Force Base, Ohio

AFIT/GAE/ENY/89D-27

EFFECT OF A SINGLE OVERLOAD UPON FATIGUE CRACK GROWTH IN AN ALUMINUM-LITHIUM ALLOY

Albert S. Perkins
Captain, USAF

AFIT/GAE/ENY/89D-27

AFIT/GAE/ENY/89D-27

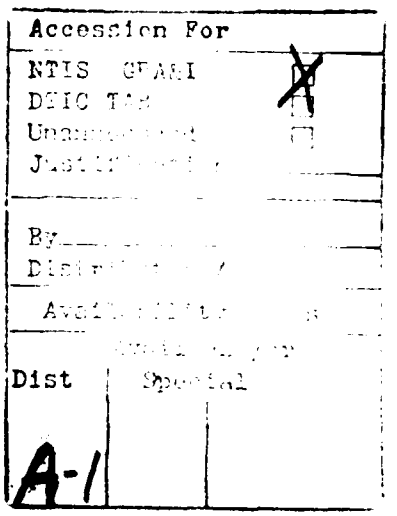

EFFECT OF A SINGLE OVERLOAD UPON FATIGUE CRACK GROWTH IN AN ALUMINUM-LITHIUM ALLOY

THESIS

Presented to the Faculty of the School of Engineering

of the Air Force Institute of Technology

Air University

In Partial Fulfillment of the

Requirements for the Degree of

Master of Science in Aeronautical Engineering

Albert S. Perkins, B.S.

Captain, USAF

December 1989

Preface

The primary goal of this study was to investigate the effects of single overloads upon the crack growth characteristics of aluminum-lithium alloy 2091, and to attempt correlation of the crack closure measured by different techniques with crack growth rates.

A method of using the laser interferometric displacement gage to measure near-field closure profiles as a function of crack length for compact tension specimens was developed. The laser IDG detected closure loads higher than those measured by far-field technique (clip gage), and also showed that closure load for aluminum-lithium 2091 in the compact tension geometry is a function of crack length and applied stress intensity range.

I'd like to thank the many people who made this all possible. An immense amount of thanks go to my advisor, Dr. Shankar Mall (AFIT/ENY), and to my sponsor, Dr. Ted Nicholas (WRDC/MLLN).

Special thanks go to George Hartman, University of Dayton Research Institute, who developed the generalized electric potential solution (Appendix B) used to track crack growth, and to Jay Anderson, who kept machinery going when it was needed.

Other large measures of praise belong to the remainder of the AFIT Aero/Astro Labs staff: Nick Yardich (Supervisor), Dan Rioux, Andy Pitts, Mark Derriso and Tim Majors.

Thanks to Jay Jira (WRDC) for hints on data reduction techniques and to Dave Maxwell (UDRI) for hints on testing techniques. Super thanks to Bob Lewis (WRDC) for spending time with me at the camera; (photos, Section IV).

And to my wife, Debby, who endured the long nights of study and shared too few moments of my precious time for the last eighteen months, I owe the most. (Don't worry, honey. Payback is on the way.)

"Some things are still a mystery to me,
While others are much too clear..."
Jimmy Buffett, "Migration", 1974

Table of Contents

List of Figures

List of Tables

ABSTRACT

The fundamental goal of this thesis was to investigate the effect of a single overload upon the behavior of fatigue crack growth in the aluminum-lithium alloy designated AlLi 2091. Specimens used in this study were compact tension (CT) specimens; crack growth was produced by a cyclic loading of constant load ratio (0.1) and a constant maximum stress intensity factor, punctuated with periodic (single) overloads.

Crack growth in the CT specimens was monitored by a variety of different instrumentations. Crack length was tracked using the electric potential (EP) method. Far-field measurements were taken via a clip gage (at the specimen mouth). Optical measurements, taken by travelling microscope, allowed for the correction of the EP crack length monitoring during the test if needed.

In addition, load-displacement measurements were taken at a set of microhardness indents near the crack tip with a laser interferometric displacement gage (IDG). These near field measurements were compared to the closure measured by the clip gage, a far-field device.

The laser IDG was found to measure a higher level of closure than the clip gage for all lengths over which a direct comparison could be made.

The level of closure measured by the laser IDG depended upon the distance from the crack tip to the most recently placed set of indents. A second order regression to the P_{cl}/P_{max} data as measured by the IDG fit the data well for most segments of crack growth. These regressions were used to normalize the data to a point 0.2 mm from the crack tip.

When the closure load data measured by the IDG was normalized to the point 0.2 mm behind the crack tip, the closure load for this material was found to depend upon the crack length and the applied stress intensity range.

Changes in load history were found to have an effect upon the crack growth behavior. The sudden transition from precracking to fatigue test caused a change in the direction of the crack growth and some secondary cracking; the secondary cracks did not propagate in this case, however.

For the tests involving overloads, 80% overloads were applied to the compact tension specimens. The overloads were observed to cause significant crack retardations for all stress intensity ranges; for the 80% overload, delay distances increased as the stress intensity range increased.

Large amounts of scatter in the P_{cl}/P_{max} data (as measured by both the IDG and the clip gage) were observed after the application of an overload. The changes in crack direction were substantial and secondary cracks propagated for a significant distance before a primary crack developed and moved through the material affected by the overload.

The Effect of A Single Overload Upon Crack Growth in an Aluminum-Lithium Alloy

I. Introduction

Overview

Man has been airborne for over five hundred years. From the first tentative tests of man-carrying kites and gliders to the high performance jet aircraft of today, successful flight has always been dependent upon the existence of high-strength materials. The further evolution of aerospace vehicles will require new materials that have extraordinary properties: high strength-to-weight ratios, tolerance of extreme temperatures and corrosive environments, etc. The development of the aluminum-lithium alloy is another step toward the realm of high strength-to-weight ratio materials.

Several aluminum-lithium alloys have been developed; from preliminary tests, AlLi 2090 has been found to be a high strength alloy, while AlLi 2091 has been found to be damage tolerant.

Background

Early emphasis in aircraft structural design was upon high strength alone; catastrophic failures were to be avoided by overbuilding the primary structure, using extra material and redundant load paths. While providing safety in most

cases, this philosophy had many drawbacks. The extra weight in the structure, while providing extra static strength for the aircraft primary structure, invoked severe penalties upon the performance of the aircraft. Of greater consequence, this approach to design neglected the possible existence of flaws in the structure which could grow and inevitably cause structural failure.

Eventual recognition that many aircraft accidents had occurred due to pre-existing flaws, rather than a simple "wearing out", led to the evolution of a damage tolerance approach of structural analysis. Research concentrated on determining what factors, such as stress levels, component geometry, characteristics of the fatigue stress cycling, heat treatment of materials, etc., affected the rate of crack growth in aircraft structural components.

An aircraft component, by virtue of being integrated into a machine in motion, is subjected not only to static stresses (when the aircraft is on the ground) but to dynamic stresses (when the aircraft is taxiing, taking off, cruising, maneuvering, landing, etc) as well. These cyclic stresses are a result of the static and aerodynamic forces applied to the aircraft over any period of time.

Stress cycles are typically thought of in terms of a "min-max" pair; the cycle begins with a minimum stress value and, after having passed through a maximum stress value, ends when the stress reaches another (not necessarily the same) minimum value. The stresses applied to an aircraft

component, in combination with the specific geometry of the component, result in stress intensity factors. (See Figure 1-1.) When the plastic zone at the crack tip is small, the analysis of crack growth can be based upon this single parameter of stress intensity, K. (1:15) The stress intensity factor (K) takes the general form:

$$K = \beta \sigma \sqrt{a} \qquad (1)$$

where σ is the far-field stress in the cracked body, a is the crack length, and β is a dimensionless quantity which depends upon the geometry of the component (1:11). β is affected by parameters such as the component thickness, width, and shape. Changes in component geometry near a crack, such as a fastener hole or a fillet radius, can have significant effects upon the stress intensity factor.

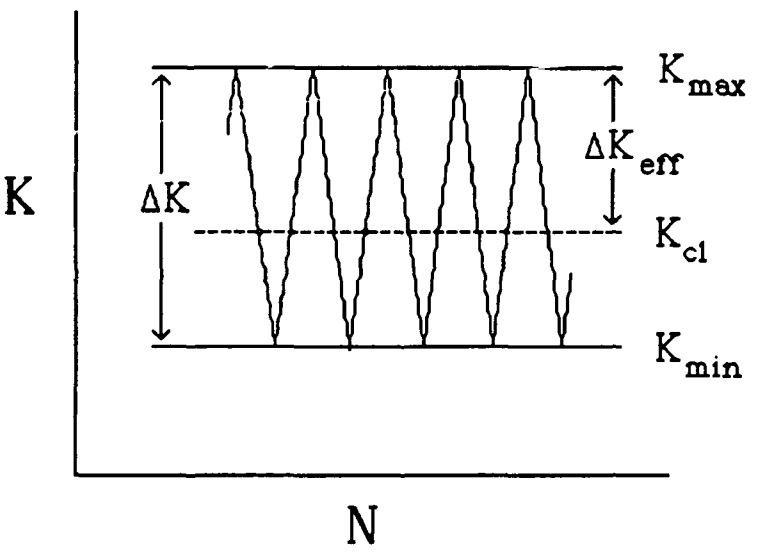

Figure 1-1. Typical Fatigue Cycle

One of the most useful relations developed in crack growth characterizations of materials has been the log-log plot of crack growth rate versus the stress intensity range for the cycle. The crack growth rate (da/dN) is measured in units of length/cycle; the stress intensity range (ΔK) is a measure of the difference in stress intensity between the maximum stress and the minimum stress of the cycle and is measured in units of "stress • $\sqrt{\text{length}}$". A typical example of this log-log plot is shown in Figure 1-2; it can usually be divided into three main regions.

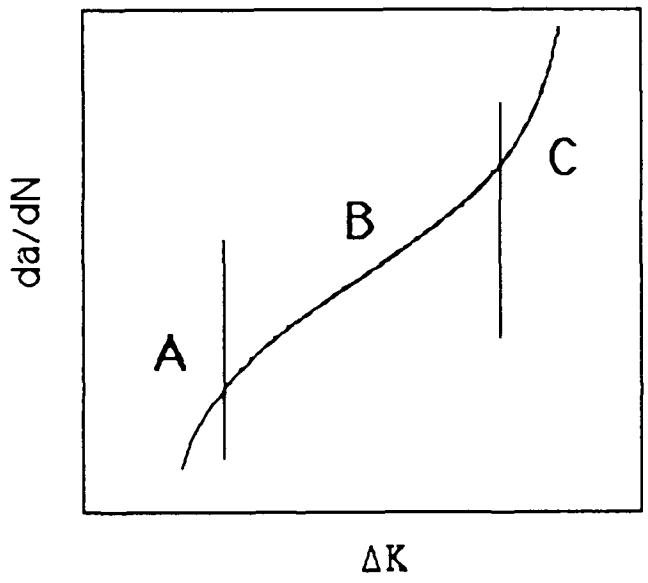

Figure 1-2. Typical Sigmoidal Relation between ΔK and da/dN

Region A shows the portion of the plot where the growth rate is very low. A very small decrease in stress intensity range can result in a dramatic decrease in crack growth rate. The term ΔK_{th} denotes the threshold stress intensity range, below which measurable crack growth does not occur. In this region, a large number of fatigue cycles are needed to produce measurable crack growth. Ideally, aircraft components would be designed such that the stress intensity ranges are always below ΔK_{th}. Realistically, due to weight, cost, and other considerations, most components are not designed for this region of the curve.

At the other extreme, Region C shows the portion of the curve where the growth rate is very high; a very small increase in the stress intensity range can result in an extreme increase in crack growth rate. Due to the large crack growth rates in this region of the curve, an aircraft component will have a very limited remaining life; at these stress intensity ranges, the remaining useful life of the component could be measured in tens of cycles, which could easily occur within minutes or seconds in an operational environment. K_{IC}, the plane strain fracture toughness, is the limiting critical value of stress intensity for a material. An aircraft component subjected to a stress intensity equal to or greater than the K_{IC} of the component material will immediately and catastrophically fail.

The central portion of the curve, Region B, depicts the stress intensity ranges where stable crack growth occurs.

Because aircraft components are not designed to experience crack growth rates in Region A (for cost and weight reasons) or Region C (for obvious reasons of ridiculously short lives), Region B is the region of most interest in structural analysis. Any damage tolerance analysis must be based upon crack growth behavior in this region.

The largest part of Region B for most materials can be modeled as a straight line. The equation of this straight line is:

$$\frac{da}{dN} = C(\Delta K)^n \tag{2}$$

where da/dN is the crack growth rate, ΔK is the stress intensity range, and C and n are material constants to be determined from data gathered in laboratory testing. Equation 2 is commonly known as the Paris-Erdogan equation. (2:528)

One of the characteristics of the fatigue stress cycling that affect the crack growth rates measured in experimental data is the stress ratio. The stress ratio is defined as:

$$R = \frac{K_{min}}{K_{max}} \tag{3}$$

where K_{min} and K_{max} are the respective minimum and maximum stress intensities encountered during a fatigue cycle. The da/dN plot will shift upward and to the left for increasing values of stress ratio.

The effective stress intensity range for a fatigue cycle is usually less than the applied stress intensity because of a phenomenon called closure. On the unloading portion of a fatigue cycle, the crack surfaces make contact before the minimum stress is reached. Similarly, on the loading portion of the fatigue cycle the crack surfaces do not break contact immediately even though load is being applied. The portion of the load cycle below the closure load does not affect the crack tip region. The minimum load that actually affects the crack tip is the load at which the crack surfaces break contact. An effective stress intensity range can be defined as:

$$\Delta K_{eff} = K_{max} - K_{cl} \qquad (4)$$

where ΔK_{eff} is the effective stress intensity range, K_{max} is the stress intensity factor associated with the maximum load of the fatigue cycle and K_{cl} is the stress intensity factor computed from the closure load.

The rate of crack growth in an aircraft component can be affected by the loading history. Components are rarely subjected to fatigue loading of constant amplitude; they are far more likely to experience random loading, where the stress intensity ranges and stress ratios vary widely from one cycle to the next. When material is subjected to an overload, the subsequent crack growth can be substantially, and sometimes even fully, retarded. The ability to quantify the retardation effects of random loading upon materials in a

service environment is essential if we wish to accurately predict component lives.

An overload introduces a large plastic zone in front of the crack tip; when fatigue cycling returns to non-overload levels, this plastic zone contains yielded material under compressive stress. These compressive stresses effectively reduce the amount of stress that the crack tip experiences, slowing the crack growth rate below the normal growth rate expected. When the crack tip moves through this region of residual stresses and reaches unaffected material, normal crack growth rates will resume. (1:272-274)

Objectives

The primary objective of this study was to investigate the effects of the single overload on the fatigue crack growth behavior in the aluminum-lithium alloy 2091. The retardation effects introduced due to this overload were investigated through correlations with the effective stress intensity ranges, as measured by both a near-field (laser interferometric displacement gage) and a far-field (clip gage) determination of closure load. To achieve this objective, three types of tests will be conducted using compact tension specimens.

The first type of fatigue test will be performed at a constant load ratio and a constant maximum load. This type of test will be used primarily to reproduce data previously

obtained by other researchers. This test will also provide data used to verify the calibration curve that relates voltage measured across the specimen mouth to the crack length in the specimen. Finally, these tests will check the function of the non-conducting clip gage constructed for this study to be used with the electric potential method for measuring crack lengths.

A second type of test will be conducted at constant stress intensity range, and will be punctuated by single overloads of various size. This test will provide information about what size of overload to use in the future tests that will form the bulk of the testing for this study. Since a fatigue test of constant stress intensity range produces a constant crack growth rate under normal conditions, the point at which crack growth returns to normal after an overload can easily be determined.

The third type of fatigue test will be performed at a constant load ratio and a constant stress intensity range. These tests will constitute the major portion of testing for this study. Several baseline tests will be performed in which fatigue cycling without overloads is applied; the primary purpose of these tests is to determine the closure loads under normal fatigue cycling, against which the closure loads obtained during non-baseline tests will be compared. In the non-baseline tests, the fatigue cycling will be punctuated with a single overload of predetermined size.

This overload will be of sufficient magnitude to significantly (but not completely) retard the crack growth.

The focus of the study will be upon the behavior of the closure loads in the region of post-overload retarded crack growth, as compared to the closure loads observed during the baseline tests. Primary emphasis will be placed upon the closure loads measured near the crack tip by the laser interferometric displacement gage; comparisons will also made with the far field measurements made by the clip gage. The closure loads observed will then be used to compute effective stress intensity ranges, which will be compared to post-overload crack growth behavior.

II. Theory/History

The Paris-Erdogan relation as given by Eq. (1) is commonly used in fatigue analysis, and relates the crack growth rate (da/dN) to the stress intensity range (ΔK). In this relation, the stress intensity range is considered to be the factor that drives the crack growth. Due to the phenomenon of crack closure, however, the crack tip does not experience the applied stress intensity range of ΔK, but the effective stress intensity range as given by:

$$\Delta K_{eff} = K_{max} - K_{cl} \tag{5}$$

where K_{max} is the stress intensity factor associated with the maximum load of the fatigue cycle and K_{cl} is the stress intensity factor associated with the closure load.

The phenomenon of closure was first considered by Elber (3:37). He compared a zero-width saw cut, a typical model of a crack, with an actual crack and found that the actual fatigue crack did not remain open during the entire load cycle. Unless the crack is fully open, propagation does not occur; therefore, the amount of load needed to overcome closure should be taken into account when analyzing crack growth.

Crack closure is detected by analyzing load-displacement data obtained from fatigue specimens. Numerous data points are obtained throughout a fatigue cycle, producing a load-displacement curve such as that shown in Figure 2-1.

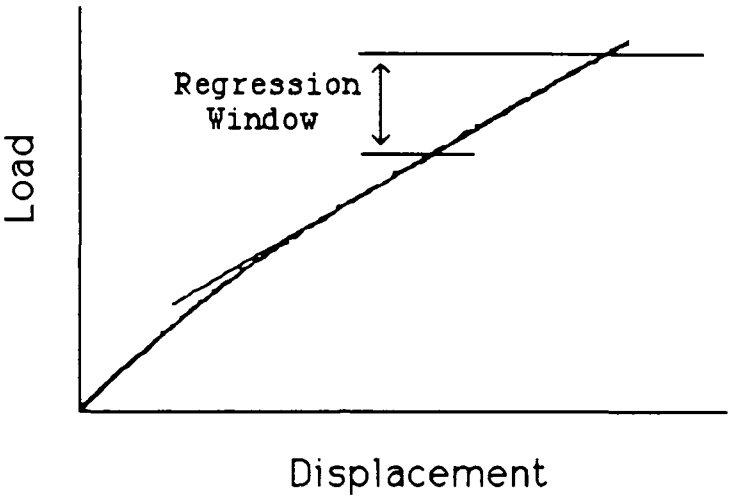

Figure 2-1. Typical Load-Displacement Curve

The linear upper portion of the load-displacement curve in Figure 2-1 indicates that the crack is fully open; the non-linear portion of the curve indicates that the crack surfaces are coming into contact and that closure is occurring.

Load-displacement plots that exhibit closure usually show three distinct regions: 1) a region where the crack is fully open, 2) a region where the crack is partially closed, and 3) a region where the crack is fully closed. The regions of the load-displacement plot where the crack is either fully open or fully closed are characterized by linear segments at the upper and lower extremes of the load range for the fatigue cycle. In the central region of the plot the slope

of the curve displays a gradual change, which indicates that the crack surfaces are coming into contact with each other. An ideal load-displacement plot would exhibit only two regions, i.e. only fully open and fully closed.

When attempting to identify the closure load from a load-displacement plot, a "window" (i.e., range or limits) of upper and lower load values upon which to base the linear regression must be selected. These values are located along the main linear portion of the plot (i.e., the upper portion of Figure 2-1). This window must contain only the linear portion of the plot. A linear regression will not accurately represent a curving portion of the plot; as a result, an inaccurate value for the closure load may be generated.

On curves that display a distinctly linear upper portion, selecting the limits of the window is relatively straightforward. In a gradually curving plot, however, the point of departure from the linear regression (which signifies the closure load) is very sensitive to the choice of upper and lower bounds for the window. Some load-displacement plots exhibit a non-linearity at the extreme upper portion of the load range; this has been attributed to non-linear deformations in the plastic zone ahead of the crack tip (4:236). Others attribute a portion of this non-linear behavior at the upper portions of the load-displacement curve to crack growth as well (5:214).

The slope of the load-displacement curve is also known as the compliance. The same regression used to determine the

closure load will provide a compliance value that characterizes the linear portion of the load-displacement curve. This compliance value can be used to calculate the length of the crack when fully open. The equation used to calculate the apparent crack length from compliance in compact tension specimens is:

$$a = W * (1.001 - 4.6695\ U + 18.46\ U^2 - 236.82\ U^3 + 1214.9\ U^4 - 2143.6\ U^5) \quad (6)$$

where a is the crack length and W is the specimen width. The quantity U is determined from the relation:

$$U = \frac{1}{1 + \sqrt{EBC}} \quad (7)$$

where E is the Young's modulus, B is the specimen thickness, and C is the compliance of the specimen as measured at the front face of the notch mouth. (6:14).

Factors Affecting Closure

Three different factors have been identified that significantly contribute to closure: material plasticity, asperity, and crack surface oxidation.

Elber originally envisioned closure as being caused by the plastic deformation left in the wake of the propagating crack, which resulted in incompatible crack surfaces (3:41-44). A plastic zone (whose size is dependent upon the maximum tensile load) is formed at the crack tip; as the

crack propagates, new plastic zones are formed and the plastic zones from previous load cycles are left behind, as depicted in Figure 2-2.

Tensile deformations in the plastic wake result in compressive stresses normal to the crack surfaces. As a result, it is possible for a crack to remain closed in the presence of a tensile load which cannot overcome the compressive stresses.

During the unloading portion of a fatigue cycle, the material surrounding the plastic zone at the crack tip returns to its former shape and size, while the material in the plastic zone cannot. As a result the yielded zone is compressed, further adding to the compressive stresses that must be overcome to fully open the crack.

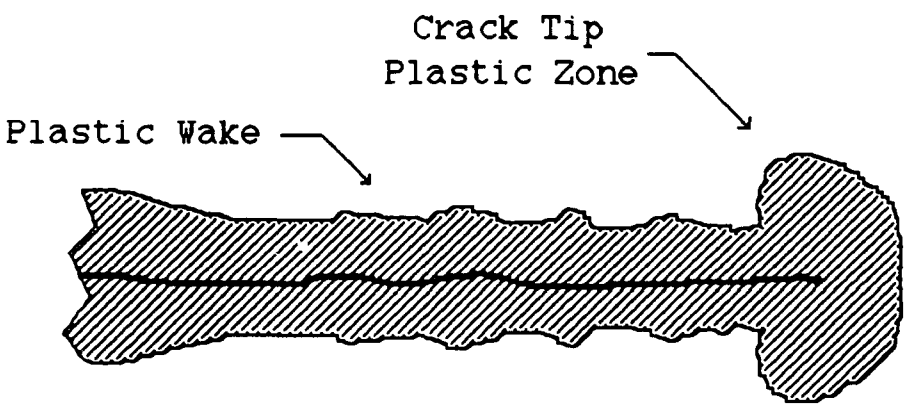

Figure 2-2. Typical Plastic Wake

A second factor that has been found to contribute to crack closure is asperity. Fracture surfaces are not perfectly flat. In some materials, especially, the grain size of the alloy dramatically affects the regularity of the crack surfaces. With any Mode II (shear) displacement during fatigue loading, the crack surfaces will not perfectly mesh during the unloading. This results in contact of the crack surfaces at loads above the minimum value for the load cycle, which reduces the effective stress intensity range. Closure due to asperity has been found to be more pronounced at crack growth rates near threshold because of larger amounts of Mode II displacements. (7:63-64)

Other asperity-related phenomena can aid in the development of closure. Meandering of the crack path can be a factor in premature contact of the crack surfaces. Some materials exhibit large amounts of crack branching; this effect can also provide an additional contribution to crack closure. (8:14)

A third factor that contributes to the development of crack closure is the formation of oxide layers on the crack surfaces (9:510, 10:553, 11:393). Many materials, especially the newly-exposed material of the crack surfaces, are susceptible to oxidation; corrosive environments can accentuate this effect. The thickness of the layer of corrosion products can approach the size of the crack tip opening displacement (CTOD), especially in stress intensity ranges near threshold. The corrosion products cause the

crack surfaces to contact before the minimum load is reached, again effectively reducing the stress intensity range.

Asperity and oxide-induced closure are usually observed at low crack growth rates (7:63-64, 12:28). These are usually associated with low stress intensity ranges and small plastic zones. On the other hand, high crack growth rates are caused by large stress intensity ranges and are usually accompanied by large plastic zones; under these conditions, the plasticity-induced closure dominates.

Measurement Techniques

It was previously mentioned that closure loads are dependent upon the method of analysis used to interpret the load-displacement plots. Closure loads are also highly dependent upon the measurement device used to generate the load-displacement plots.

Three different measurement techniques were used in this study; they were: 1) electric potential, 2) laser interferometric displacement gage (IDG), and 3) clip gage. Each of these techniques can be used to measure closure. In this study, however, the electric potential method was not used to measure closure. The sole use of the electric potential method was to monitor the crack length, which was used as feedback to the computer software which controlled the test machine.

Because this study used both electric potential method and clip gage method, a special non-conducting clip gage was

needed. Details of the constructions of this clip gage are included in Appendix A.

Each of the measurement techniques used in this study will now be discussed.

Electric Potential

When a flawless compact tension specimen has a constant electric current passing through it, the electric field set up within the specimen has a specific distribution. This distribution of electric potential will change as a crack forms and grows under cyclic fatigue. If potential leads are spot-welded to the specimen near the specimen mouth, voltage differences between the lead points can be measured as the crack grows. These changes in the electric field can be used to monitor the growth of a crack in the specimen. This technique has been used to track crack growth to accuracies of 0.05 mm (13:442).

Crack closure and thermal emf have been identified as factors that can affect the accuracy of the electric potential method for monitoring crack growth (14:107, 15:20, 16:104,114). The effect of these factors are minimized in this study. Thermal EMF is accounted for during data sampling, and the effect of closure is minimized by only using voltage values obtained during the highest portions of the load cycle, when the crack surfaces are fully open.

The generalized electric potential solution used in this study was produced using a finite element analysis. This

solution was used to initialize the curve for each segment of crack growth and to track the subsequent crack growth in that segment. The development of this generalized solution for the compact tension specimen geometry used in this study are discussed in Appendix B.

The specimen was removed from the test fixture at regular intervals in order to place microhardness indents on the specimen for use with the laser IDG. To facilitate this removal, the electrical connection where the current passed through the specimen was made through spade connectors; these were attached to the face of the specimen by screws into tapped holes shown in Figure 2-3. This figure also shows the locations where potential leads were spot-welded.

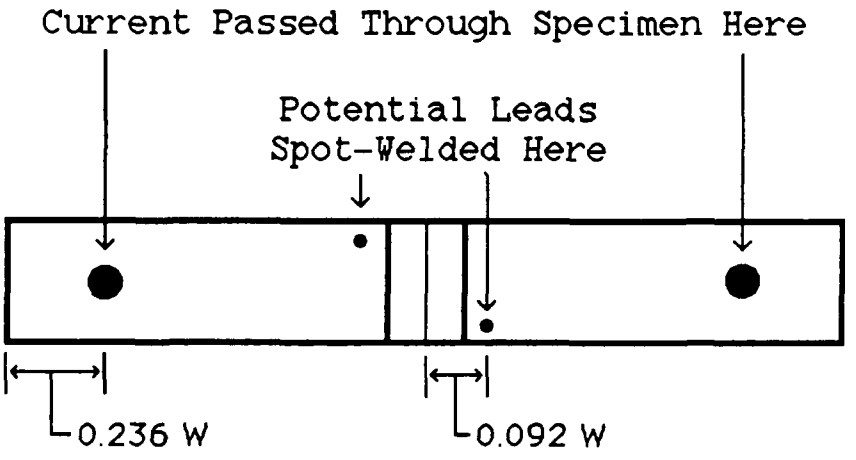

Figure 2-3. Electrical Connections on Front Face of Compact Tension Specimen

In the electric potential method used for this study, a constant electric current of 10.0 amps was run through the specimen. A constant electric current was generated by a Hewlett-Packard 6033A System Power Supply. The potential across the leads was measured by a Hewlett-Packard 3456A Digital Voltmeter. These two instruments were interfaced to the computer which controlled the loading conditions for the fatigue tests.

Clip Gage

The clip gage is one of the most commonly used devices in monitoring crack growth. Clip gages are used to monitor the displacement between points across the crack mouth, usually between machined notches located at the front face of the specimen or at the load line of the specimen. Measurements are taken by the clip gage at some distance from the crack tip, where crack growth is taking place. The "remote" location of the clip gage affects the sensitivity of the measurements; as a result, closure loads are more difficult to determine accurately from far-field measurements (17:378).

Because the clip gage is a "contact" measurement device, the measurements of load and displacement can be affected by friction between the clip gage and the specimen. This, in turn, will affect the load-displacement plot and will result in an inaccurate determination of the closure load.

In spite of the drawbacks mentioned above, the clip gage has many advantages. It is convenient to use. Closure loads obtained from clip gage data are thickness-averaged values. Compliance values determined from clip gage load-displacement data can also be used to calculate a thickness-averaged value for crack length.

Due to the ease of use and the acquistion of thickness-averaged data, many computer-controlled fatigue programs use the input from clip gages to control the loading.

Laser Interferometric Displacement Gage

The laser interferometric displacement gage (IDG) is one of the latest methods developed to measure relative displacements. The coherent laser light, upon reflection from the surfaces of microhardness indents, produce well-defined patterns of interference fringes. These fringe patterns consist of light and dark bands, formed when the two reflected rays of laser light constructively and destructively interfere with each other.

The schematic shown in Figure 2-4 depicts the IDG setup, and also shows a typical interference fringe pattern. Destructive interference, resulting in a dark band, occurs when the difference in path length is an odd multiple of half the wavelength of the laser light. Constructive interference produces a bright band and occurs when the difference in path length of the two reflected rays of light is a multiple of the laser wavelength.

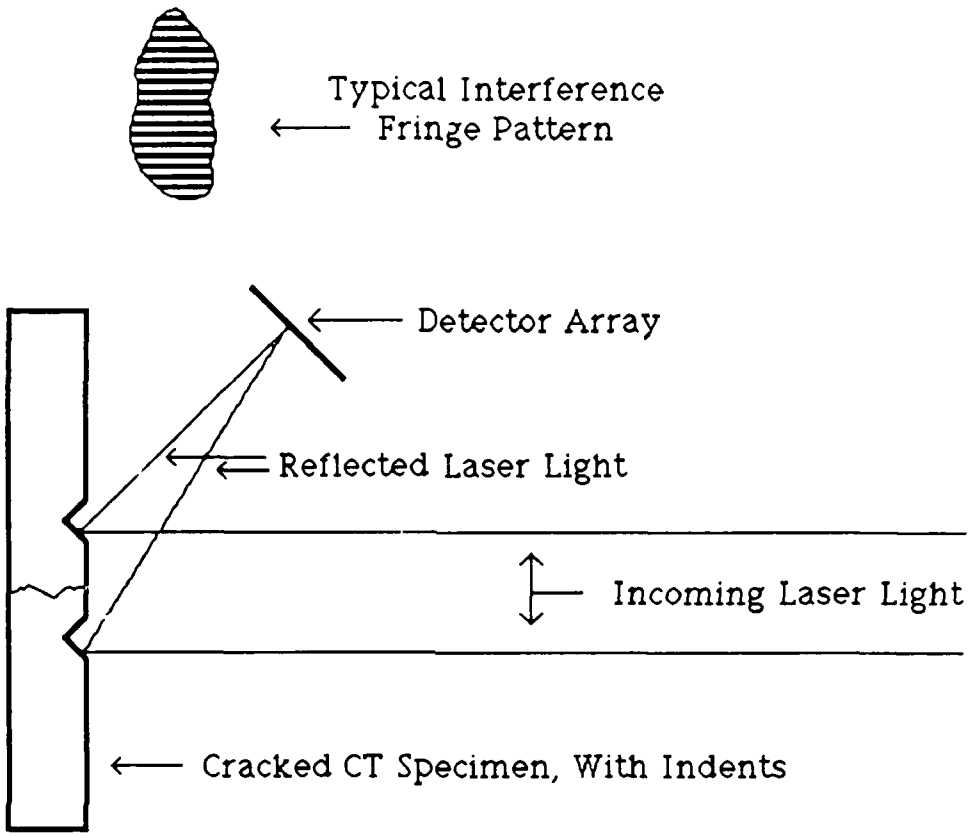

Figure 2-4. Schematic of Laser IDG

For this study, a Vickers microhardness indent was placed on each side of the crack, as shown in the schematic in Figure 2-5. These indents are pyramidal in shape, with sides angled at 45°. Each indent has four sides; therefore, the two indents will produce four sets of fringe patterns. Only two of them, however, are used in this study; these are the two "above" and "below" the plane of the crack as depicted in Figure 2-4.

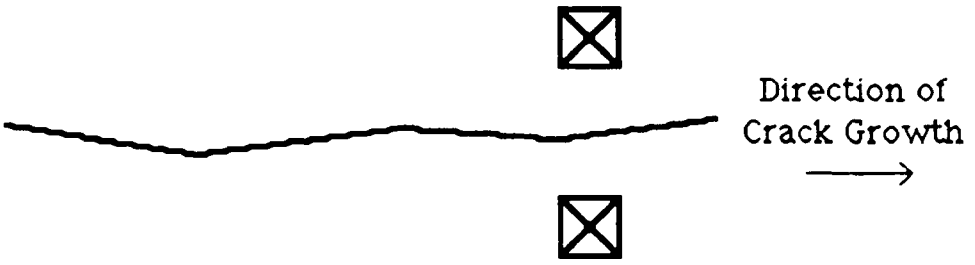

Figure 2-5. Placement of Microhardness Indents

As the specimen undergoes cyclic loading the crack surfaces will open and close, resulting in movement of the indents. The relative displacement causes the interference patterns to move as well; the movement of the bright and dark bands across a linear array of photodetectors can be correlated to the actual displacement of the indents. The displacement, when accompanied by input from the load cell, produces a load-displacement curve. The IDG has an accuracy of approximately 10^{-5} mm when a helium-neon laser is used to illuminate the microhardness indents. (18:24)

Because the laser IDG is a non-contact method of measurement, some possible sources of hysteresis in the load-displacement data are removed. Another advantage of the laser IDG is that the microhardness indents can be placed at any point desired along the crack path; this allows near-field measurements of compliance and closure to be made if desired.

Comparisons Between Clip Gage and IDG Measurements

As mentioned earlier, the clip gage and the laser IDG both perform the same function: they take measurements of load-displacement data at specified locations on a compact tension fatigue specimen. The primary difference between the two is that the clip gage is restricted to take measurements at locations determined by the specimen design, whereas the laser IDG can take measurements almost anywhere along the crack path.

Due to the flexibility in placing microhardness indents, the laser IDG can provide measurements of load-displacement data and closure loads very near the region of the crack tip. The load-displacement data taken in the region near the crack tip can be dramatically different from the measurements taken in the far field by the clip gage.

Figure 2-6a shows a typical load-displacement curve obtained by a clip gage, and Figure 2-6b shows the load-displacement curve obtained by the laser IDG for the same loading conditions and the same crack length. (These curves were obtained on two consecutive fatigue cycles during one of the baseline tests for this study. The crack growth from one cycle to the next can be taken to have a minimal effect.) The differences are readily apparent; the clip gage load-displacement curve shows a much more gradual change in compliance as the crack surfaces come into contact, while the load-displacement curve for the IDG shows a dramatic change in compliance once closure occurs.

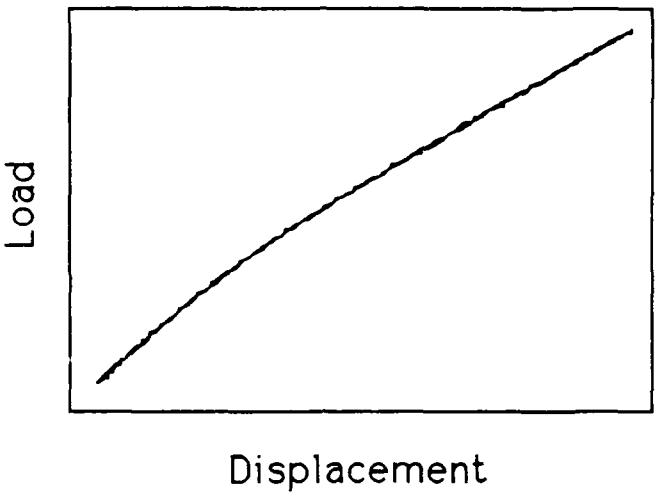

a. Data Obtained from Clip Gage

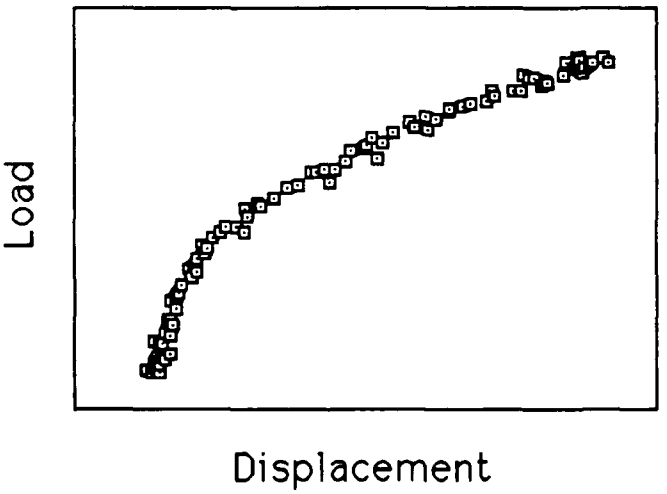

b. Data Obtained from IDG

Figure 2-6. Load-Displacement Data from Clip Gage and IDG

The difference between the two load-displacement curves is a direct result of the different locations of measurements for the two techniques. The distance of the load-displacement measurement location from the crack tip has been found to affect the measurement of closure load (19:211).

This finding is contradicted by a study performed using finite element analysis (17:378) which generated load-displacement plots for both far-field (at the crack mouth, 65 μm behind the crack tip) and near-field (4 μm behind the crack tip) measurement locations. Despite dramatic differences in the appearance of the load-displacement plots generated, the finite element analysis found that the closure load is independent of the measurement location. The finite element analysis also confirmed, however, that the sensitivity and resolution necessary to determine the closure load is greatly affected by the distance of the measurement location from the crack tip.

Some studies attribute the differences in near-field and far-field load-displacement plots to differences in the behavior of the closure phenomenon itself. In the near field, closure occurs in a three-dimensional manner; during the fatigue loading cycle, shear lips on the surface of the specimen are the first portion of the crack faces to make contact and are the last portion of the crack faces to break contact (19:213, 21:586). The measurements of displacement near the crack tip are highly influenced by the complex residual stress field in the region of the crack tip; this

three-dimensionality can be caused by differential yielding of surface material as compared to material inside the specimen, or by crack tunneling (12:11).

In the far field, the closure phenomenon exhibits a more thickness-averaged behavior (12:11). A sensitive instrument could discriminate among the different stages of this behavior and possibly detect the first contact of the crack surfaces; however, as discussed before, far-field measurements suffer from an inherent lack of sensitivity due to the remoteness of the measurement location from the crack tip.

The general consensus seems to be that near-field measurements are a better way to ascertain the effective stress intensity range experienced by the crack tip; in this study, these measurements will be obtained from the laser IDG. The near-field measurement location will provide an increased instrument sensitivity and will allow better determination of the load at which full crack surface separation occurs. Closure loads measured by the IDG should more accurately reflect the effective stress intensity range experienced by the crack tip region.

For this study, the microhardness indents used with the IDG were initially placed approximately 150 microns behind the crack tip. As the crack grows under subsequent fatigue cycling, the tip of the crack moves away from the indents. At some point during the growth of the crack, obviously, a transition from near-field to far-field measurement is made.

Closure loads determined from laser IDG measurements made more than 0.1 times the specimen width behind the crack tip are nominally equal to the closure loads determined from other far-field measurement techniques such as clip gage and back face strain gage (20:195). In order to retain the near-field nature of the load-displacement measurements in this study, new indents were placed at the crack tip after approximately 2.5 mm of crack growth from the previous placement of indents. Therefore, any closure measured by the IDG occurred between the microhardness indents and the crack tip, a distance no longer than 2.5 mm.

Any contact of the crack surfaces (closure) measured by the clip gage has a much longer distance over which to become apparent. Once the crack at the location of the microhardness indents has come into contact, no further motion of the indents should occur until the next fatigue cycle is applied and the load rises above that needed to open the crack at that point. Any further closing of the crack surfaces beyond the indents would go unnoticed, however; the IDG is sensitive only to changes in geometry that occur between the indents and the crack tip.

Contact of the crack surfaces beyond the indents will be detected by the clip gage. The distance over which crack surface contact occurs can be indirectly obtained from the load-displacement curve obtained from the clip gage. Just as the compliance of the upper portion of the curve can be used to determine the length of the crack when it is fully open, a

regression can be performed to find the compliance of the lower portion of the curve; this "closed crack compliance" can be used to determine the apparent length of the crack when it is fully closed. Figure 2-7 shows a load-displacement curve obtained from a clip gage, with both open and closed crack compliances computed.

The region of gradual compliance change for load-displacement curves obtained from a clip gage indicate that the crack surfaces do not come into contact instantaneously, but that the crack surfaces come into contact over a finite interval of load values. This gradual closing of the crack surfaces during unloading of the specimen has been noted in many studies (21:586, 22:59, 23:560-561).

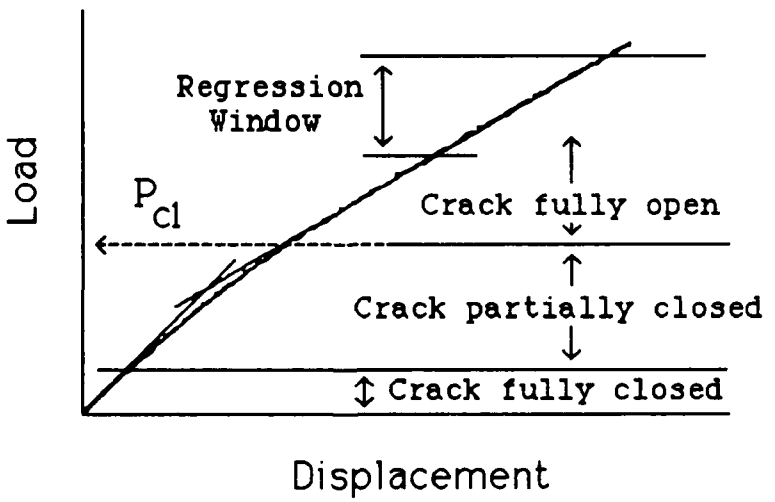

Figure 2-7. Load-Displacement Plot With Open Crack and Closed Crack Compliances

Using Eq (5), the open crack compliance and the closed crack compliance can be used to compute the apparent lengths of the crack when fully open and when fully closed. The difference between these two lengths gives the distance over which the crack surfaces are in contact at minimum load for the fatigue cycle. The calculation of the contact length was performed for the constant maximum amplitude load test for this study; results are shown in Figure 2-8. The contact length measured by the clip gage was significantly longer than the maximum IDG measurement distance of 2.5 mm.

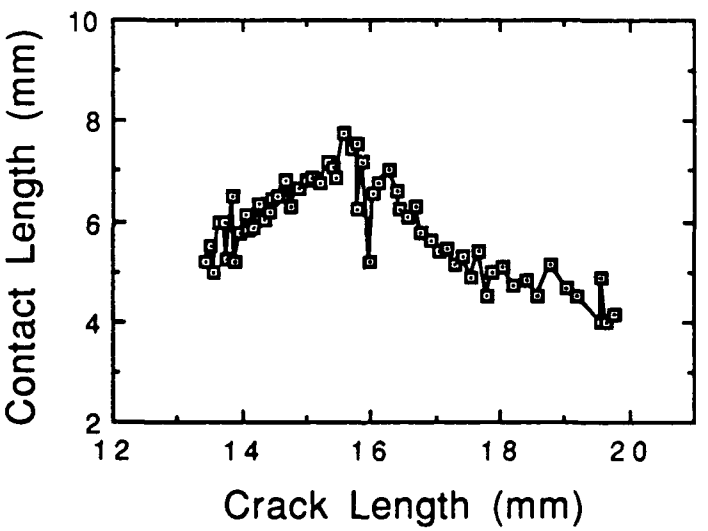

Figure 2-8. Contact Length as a Function of Crack Length for the Constant Maximum Amplitude Load Test

The existence of a region of gradual compliance change makes it possible to define the closure load in many different ways; one can either use the load at which the crack first begins to open, the load at which the crack is fully open, or a load value somewhere between these two that might represent an "average" value of closure load (24:172).

Some studies (25:706) have defined the closure load as the value for load at the point of intersection of the open crack and closed crack compliances, depicted in Figure 2-6. Many other studies have defined the closure load to be where the load-displacement plot first begins to deviate from linearity, designated as P_{cl} in the same figure (5:220, 20:187, 23:562, 26:205-206, 27:96). In this study, where the emphasis is on closure near the crack tip, the point at which the load-displacement plot begins to deviate from linearity will be considered to be the closure load.

Previous Studies

Overloads during fatigue cycling can cause retardation in subsequent crack growth. These overloads also result in an increase in closure load, which in turn decreases the effective stress intensity range. Some studies have been able to correlate the retarded crack growth rates with the decrease in effective stress intensity range due to the increased closure. Others studies claim that retarded crack growth rates after an overload are related to, but not caused

by, the phenomenon of closure. This conflicting evidence will now be evaluated.

In a study that used single overloads of 100% and 150% over a constant baseline stress intensity range fatigue test in a titanium alloy, the near-field and far-field closure loads were compared to the post-overload crack growth rates. The effective stress intensity range calulated using far-field closure loads showed no correlation with the post-overload crack growth rates, while the effective stress intensity range calculated using the near-field closure loads corresponded with the post-overload crack growth rates (27:106).

In a similar study involving aluminum-lithium 2090-T8E41, the effect of a single 150% overload applied above a baseline constant stress intensity range of 8 $MPa\sqrt{m}$ was investigated. The far-field measurements (using a back face strain gage) showed no detectable changes in closure load, while the use of side face strain gages near the crack tip showed a correlation between the crack growth rates and the closure load. The maximum closure loads occurred at the minimum post-overload crack growth rate, and the closure loads subsequently were reduced as the crack growth rate gradually returned to that measured prior to the overload (28:2854).

In non-overload fatigue tests, the effective stress intensity range (ΔK_{eff}) has been found useful in correlating crack growth rates from tests of various materials, stress

levels and stress ratios. In tests with the titanium-aluminum alloys Ti-8Al(a) and Ti-4Al(s) that involved both large cracks in compact tension specimens and small surface cracks, crack growth data could be consolidated using the effective stress intensity range at all but the shortest crack lengths (29:160-163).

In another study that analyzed surface cracks in Ti 6246, the ΔK_{eff} was used to consolidate the crack growth data into a single band of values (30:633). Again, however, ΔK_{eff} did not consolidate crack growth rates well for the small crack data.

Another study that involved Ti 6246 was able to correlate the ΔK_{eff} with fatigue crack growth rates near threshold at low stress ratios (31:1013). The same study found difficulty in correlating ΔK_{eff} and crack growth rates in tests where threshold was attained at higher stress ratios; this was attributed to the difficulty in determining closure load because of the proximity of closure load to minimum load.

Other studies have inferred that the closure does not fully explain the retardation of crack growth following an overload. In a study involving overloads in 7475-T731 aluminum alloy (32:528-535), tests were conducted at stress ratios of 0.7. Crack closure was measured using a surface-mounted Elber CTOD gage; each measurement was taken at a location one-half of the specimen thickness behind the crack

tip. For the two thicknesses of specimen studied, this distance was 1.015 and 3.25 mm, respectively. The study found that there was no measurable closure, either before or after the overload was applied, even though various amounts of crack retardation were observed.

From fractographic analysis of the crack surfaces, it was suggested that these post-overload retardation effects were due to crack tunnelling and/or crack tip blunting. The possibility exists that there was undetected near-field closure, however. The small amount of closure that might be expected at a high stress ratio could be masked by the lack of sensitivity of a far-field measurement.

III. Test Procedures

Specimen Preparation

All fatigue tests performed for this study were conducted using the aluminum-lithium alloy 2091. Refer to Table 1 for the chemical composition of this alloy (33). Material was obtained in sheet form with a thickness of 3.66 mm (0.144 in); standard compact tension specimens were machined from this material according to the dimensions specified in ASTM E647-86a (34:912).

The properties of this material vary in the various directions of grain orientation and with the various heat treatments available. This study used material with the T-3 heat treatment, and compact tension specimens were machined in the L-T orientation. In the longitudinal direction, this material has been found to have a yield strength of 50.1 $MPa\sqrt{m}$

Table 3-1. Chemical Composition of AlLi 2091 Alloy

Element	% Weight
Si	0.20
Fe	0.30
Cu	1.8 - 2.5
Mn	0.10
Mg	1.1 - 1.9
Cr	0.10
Zn	0.25
Li	1.7 - 2.3
Zr	0.04 - 0.16
Ti	0.10
Others, each	0.05
Others, total	0.15
Al	Remainder

(45.5 ksi) and an ultimate yield strength of 65.3 MPa$\sqrt{m}$ (59.4 ksi). The Young's modulus nas been evaluated as 12.7 X 10^3 MPa$\sqrt{m}$ (11.5 X 10^3 ksi) (33).

Both faces of each specimen were polished to a mirror-like, 1-micron finish; this was done to minimize the random reflections from an unpolished surface, enabling the detector arrays of the laser IDG to more easily distinguish the interference fringes from background reflections. Polishing of the specimens, performed in several stages with progressively finer grits, removed quite a bit of material from the faces of the specimens.

The specimens were machined and polished in two sets. There were slight differences between the two sets of specimens, especially in the dimensions of notch length and post-polish thickness. Actual dimensions of the specimens are listed in Table 3-2. Figure 3-1 shows a compact tension specimen and depicts the terms referred to in Table 3-2.

Table 3-2. Actual Dimensions of Compact Tension Specimens

Specimen Number	Width (mm)	Notch Length (mm)	Thickness (mm)
1	39.934	7.013	3.193
2	39.949	6.891	3.310
3	39.878	7.041	3.256
4	39.987	7.097	3.325
5	40.084	7.145	3.218
6	39.822	6.807	2.804
7	39.761	6.764	2.842
8	39.799	6.797	2.898
9	39.896	6.850	2.908

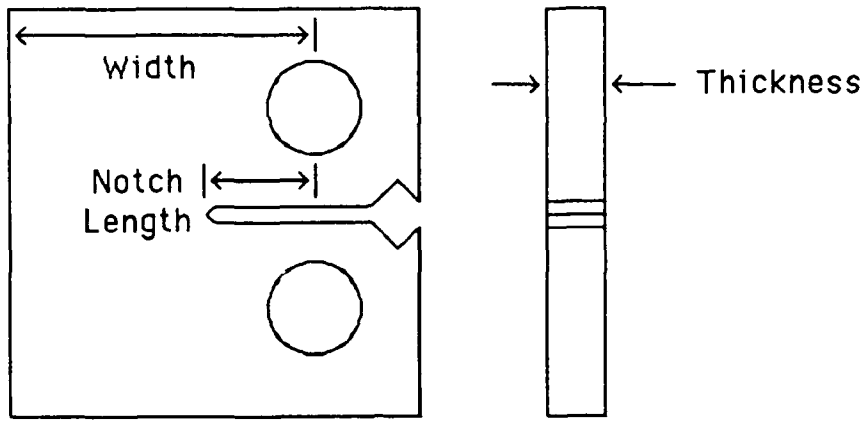

Figure 3-1. Dimensions for Compact Tension Specimen

Testing Procedure

Precracking

The precracking for each compact tension specimen used in this study was performed in accordance with ASTM recommendations (34:906). The final precracking crack length in each specimen was 11.43 mm (0.45 in) as measured from the load line. If the microhardness indents for use with the laser IDG were placed at crack lengths less than 11.43 mm, the grips used to hold the specimens obstructed the interference fringe patterns produced by the laser light reflected from the indents. In addition, a final precrack length of 11.43 mm placed the crack tip beyond the notch tip by at least a notch width, per ASTM recommendations. This

precaution minimized any effects that notch tip geometry may have had upon the crack tip stress field.

The maximum stress intensity level (K_{max}) at the 11.43 mm crack lergth was chosen to be 4.4 MPa$\sqrt{m}$ (4.0 ksi). This value for K_{max} placed the final precracking ΔK just above threshold value for this material. In this study, all tests involved maximum stress intensity levels above 4.4 MPa$\sqrt{m}$; this removed the possibility of precracking load history affecting the subsequent fatigue test. The initial K_{max} for the precracking, to be applied at the initial crack length (equal to the specimen notch length beyond the load line) was chosen to simultaneously satisfy two criteria: 1) a final K_{max} of 4.4 MPa$\sqrt{m}$ at 11.43 mm, and 2) a load shed rate near the ASTM-recommended value of 20%.

Crack Growth

For fatigue crack growth beyond the precracking of the specimen, the loading consisted of fatigue cycling at 30 Hz (sine wave function) in a laboratory air environment. The test system was fully automated and controlled by an IBM AT computer. Inputs from the load cell and from the various measurement techniques (electric potential, clip gage, and laser IDG) were interfaced to the computer through an analog-to-digital board.

One baseline test was conducted under constant amplitude load conditions. For this test, the load did not depend upon crack length; in other words, feedback of crack length to the

controlling computer was not required to actively control the load parameters. Because the laser IDG required the placement of microhardness indents on the specimens at regular intervals, however, the crack length as measured by the electric potential method was used as feedback to the computer to limit the amount of crack growth during any one segment of testing. During the constant amplitude load tests, feedback from the load cell to the computer was used to control the load level.

In the next series of tests, a constant stress intensity range was used in order to maintain a constant crack growth rate. The constant stress intensity range tests required a feedback of crack length to the controlling computer; the crack length (as measured by the electric potential method) was used by the computer to determine the load required to meet the stress intensity range specified for the test.

In all tests, crack growth in the specimen was controlled by specifying a final crack length for that portion of the test. Proper use of the laser IDG required the crack tip be no farther than 0.1 times the width of the specimen (20:195); this limited each segment of crack growth to approximately 4.0 mm, although usually the segments were limited to 2.5 mm of crack growth. When the final crack length for a segment of crack growth was reached, the computer placed the fatigue test on hold at 10% of the maximum load.

Data Collection

Data from each of the measurement techniques (electric potential, clip gage, and laser IDG) were taken at specified time intervals which depended on the crack growth rates observed during the tests. For ΔK = 5.5 MPa$\sqrt{m}$ (5 ksi) tests, data was collected at intervals of 600 seconds (10 minutes). For ΔK = 7.7 MPa$\sqrt{m}$ (7 ksi) tests, data was collected at intervals of 120 seconds (2 minutes). For ΔK = 9.9 MPa$\sqrt{m}$ (9 ksi) tests, data was collected at intervals of 60 seconds (1 minute). These intervals ensured the collection of a sufficient number of data points for each fatigue test. These data collection rates also updated the crack length measurement at crack length intervals short enough to allow load shedding for the fatigue test to occur at the proper rate, maintaining the stress intensity range near the specified value for the test.

At each data collection point, the computer slowed to 0.1 Hz for three load cycles. During the first of these load cycles, the electric potential data was taken; crack length was determined from the data taken during this first data cycle. During the second cycle, 1000 points of data were taken from the clip gage; these 1000 points were then converted by the computer into a load-displacement plot for the specimen notch mouth. During the third cycle, 500 data points were taken from the laser IDG; these 500 points were similarly converted by the computer to produce a load-

displacement plot for the most recently placed set of microhardness indents.

After these three load cycles were completed, load-displacement data obtained from the clip gage and the laser IDG were stored on the computer's hard disk and the electric potential crack length was added to a log file. Based upon the newly-measured crack length, a maximum load for the load cycles prior to the next data acquisition cycle was computed. Fatigue cycling then returned to the baseline rate of 30 Hz. If the newly-measured crack length exceeded the specified maximum crack length for that segment of crack growth, the test was placed on hold.

Before removing the specimen from the testing machine to prepare for the next segment of crack growth, a restart file was saved; this allowed the final parameters of the current portion of the fatigue test to be saved so that the testing machine could be reinitialized at the beginning of the next segment of crack growth.

Placing Microhardness Indents

After the completion of each segment of crack growth, the specimen removed from the testing machine. Optical measurement of the crack lengths on front and back were made; these measurements were averaged and compared to the crack length as measured by the electric potential method. The front and back crack lengths were monitored to make sure that they were within 5% of each other per ASTM recommendations

(34:908-909); the specimen was reversed in the grips if the crack on one surface began to extend far ahead of the crack on the other surface.

A pair of pyramidal microhardness indents were placed on the side of the specimen facing the IDG detectors during the next segment of the test. For this study, the size of each microhardness indent was approximately 26 - 27 microns across; they were placed approximately 100 - 150 microns apart, straddling the crack. In general, the indents were placed approximately 100 - 150 microns behind the crack tip. The distance of the indents behind the crack tip was measured and recorded; this would be used later in the data reduction.

The specimen was then returned to the testing machine, which was reinitialized (using the restart file) for the next segment of crack growth. Testing could not immediately begin, however; the temperature of the specimen was significantly affected by the 10.0 amps of current flowing through the specimen used in the electric potential method of crack measurement. Thermal equilibrium was essential for proper calibration of electric potential measurements.

After the specimen had reached a thermal equilibrium (which took approximately 5 minutes), the clip gage was inserted into the specimen mouth, the laser was aligned to illuminate the microhardness indents, and the IDG detectors were adjusted such that the interference fringes fell upon the linear detector arrays. If the electric potential crack length had drifted away from the optically-measured crack

length, the electric potential calibration constant was adjusted before the test was restarted.

Once the load cycling had resumed, the IDG was watched closely to assure that the interference fringes were tracked properly; it was not unusual for the first few cycles to cause the specimen to shift in the grips, causing the interference fringes to be thrown off the detectors. When the specimen had stabilized in the grips and all gages were determined to be functioning properly, the test machine could be left unattended. The computer continued to monitor test conditions, applying load cycles and periodically taking data until the specified maximum crack length was reached.

As mentioned before, for the constant stress intensity range tests the maximum load applied to the specimen depended upon the most recent crack length (as measured by the electric potential method). As the crack grew, the maximum load applied to the specimen decreased. At some point in each test, the load decreased to a level where the load cell could not provide accurate feedback to the computer that controlled the loading; at this point, the computer automatically stopped the test. Due to the varying thicknesses of the specimens, this point varied for each test. For the $\Delta K = 5.5$ MPa$\sqrt{m}$ tests, the loss of load control occurred near crack lengths of 25.5 mm. For the $\Delta K = 7.7$ MPa$\sqrt{m}$ tests, loss of load control occurred near 28 mm, and for $\Delta K = 9.9$ MPa$\sqrt{m}$ tests, loss of load control occurred near 30.5 mm.

Data Reduction

Step 1: Correction of Electric Potential Crack Length Data

As discussed earlier, the DC electric potential (EP) method is the most accurate method (of those used in this study) for determining crack length. Even so, some drift in the EP measurements was found during crack growth from one set of microhardness indents to the next. Reinitialization of the EP method after each placement of microhardness indents resulted in discontinuous crack length data for the specimen. (See Figure 3-2.)

The actual crack lengths at the beginning and the end of each segment are known, having been optically determined at the time of indent placement. Initial and terminal EP crack lengths, however, will not match these optical crack lengths; the initial EP crack length was determined from the regression equation obtained from the generalized electric potential solution, and the EP terminal crack length will not match the actual terminal crack length due to drift in the EP measurements during the growth of the crack. EP crack lengths between the segment endpoints provide a smooth set of data points between the initial and terminal EP crack lengths.

Through the use of a linear interpolation which uses the mapping scheme shown in Figure 3-3, initial and terminal EP crack lengths for each segment can be corrected such that they match the actual crack lengths measured at indent placement.

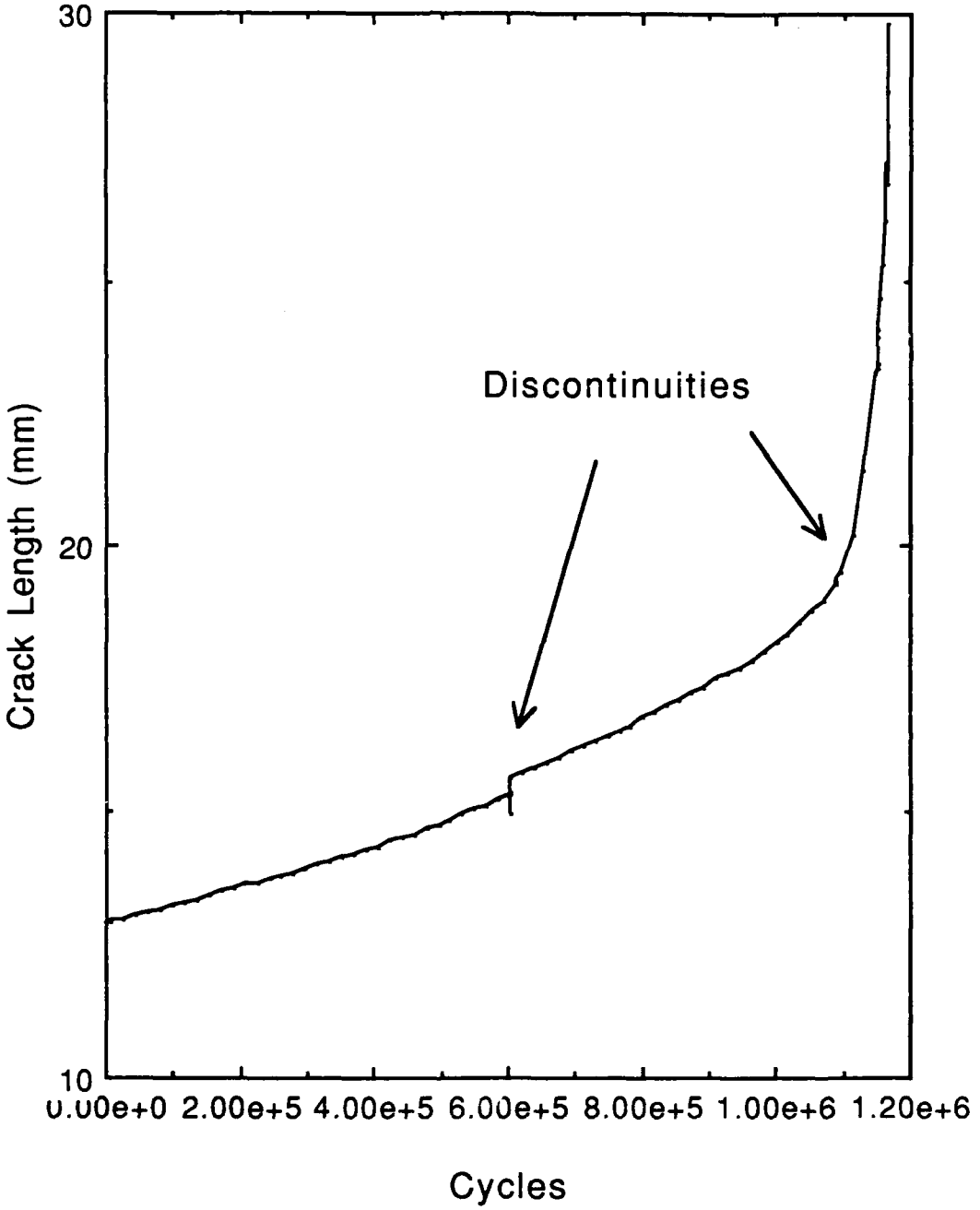

Figure 3-2. Uncorrected Electric Potential Crack Length Data

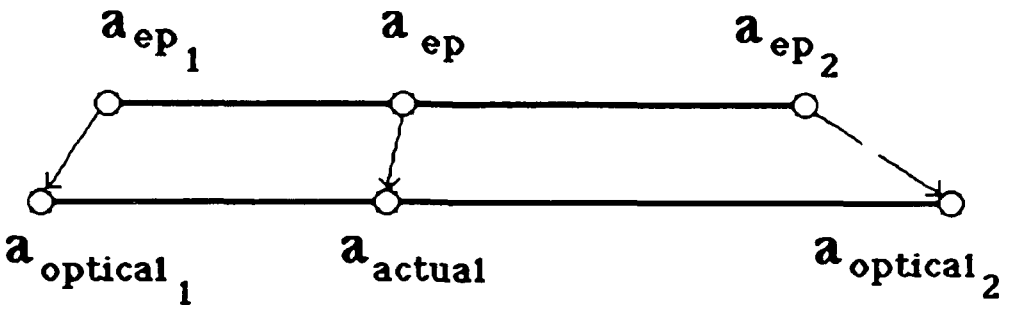

Figure 3-3. Linear Interpolation Scheme used to Correct EP Crack Length Measurements.

The formula used in this interpolation scheme is:

$$a_{actual} = a_{optical_1} + \frac{a_{ep} - a_{ep_1}}{a_{ep_2} - a_{ep_1}} * (a_{optical_2} - a_{optical_1}) \quad (8)$$

This linear interpolation also preserves the smoothness of crack length data within the segment of crack growth and results in a crack length vs cycles curve that is smooth from start to finish over the entire specimen (See Figure 3-4). Smoothness of the crack length vs cycles (a vs N) data is vital for calculation of accurate crack growth rates (da/dN).

The corrected crack length replaced the EP-measured crack length in all data files used in subsequent analysis. All other data contained in these files (such as compliance values, closure load values, etc.) remained the same.

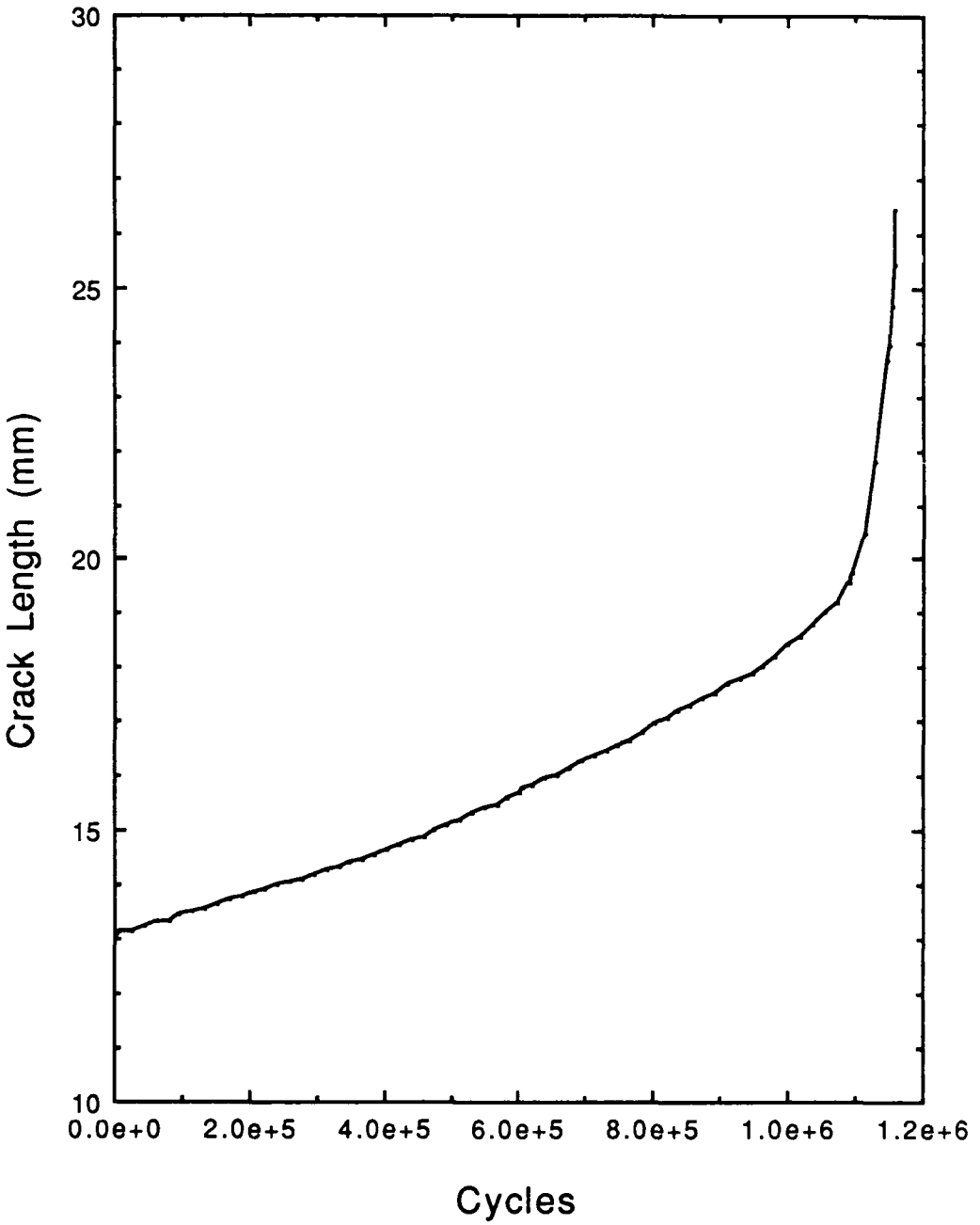

Figure 3-4. Corrected Electric Potential Crack Length

Special Note about Figures 3-2 and 3-4

Because the test results depicted in Figures 3-2 and 3-4 were obtained from a constant amplitude maximum load test, it was possible to test the specimen to failure. The lack of an identifiable upper optical crack length for the last segment of crack growth resulted in the loss of data from this segment. Because of the extremely large crack growth rates in this segment of the test, however, this loss was limited to three data points.

The tests conducted under constant stress intensity ranges experienced a loss of load control as the crack achieved a certain length. Because of this loss of load control, specimens were not tested to failure. Therefore, accurate optical measurements of the final crack length could be made, and data from all segments of crack growth could be retained and analyzed.

Step 2: Analysis of Load-Displacement Curves for IDG and Clip Gage

Even though the load-displacement curves for the IDG and for the clip gage are usually quite different in appearance, they each possess the characteristics from which two items of information are obtained, i.e. the compliance, or slope, of the linear portion of the plot; and the closure load, the load at which the load-displacement plot deviates from the linear trend of the upper portion of the curve. Therefore, the load-displacement curves obtained from the IDG were

analyzed separately from those obtained from the clip gage, but the analysis techniques used on each type of curve were the same. The technique described below applies to both types of data.

Each set of individual load-displacement plots (the set obtained from the clip gage and the set obtained from the laser IDG) were graphically displayed in sequence on an IBM PC. An imaginary grid was superimposed upon each plot, with the maximum and minimum load of the plot being identified with the values 1.0 and 0.0, respectively. For each plot, an upper and a lower value for load were chosen; these upper and lower values of load formed a "window", and were selected such that the linear portion of the load-displacement curve fell within the window. For the plots in this study, unless otherwise noted in the section entitled "Results", the upper and lower limits of the window were chosen to be 0.95 and 0.70, respectively. A linear regression was performed for the points that fell within the window; this regression provided the compliance, or slope of the load-displacement curve.

The linear regression through the upper portion of the curve also provided the basis for determining closure load. In this study, the closure load was identified as the load at which the load-displacement plot deviated from the linear regression by two standard deviations.

The analysis of the load-displacement curves from the clip gage and from the laser IDG yielded data files that

contained one data record for each load-displacement plot. (As mentioned above, the IDG and the clip gage data were analyzed separately; two separate data files were produced.) Each individual record in the data files contained: 1) the data sample number of each plot, which identified the time at which the data was taken, 2) the compliance value for the linear portion of the curve, and 3) the closure load.

In some cases it was impossible to perform a regression upon the load-displacement plots; either the linear array detectors did not track the interference fringes properly, the fringes did not fall upon the detector arrays, electrical connections were broken loose, etc.

In any case where regression was impossible, all data collected for that data sample were discarded. For example, if the IDG load-displacement plot for a data sample was poor but the clip gage plot was good, the data were discarded anyway. This was done so that subsequent steps in the data analysis did not yield different values due to a differing number of data records.

Step 3: Combination of Closure Loads and Log File Data

A simple FORTRAN program was executed that combined the data generated from the analysis of the load-displacement plots with the data collected in the log file, which included: 1) the crack length measured by electric potential method, 2) the number of load cycles applied since the test began, 3) the maximum load applied during the data

acquisition load cycle, and 4) the load ratio applied during the data acquisition cycle.

The log file data were combined with the IDG closure file and the clip gage closure file to produce two data files. One file included the data pertaining to that measured by the clip gage, and the other file contained data pertaining to that measured by the laser IDG. Separate data analysis was performed for each of these files.

Step 4. Incremental Polynomial Regression of Raw Data

ASTM E647 recommends analyzing crack growth data using an incremental polynomial method (34:919-920). This involves fitting a second-order polynomial to a specified subset of data points, usually seven. From this regression, the values of crack growth rate and stress intensity range are calculated for the midpoint of the subset of data points. An identical regression (using additional information from the same data samples) was performed to determine the values for closure load, maximum load, K_{max}, and load ratio; these parameters were then used to compute an effective stress intensity range. Fitting of second-order polynomials to new subsets of data points continued until data points were exhausted.

The two data files generated in Step 3 will contain the same number of data records; each data record in the file containing clip gage data will have a corresponding data record from the file containing the IDG data. These

corresponding data records were obtained at the same crack lengths; therefore, the separate polynomial regression of the two data files will yield identical values for crack length and crack growth rates.

The files produced by the regression will contain different closure load data, however, because two different methods were used to measure the load-displacement data; the near-field closure measured by the laser IDG should be considerably higher than that measured in the far-field by the clip gage. Because closure loads measured by the IDG are higher, the effective stress intensity range computed from the IDG data will be lower.

Step 5. Further Analysis of IDG Closure Data

When the ratio of closure load and maximum load (P_{cl}/P_{max}) over each data acquisition cycle is plotted against crack length, a distinct trend in closure is seen. Figure 3-5 shows this plot over three segments of crack growth for a typical constant amplitude load test. Also shown in this figure are the crack lengths at which the microhardness indents used with the IDG were placed. The general trend and discontinuity of this curve clearly demonstrate that the closure load measured by the laser IDG is highly dependent upon the instantaneous distance of the microhardness indents from the crack tip. The closure measured by the IDG decreased as the distance between the crack tip and the indents increased.

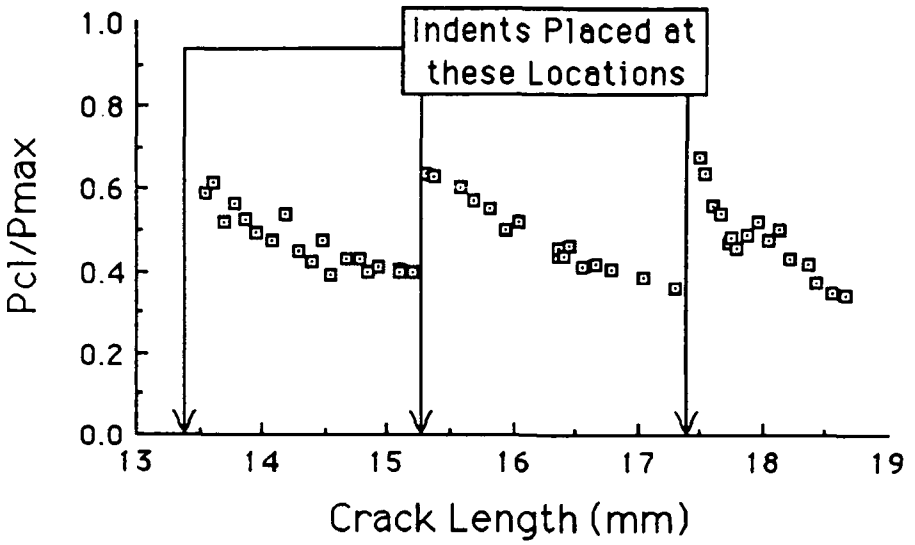

Figure 3-5. Typical Relation Between P_{cl}/P_{max} and Crack Length for a Constant Amplitude Load Test

As mentioned previously, new indents were placed after each segment of crack growth of two to three millimeters. This placement of indents occurred several times during a typical test. By using the location of the microhardness indents, the distance from the crack tip to the most recently placed set of indents could be calculated for any data sample. P_{cl}/P_{max} data from several different segments of crack growth in a constant maximum amplitude load test are plotted against the distance of the crack tip from the microhardness indents in Figure 3-6.

With a regression analysis, the ratio of P_{cl}/P_{max} for these data sets could be expressed as a function of crack tip

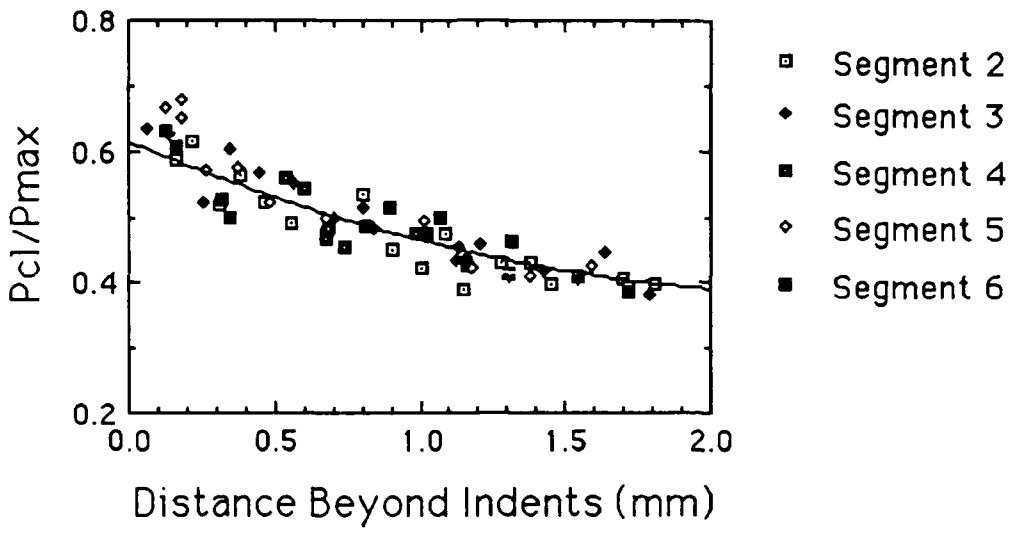

Figure 3-6. Typical Relation Between P_{cl}/P_{max} and IDG Indent Location for Several Segments of Crack Growth from a Constant Amplitude Load Test

distance beyond the indents. A second-order polynomial regression was chosen for the regression. In Figure 3-6, this regression curve is shown superimposed upon the data.

To eliminate the effect of indent location upon the measurement of crack closure, a fixed distance behind the moving crack can be selected at which the closure load from the IDG can be normalized. As seen in Figure 3-6, the second order regression chosen to fit the P_{cl}/P_{max} data fits the data over a large portion of the curve, but the behavior of the P_{cl}/P_{max} data changes when the indents are located very near the crack tip. The values of P_{cl}/P_{max} take a sudden and dramatic upturn when the crack tip is near the indents. The

closure behavior appears to change when the crack tip is approximately 0.2 mm beyond the indents.

This location could be the point at which the behavior of the closure phenomenon changes from the three-dimensional nature near the crack tip to the bulk closure behavior; if so, adjustment of all closure loads to match those at this location will retain the near-field nature of the load-displacement measurements without adding the three-dimensional effects seen at locations closer to the crack tip. This should also give the best estimate of the effective stress intensity experienced by the crack tip, which should be independent of measurement location.

Due to changes in loading history from one type of test to another, the regression curve may be different for each type of baseline test. Also, regression curves may change from one segment of crack growth to another within the same test. For example, a fatigue test that involved maintaining a constant stress intensity range would have a different loading history than a fatigue test that used a constant maximum amplitude loading. Therefore, the function that relates the closure load, maximum load and distance of crack tip beyond the indents would be expected to have a different relation for each specific test. The regression curves for individual segments of crack growth will be discussed in Section IV.

When the data for each segment of crack growth is analyzed individually, a value of P_{cl}/P_{max} at a distance of

0.2 mm beyond the indents can be obtained for that segment of crack growth from the best-fit regression for that segment. Since the placement of the indents is known, this value of P_{cl}/P_{max} can be associated with a specific crack length. The P_{cl}/P_{max} data for a typical single segment of crack growth from a constant stress intensity range test of 7.7 MPa$\sqrt{m}$, along with the regression curve that fits the data, is depicted in Figure 3-7.

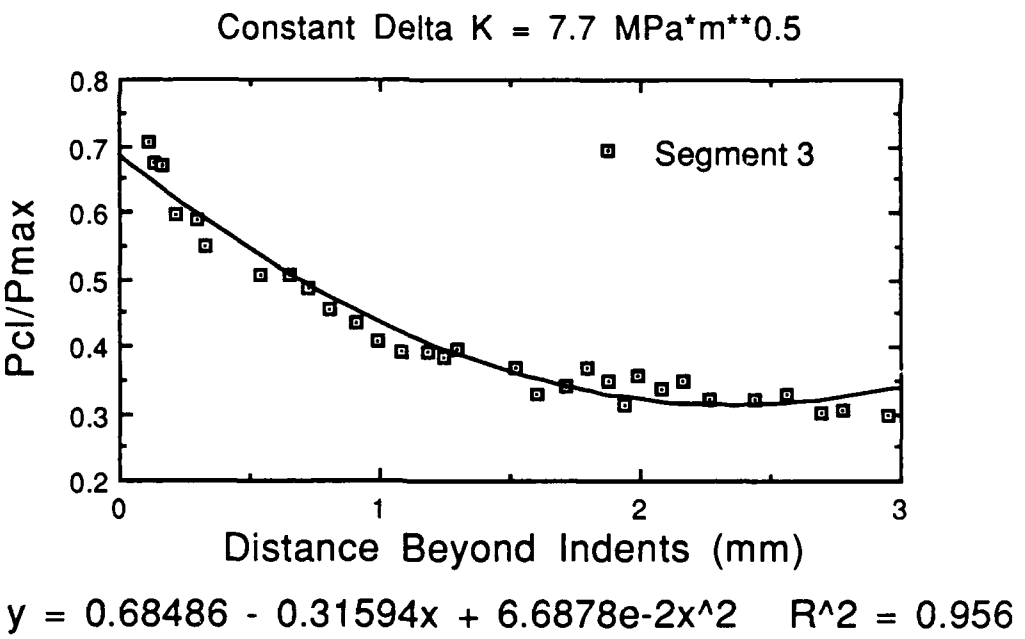

Figure 3-7. Typical Relation Between P_{cl}/P_{max} and IDG Indent Location for a Single Segment of Crack Growth (Best-Fit Second Order Regression Shown)

When the data from all segments of crack growth for a specimen are taken as a whole, a profile of P_{cl}/P_{max} as a function of crack length for that specimen can be obtained. A linear interpolation between these specific data points will give a value of P_{cl}/P_{max} for any crack length. This value can be thought of as the value of P_{cl}/P_{max} that would be measured if the indents were travelling at a fixed distance of 0.2 mm behind the growing crack tip. Since the maximum load and crack length are known for each data acquisition cycle, a value of closure load can be calculated for each data cycle. (The P_{cl}/P_{max} profiles and closure load profiles for each specimen are discussed in the Results section.)

These new values of closure load, adjusted to account for the dependence of the distance of crack tip beyond the indents, can be substituted into the data file that contains the original closure data measured by the IDG that was generated in Step 3.

This new file, containing closure loads based on the value of P_{cl}/P_{max} as if it were measured 0.2 mm behind the crack tip, was analyzed using the seven-point polynomial incremental regression technique described in Step 4. Only the IDG closure data had been changed; the remaining log file data was the same as that for the previous incremental polynomial regressions. Therefore, the crack growth data remained unchanged. The increase in closure load due to the

adjustment to a distance of 0.2 mm behind the crack tip led to a corresponding decrease in effective stress intensity range. These values were then correlated with the crack growth rates.

Further Comments on the Incremental Polynomial Regression

When the ASTM-recommended (34:919-920) incremental polynomial regression is performed, an interval of distance and a number of data points are chosen. The data points from the fatigue tests are divided into subsets; if the specified number of points (or more) lie within the chosen interval of distance, a second-order polynomial is fit to the data. Otherwise, the interval is extended from the initial data point until the specified number of points are found; the regression is then performed for this extended interval. Regressions continue until subsets of data points are exhausted.

The incremental polynomial regression is therefore sensitive to the interval of distance chosen. A larger interval of distance will include more data points and yield a smoother curve, while a shorter interval will be more sensitive to changes that occur over a small distance or a small number of data points. On the other hand, a small regression interval, while being sensitive to changes which occur over a short distance of crack growth, does not remove the effect of any scatter that may exist in measurements.

In the baseline tests (which included the constant maximum amplitude load test and the constant stress intensity tests without overloads), a regression interval of 0.504 mm (0.02 in) was used. For the tests in this study that involved overloads, the incremental polynomial regression was performed in a slightly different manner.

Figure 3-8 shows a schematic plot of a crack growth history (crack length vs number of cycles) following an overload of sufficient size to cause crack growth retardation. A dramatic discontinuity in slope is noted at the point of application of the overload (Point C).

If the incremental regression is performed over an interval which happens to be centered on Points B, C, or D (refer to Figure 3-8), the discontinuity in slope at the point

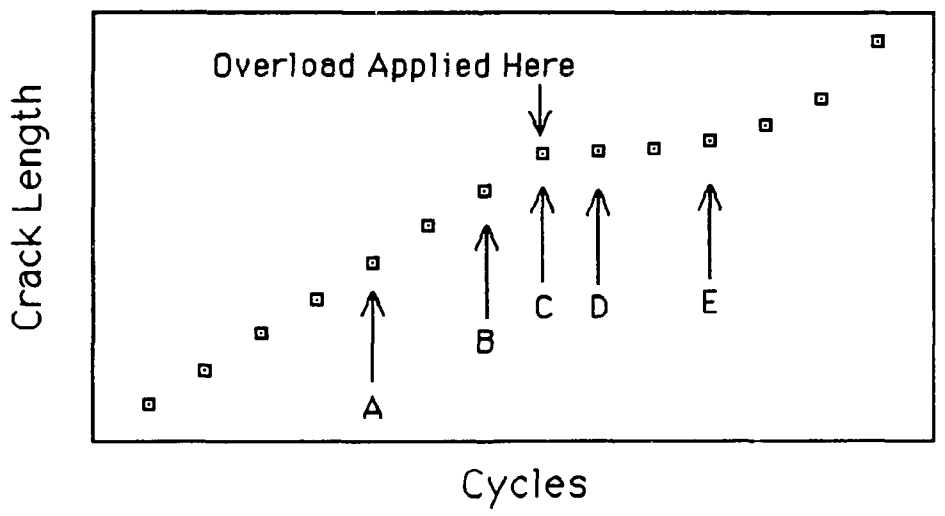

Figure 3-8. Schematic of Crack Growth History at an Overload

of overload will adversely affect the values provided by the regression. If the seven point regression is performed over an interval centered on Point A or on Point E, the regression should provide values that are proper.

To avoid the problems introduced by the discontinuity in slope at the point of an overload, the data files were split into two different sections; one section contained data cycles obtained before the overload and one contained data cycles obtained after the overload.

Then, in order to get the best resolution of crack growth retardation after the overload, a regression interval of 0.127 mm (0.005 in) was used on each portion (pre- and post-overload) of the test. The data files resulting from these separate regressions were recombined to provide a single data file. The delay distances and delay cycles were then calculated from the values of crack length and crack growth rate obtained from the regression.

IV. Results and Discussions

The crack growth characteristics of aluminum-lithium alloy 2091 will be discussed in light of the fatigue tests conducted for this study. All fatigue tests were performed on standard compact tension specimens. The applied load cycles were sinusoidal with a stress ratio of 0.1 and a frequency of 30 Hz.

All specimens were precracked such that a maximum stress intensity (K_{max}) of 4.4 $MPa\sqrt{m}$ (4 ksi) was achieved at a crack length of 11.43 mm (0.45 in). As per ASTM guidelines (34:906), the initial K_{max} of fatigue loading after precracking was always larger than the final K_{max} of precracking. By using this procedure, the effects of precracking upon subsequent fatigue crack growth were eliminated.

Three different measurement techniques were used in this study. A direct-current electric potential method was used to measure the growth of the crack in the specimen. A constant current of 10.0 amps was passed through the specimen, while a digital voltmeter read the voltage across potential leads spot-welded to the specimen. A calibration curve obtained from a finite element analysis provided the means to track the crack growth.

A non-conducting clip gage was used to obtain load-displacement relations at the mouth of the specimen. In regions closer to the tip of the crack, the laser IDG

provided load-displacement relations at the location of the most recently placed set of microhardness indents. The load-displacement relations provided by the clip gage and the laser IDG were analyzed to yield compliance values and closure loads.

Measurements were taken by the clip gage and the laser IDG at specified time intervals that were dictated by the crack growth rate; with larger stress intensity ranges, the crack growth rate was higher and the rate of data acquisition was increased accordingly. Load-displacement measurements were taken by the clip gage and the laser IDG on consecutive load cycles; any difference in the specimen response to loading due to crack growth during a single load cycle should be minimal.

Microhardness indents used with the laser IDG were placed on the polished face of the specimen after precracking had ended, and were replaced with new indents after each pre-programmed segment of approximately 2.5 mm (0.1 in) of crack growth. In each instance, the indents were placed approximately 100 to 150 microns behind the crack tip.

At the time indents were placed upon the face of the specimen, optical measurements were made of the crack length. Crack growth was monitored with the use of the electric potential method. The optical measurements of crack length allowed for the recalibration of the electric potential method during the test, if required.

After the data for each test had been collected, the crack length data were corrected using the linear interpolation technique discussed in Section III. The crack growth histories for each test are presented in the graphs in Appendix C. Since each specimen was precracked in a slightly different manner (due to slight differences in specimen thickness and notch length), cycle numbers have been adjusted so the first load cycle immediately after precracking is considered to be cycle number one.

For fatigue tests that involved overloads, the location of the overloads are depicted on the graphs. Unless otherwise noted on the graph, the overloads are 80% above the baseline value of stress intensity at the time of overload. (NOTA BENE: Because Test #2 involved complete retardation of crack growth for over 4 million cycles, the graph depicting the crack growth history for this test was divided into two different portions. The first and second portions of this test are presented in Figures C-2a and C-2b, respectively.)

After the correction of the crack lengths was made, a seven-point incremental polynomial regression was performed as per ASTM guidelines (34:919-920). This regression provided values for crack length, crack growth rate, maximum stress intensity, stress intensity range, closure load, closure stress intensity, and effective stress intensity range at points throughout the fatigue test. This data could then be analyzed to reveal characteristics of material behavior.

For fatigue tests that involve overloads, the data were split into separate data files; one contained pre-overload data and one contained post-overload data. The data files produced from the incremental polynomial regression of the separate files were recombined and used to calculate delay cycles and delay distance.

Insight into the amount of crack growth retardation after an overload can be gained by plotting crack growth rate as a function of crack length. For the tests in this study that involved overloads (Tests #6 through #9), the crack growth rates are plotted as a function of distance beyond the overload in Appendix D.

(NOTA BENE: Test #6 involved two overloads applied to the same specimen; the results of the two overloads are depicted separately in Figures D-1a and D-1b.)

Background of All Tests

The fatigue tests conducted for this study involved cyclic loading at constant stress intensity ranges. All tests were conducted at a stress ratio of 0.1. Table 4-1 describes the tests conducted for this study; the applied stress intensity range and the crack lengths at which overloads were applied (if any) are listed.

To collect baseline data for the material over a range of stress intensity ranges, a constant maximum amplitude load test (Test #1) was performed.

Table 4-1. Description of All Tests *

Test Number	Stress Intensity Range ($MPa\sqrt{m}$)	Crack Lengths at which Overloads were Applied (mm)
1	**	***
2	5.5	13.30 mm (50%) 14.71 mm (100%) 18.77 mm (80%)
3	5.5	N/A
4	7.7	N/A
5	9.9	N/A
6	5.5	14.78 mm, 20.37 mm
7	7.7	15.03 mm
8	9.9	14.91 mm
9	9.9	22.60 mm

* All overloads, unless otherwise noted, are 80% level above the instantaneous maximum load value.

** Test #1 was a constant maximum amplitude load test.

*** No overloads were applied during Test #1.

To determine the effect of magnitudes of overloads, a constant stress intensity range test punctuated by several single overloads (Test #2) was conducted. This test was conducted with an applied constant stress intensity range of 5.5 $MPa\sqrt{m}$, where overloads of 50%, 80%, and 100% were applied.

Baseline constant stress intensity range tests which involved no overloads (Tests #3, #4, and #5) were conducted for each stress intensity range studied. To maintain a constant stress intensity range, the maximum load value for each load cycle must decrease as the crack grows. By using a computer to control fatigue cycle loading, the stress intensity range was kept at the specified level until the decrease in applied load resulted in the loss of load control by the testing machine.

Because the maximum load for each fatigue cycle changed throughout the tests, the amount of closure in the specimen was expected to change as well. The baseline tests were performed in order to provide closure values against which to compare the closure values obtained from non-baseline tests.

After the baseline tests were conducted, the tests in which overloads were applied to the specimens were performed. The same stress intensity ranges were used, but the fatigue loading was punctuated by a single 80% overload. Overloads were applied at two different crack lengths, to investigate the possible effect that crack length might have upon the amount of post-overload crack growth retardation. Overloads were applied at approximate crack lengths of 15 mm and 21 mm. Separate compact tension specimens were used in the 9.9 $MPa\sqrt{m}$ overload tests to ensure that the effects of the overload at the shorter crack length did not influence the behavior of the crack growth after the overload at the longer crack length.

Baseline Tests

The following baseline tests were conducted in this study:

Test #1. Constant Maximum Amplitude Load Test

Test #3. Constant Stress Intensity Range of 5.5 $MPa\sqrt{m}$

Test #4. Constant Stress Intensity Range of 7.7 $MPa\sqrt{m}$

Test #5. Constant Stress Intensity Range of 9.9 $MPa\sqrt{m}$

Results of Test #1 Compared with a Previous Study

A fatigue test with a constant maximum amplitude load of 0.125 kips and a stress ratio of 0.1 was performed. The constant maximum amplitude load test provided crack growth data over a broad range of stress intensity range values.

After precracking of the specimen had ended, the maximum amplitude of the load cycle (0.125 kips) was selected to provide crack growth rates near threshold at the beginning of the test. As the crack grew, the maintenance of a constant maximum load level for each cycle resulted in an increase in stress intensity range. With this type of test the full range of crack growth rates, from near threshold to material failure, were attainable.

Figure 4-1 shows the comparison between the crack growth data obtained from this constant maximum amplitude load test and results obtained from a similar experiment conducted at the Wright Research and Development Center, Air Force Materials Laboratory, (WRDC/MLLN), Wright-Patterson Air Force Base, Ohio.

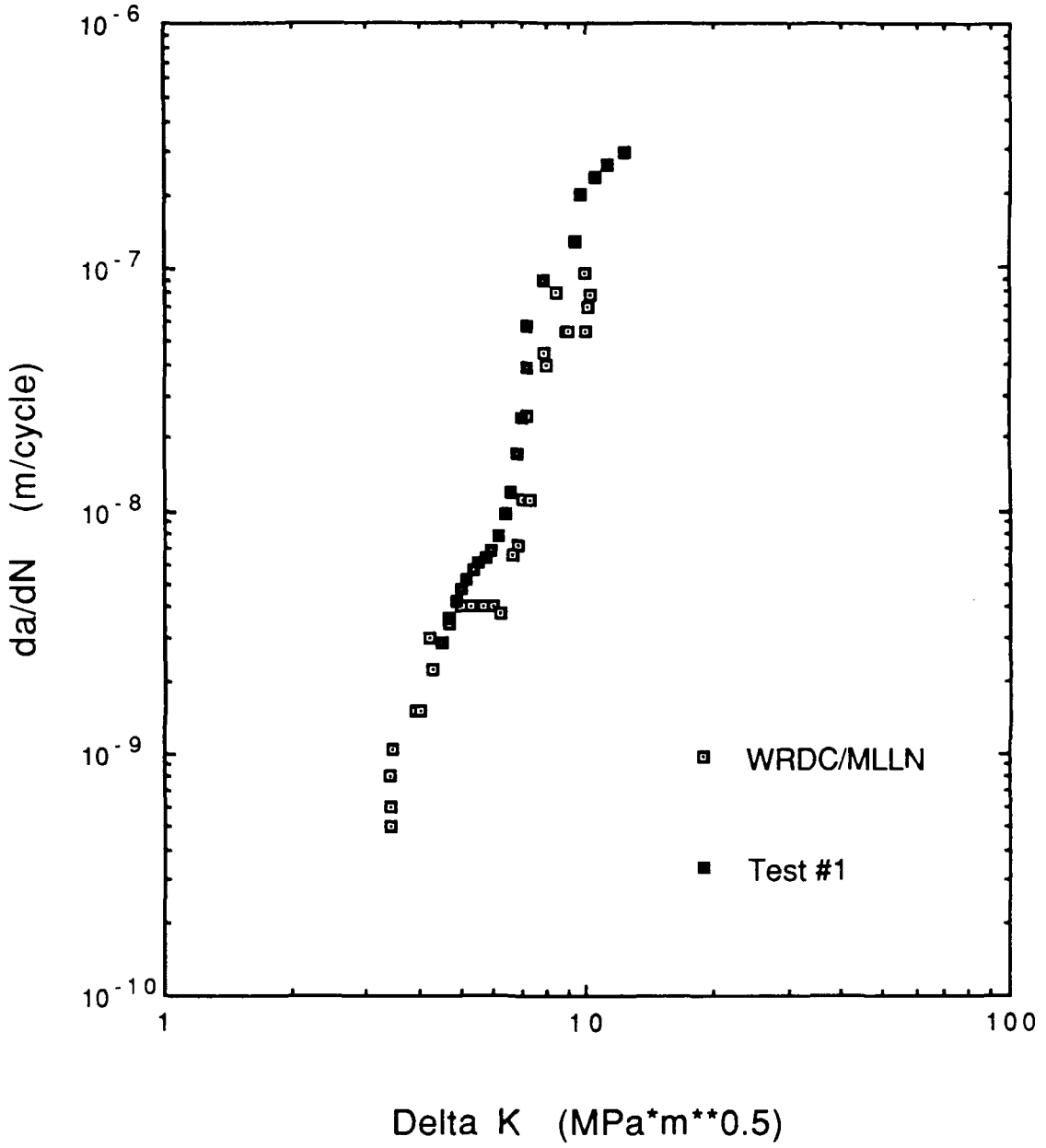

Figure 4-1. Comparison of Crack Growth Data from Test #1 with WRDC/MLLN Data

From the comparison shown in Figure 4-1, it is concluded that:

1. The applied stress intensity range vs. crack growth rate data obtained from this test are in very good agreement with the data obtained by another study throughout the span of stress intensity ranges encountered.

Discussion of Closure Measurement Techniques

Two different techniques were used to obtain load-displacement relations for the specimens. A non-conducting clip gage was used to obtain far-field measurements at the specimen mouth, and the laser IDG was used to obtain measurements at locations much nearer the crack tip. Analysis of the load-displacement relations provided a closure load; from this closure load the closure stress intensity (K_{cl}) could be computed. This value for closure stress intensity was subtracted from the maximum stress intensity (K_{max}) for the cycle, yielding a value for effective stress intensity range (ΔK_{eff}).

a. Laser IDG

As previously discussed in Section III, the closure load measured by the laser IDG was dependent upon the distance of the microhardness indents from the crack tip. The laser IDG data was analyzed on an individual segment-by-segment basis

by plotting the ratio of closure load to maximum load (P_{cl}/P_{max}) against the distance from the crack tip to the most recently placed set of indents. A second order polynomial was fit to the data so that a value of P_{cl}/P_{max} could be determined for a point 0.2 mm behind the crack tip for that particular segment of crack growth.

For all segments of crack growth (with the exception of the first segment of crack growth from each specimen) the P_{cl}/P_{max} data showed a definite trend, and a second order regression fit the data relatively well. For the first segment of crack growth following precracking, however, the P_{cl}/P_{max} data did not show a definite trend, and there was a lot of scatter in the data. Figures 4-2 and 4-3 show these dramatic differences between the P_{cl}/P_{max} trends shown in the first and second segments, respectively, of crack growth for the constant maximum amplitude load test. (The plots of P_{cl}/P_{max} vs distance beyond the indents for all segments of crack growth in all specimens are included in Appendix E.)

As demonstrated by Figures 4-2 and 4-3, the scatter in P_{cl}/P_{max} data had disappeared by the time the second set of indents were placed, and regressions on subsequent segments of crack growth could be performed without difficulty. This lack of identifiable trend for P_{cl}/P_{max} in the first segment of crack growth was observed in all specimens, and was attributed to the sudden change in loading history experienced when precracking had ended and the fatigue test had begun

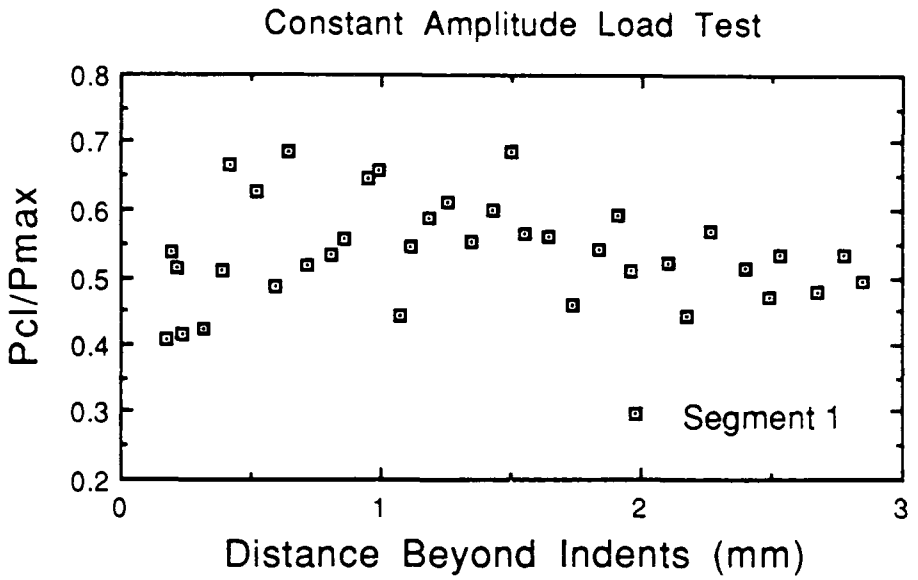

Figure 4-2. P_{cl}/P_{max} (as measured by Laser IDG) vs Distance Beyond Indents for Crack Growth over Segment #1, Constant Maximum Amplitude Load Test

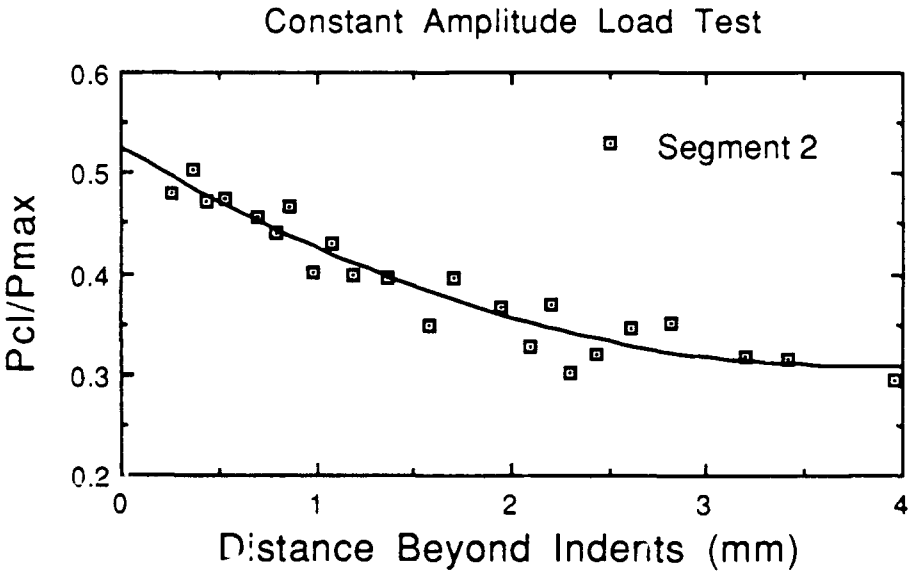

$y = 0.52526 - 0.11522x + 1.5219e\text{-}2x^2 \quad R^2 = 0.906$

Figure 4-3. P_{cl}/P_{max} (as Measured by Laser IDG) vs Distance Beyond Indents for Crack Growth over Segment #2, Constant Maximum Amplitude Load Test

Because the first segment of crack growth produced no definite trend in the IDG closure data, no value of P_{cl}/P_{max} could be obtained for the value of crack length associated with a distance of 0.2 mm behind the crack tip for this segment. Therefore, a confident calculation of closure load could not be made for the first segment of crack growth after precracking from any specimen.

Using the regressions from the remaining segments of crack growth, a value of P_{cl}/P_{max} could be determined at a point 0.2 mm behind the crack tip for each segment. These values of P_{cl}/P_{max} could be associated with specific values of crack length; a linear interpolation between these values would provide a continuous profile of P_{cl}/P_{max} as a function of crack length. The profiles for the baseline tests conducted in this study are shown in Figure 4-4.

Because the crack length and maximum load (P_{max}) for each data acquisition cycle are known, the closure load for any data sample can be calculated by multiplying the value of P_{cl}/P_{max} (obtained by a linear interpolation from the data presented in Figure 4-4) by P_{max}. Since the values for P_{cl}/P_{max} in Figure 4-4 are normalized to a point 0.2 mm behind the crack tip, the value for closure load obtained from this curve can be thought of as the value of closure that would be measured by the laser IDG if the indents were travelling along behind the crack tip at a fixed distance of 0.2 mm. Figure 4-5 shows the value for closure load as a

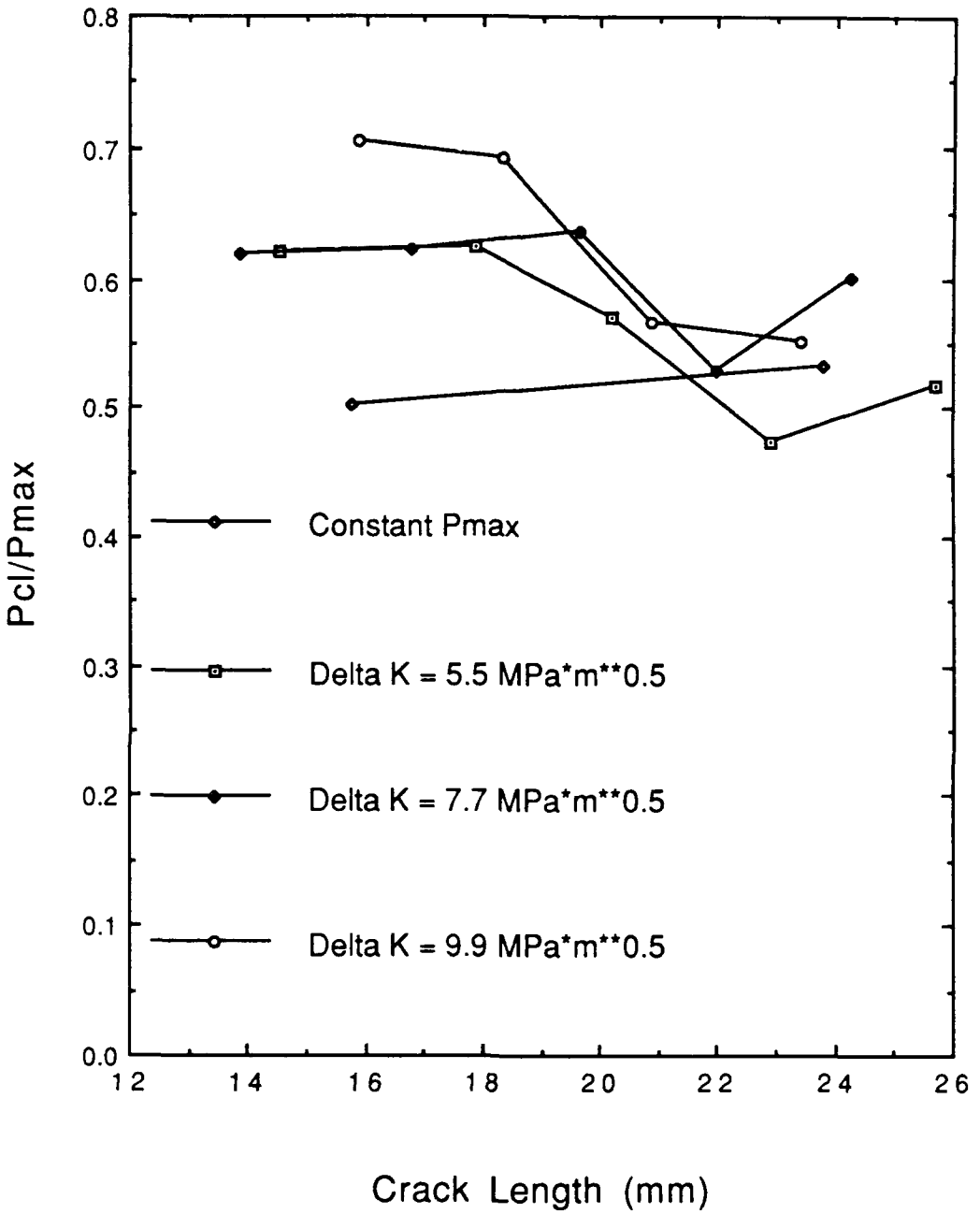

Figure 4-4. Pcl/Pmax Profiles for Baseline Tests

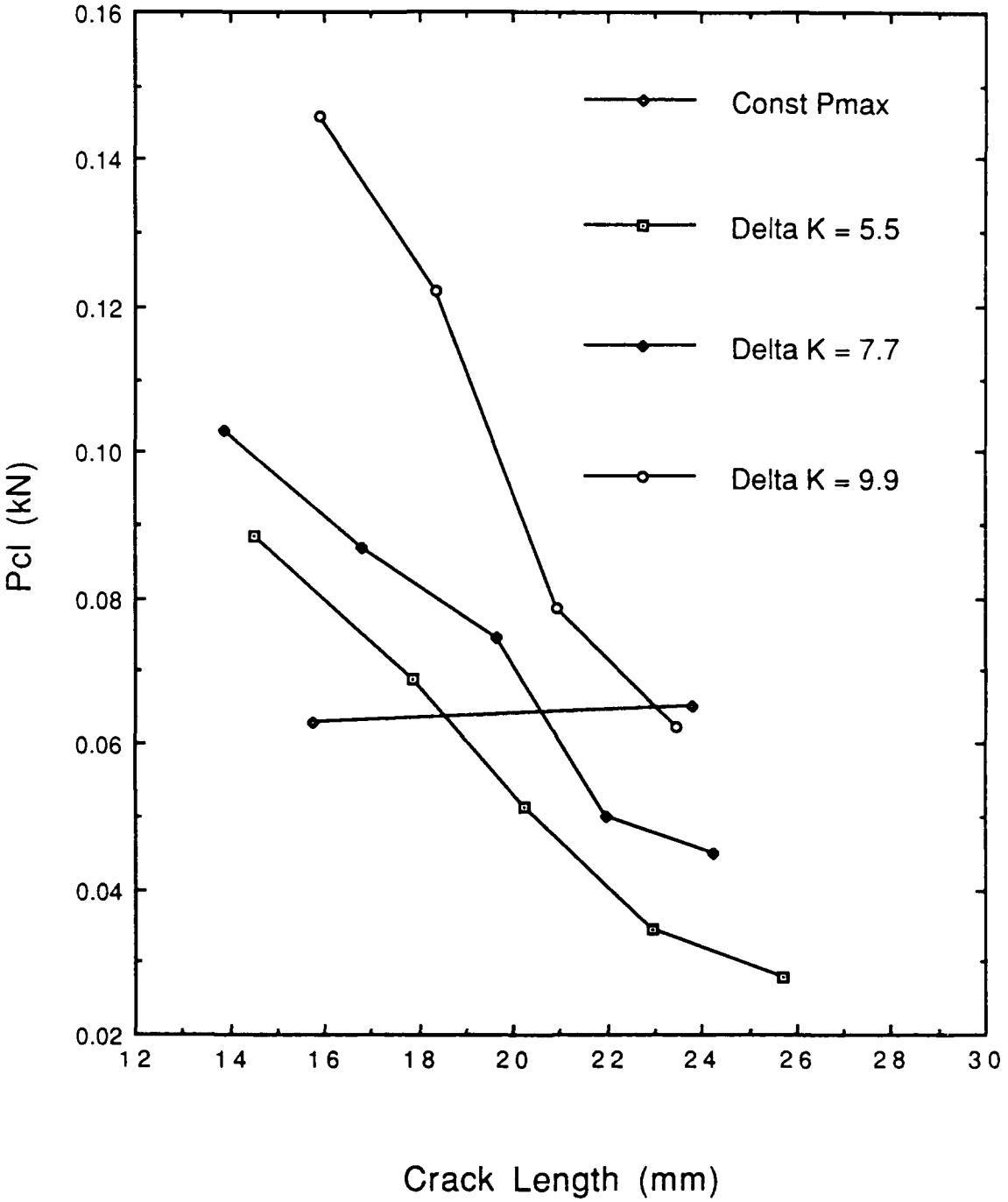

Figure 4-5. Profiles of Closure Load for Baseline Tests

function of crack length for the baseline tests conducted for this study.

The closure values for the constant stress intensity tests are seen to be separate, as shown in Figure 4-5. It is noted that the values for closure load for the higher stress intensity tests fall above those measured for the lower stress intensity ranges.

The closure values for the constant maximum amplitude load test cross the curves for the constant stress intensity range tests. This is expected, because the constant maximum amplitude for each load cycle causes an increase in stress intensity range as the crack grows. The value for closure load obtained at 15.771 mm occurred when the instantaneous stress intensity range was 5.4 $MPa\sqrt{m}$, and the value for closure load obtained at 23.784 mm occurred when the instantaneous stress intensity range was 9.4 $MPa\sqrt{m}$. These values are seen to fall near the appropriate bands of closure values obtained from the corresponding constant stress intensity range tests.

From the data obtained from the laser IDG during the baseline tests (which involved no overloads) we can conclude the following:

1. A region of transition in the behavior of closure was observed after a change in load history. This was evident from the lack of an

identifiable trend in P_{cl}/P_{max} data in the first segment of crack growth after precracking.

2. For segments of crack growth with identifiable trends in P_{cl}/P_{max} data, a regression analysis can be used to find a value for P_{cl}/P_{max} at a distance of 0.2 mm behind the crack tip. This value, along with the location of the microhardness indents for that segment of crack growth, can be used to produce a profile of P_{cl}/P_{max} vs crack length for that particular compact tension specimen and/or type of fatigue test.
3. For aluminum-lithium 2091 in the compact tension specimen geometry, closure load is a function of crack length and of stress intensity range in the following manner:
   a. For any given stress intensity range, the value for closure load decreases with an increase in crack length.
   b. For any given crack length, the value for closure load increases with an increase in stress intensity range.

b. Clip Gage

1. Data Obtained During Test #1, Constant Maximum Amplitude Load Test

Load-displacement relations at the mouth of the specimen were obtained using a clip gage. These measurements, which were taken at a location 20 to 40 mm away from the crack tip, were considered to be far-field measurements when compared to the laser IDG measurements, which were taken within 2 to 3 mm of the tip of the crack.

Since the laser IDG displayed a transitional region in the behavior of closure data during the first segment of crack growth after precracking, the clip gage data for the same segment of crack growth was analyzed to see if any recognizable trend was evident. Figure 4-6 shows P_{cl}/P_{max} as measured by the clip gage plotted against crack length for the first segment of crack growth following precracking in the constant maximum amplitude load test. As observed in the data obtained from the laser IDG for the same segment of crack growth (compare to Figure 4-2), the P_{cl}/P_{max} data showed a lot of scatter; a regression through this data would not provide a definite trend. For this reason, data obtained from the clip gage during the first segment of crack growth data was discarded before further analysis was performed.

Data from the remaining segments of crack growth for the constant maximum amplitude load test are shown in Figure 4-7. The P_{cl}/P_{max} data show a definite trend. No segmentation in the clip gage data (such as that found in the data obtained

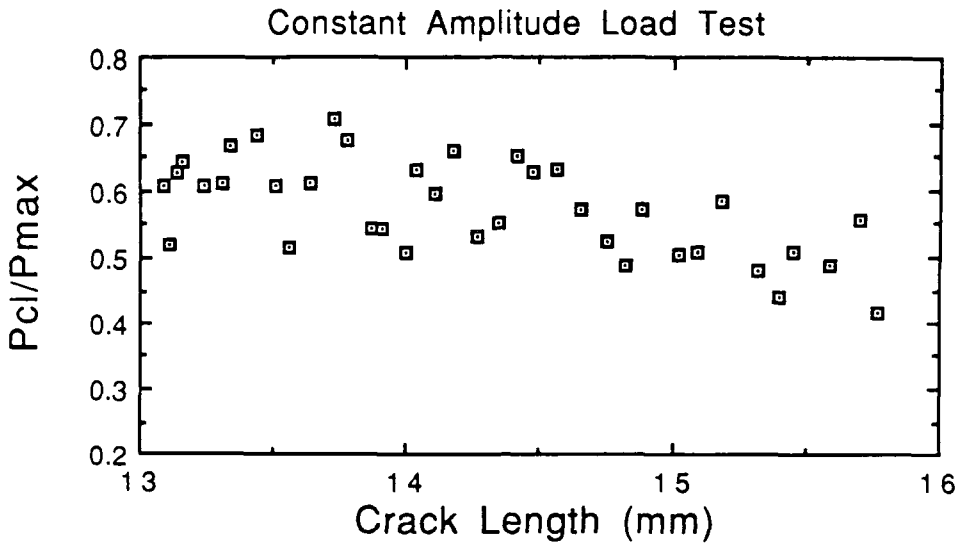

Figure 4-6. P_{cl}/P_{max} (as Measured by Clip Gage) vs Crack Length for Crack Growth Segment #1 of Constant Maximum Amplitude Load Test

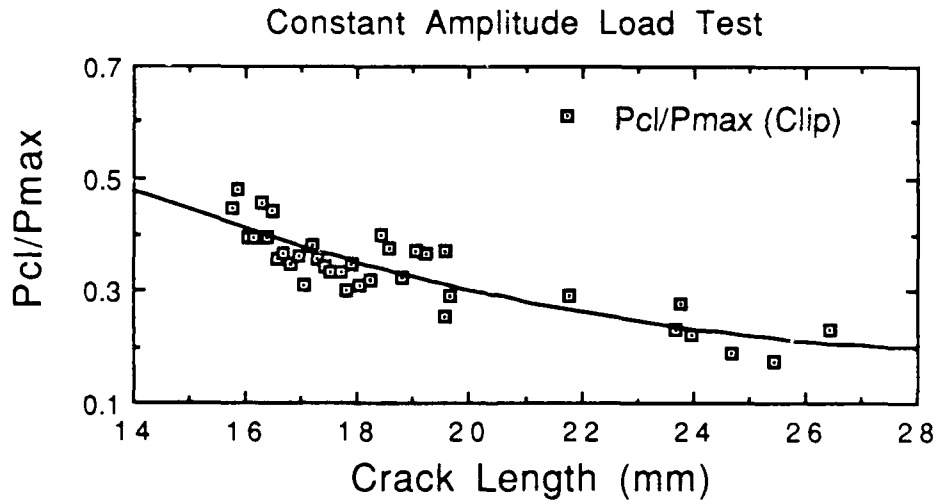

y = 1.2087 - 6.8432e-2x + 1.1531e-3x^2 R^2 = 0.737

Figure 4-7. P_{cl}/P_{max} (as Measured by Clip Gage) vs Crack Length for Crack Growth Segments #2 - #4 of Constant Maximum Amplitude Load Test

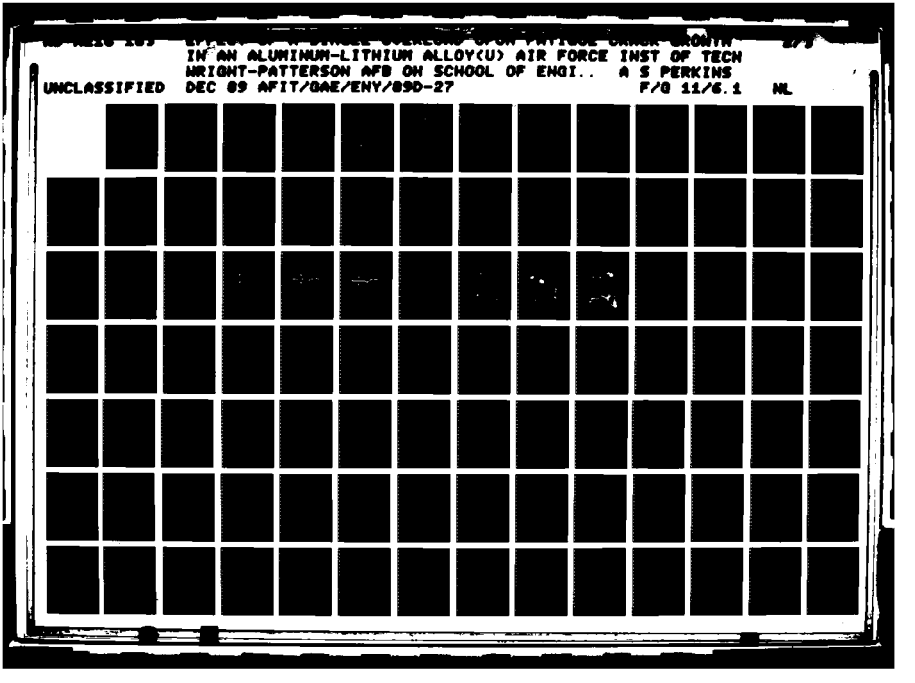
IN AN ALUMINUM-LITHIUM ALLOY(U) AIR FORCE INST OF TECH
WRIGHT-PATTERSON AFB OH SCHOOL OF ENGI.. A S PERKINS
UNCLASSIFIED DEC 89 AFIT/GAE/ENY/89D-27 F/G 11/6.1 NL

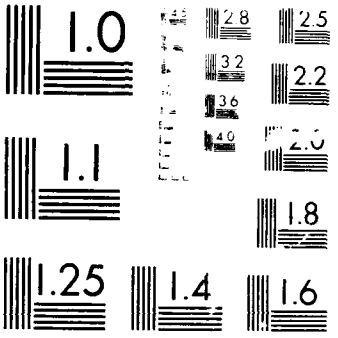
1.0
1.1
1.25
1.4
1.6
1.8
2.0
2.2
2.5
2.8
3.2
3.6
4.0

by the laser IDG) exists, and this was not expected because the clip gage measurements were taken at a location which did not change from one segment of crack growth to the next.

In the crack growth segments where laser IDG data showed distinct trends, scatter in the P_{cl}/P_{max} data recorded by the clip gage is evident. A second order polynomial was fitted to the raw data obtained from the clip gage to provide a distinct trend for P_{cl}/P_{max} as a function of crack length. This trend is considered to be valid for crack lengths over which the regression was performed (15.771 mm to 26.444 mm).

The regression curve determined from Figure 4-7 was used to calculate closure loads, which then replaced the original closure loads as measured by the clip gage. The incremental polynomial regression was then performed upon both the raw data and the data calculated from the regression trend to provide crack growth rate and effective stress intensity range data for the crack growth segments where the P_{cl}/P_{max} data showed a distinct trend. These data are presented in Figure 4-8.

The effective stress intensity range data generated from the regression trend show a smoother trend at the shorter crack lengths. The presence of a transitional region of closure in the first segment of crack growth should not invalidate the data regarding the applied stress intensity range; data from that segment of crack growth is included in Figure 4-8.

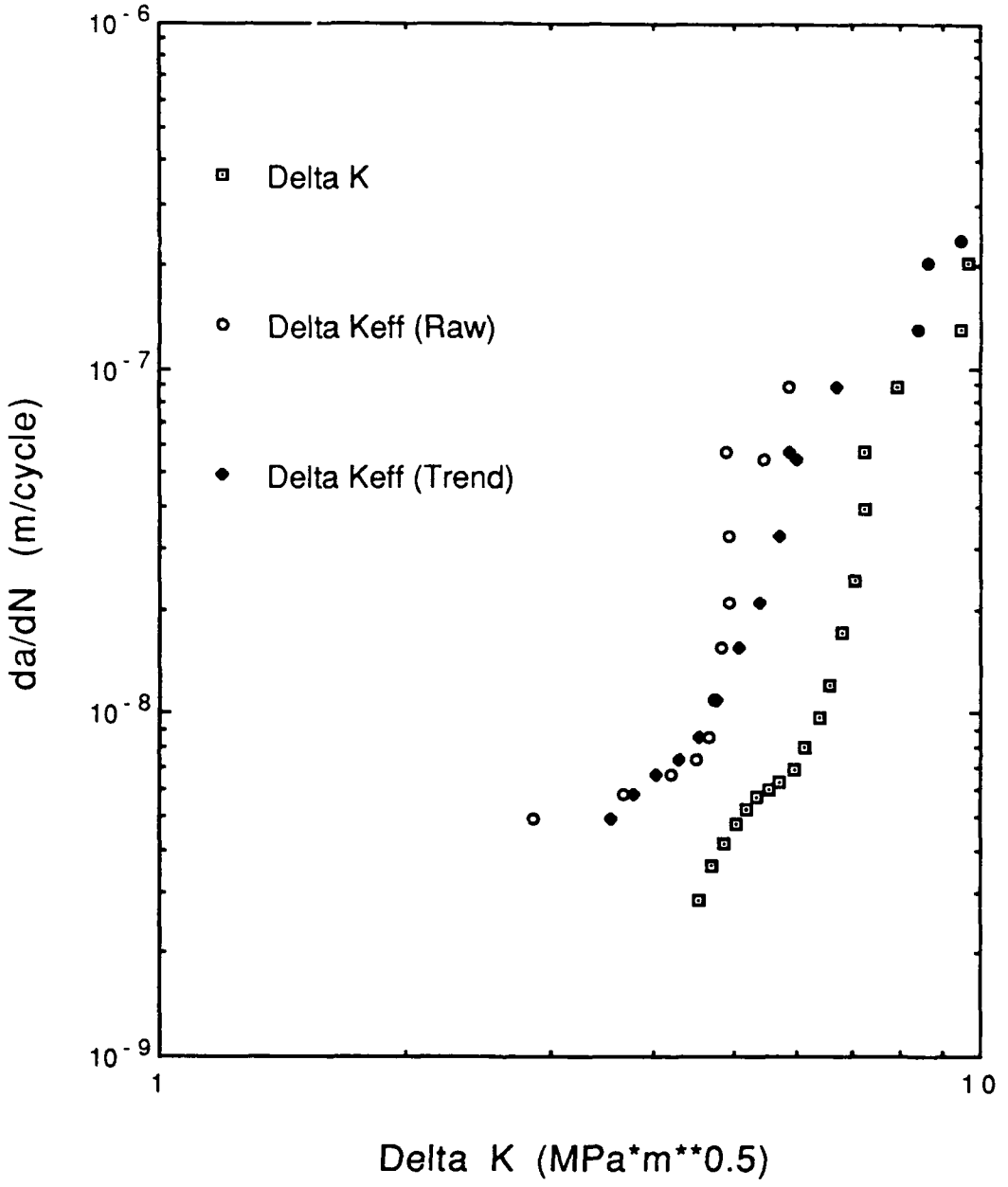

Figure 4-8. Crack Growth Data from Constant Amplitude Load Test, (Delta Keff from Clip Gage)

From the clip gage data obtained during the constant maximum amplitude load test, we can conclude the following:

1. The region of transition in the behavior of closure observed with the laser IDG after the change in load history was also present in the measurements obtained by the clip gage.
2. Even after the transitional region of closure has been traversed, the P_{cl}/P_{max} data obtained by the clip gage displays a degree of scatter. This scatter can be attributed to the far-field nature of the clip gage measurement, which results in a more gradual slope of the load-displacement curve and makes identification of the closure load more difficult.

2. Data Obtained During Tests #3, #4, and #5: Constant Stress Intensity Tests

When the clip gage data for the constant stress intensity tests were analyzed, it was found that the P_{cl}/P_{max} data for these tests showed even more scatter than that displayed by the P_{cl}/P_{max} data obtained from the constant maximum amplitude load test.

Figures 4-9, 4-10, and 4-11 show P_{cl}/P_{max} plotted against crack length for the constant stress intensity range tests (Test #3, #4, and #5, respectively).

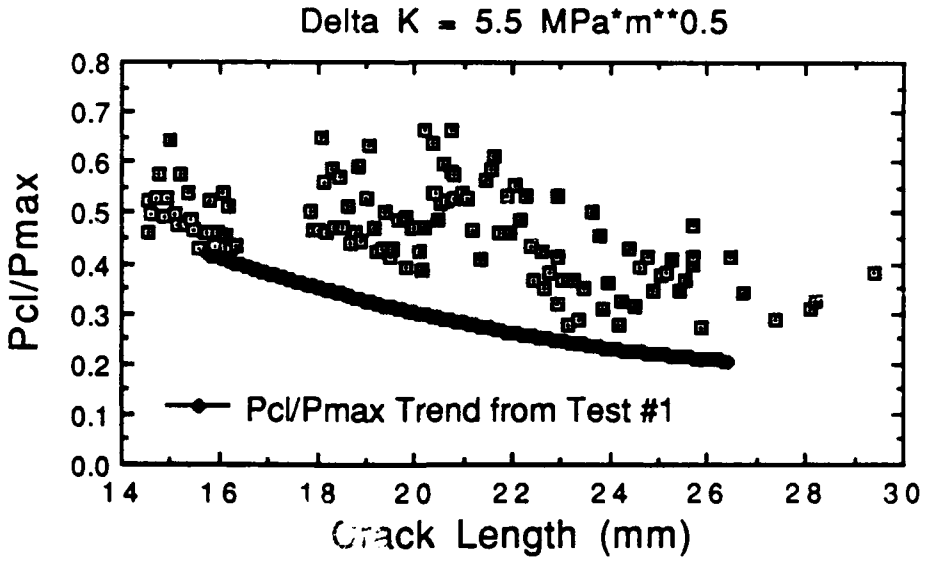

Figure 4-9. P_{cl}/P_{max} (as Measured by Clip Gage) vs Crack Length for Crack Growth Segments #2 - #6 of Test #3 (Constant Stress Intensity Range = 5.5 MPa$\sqrt{m}$)

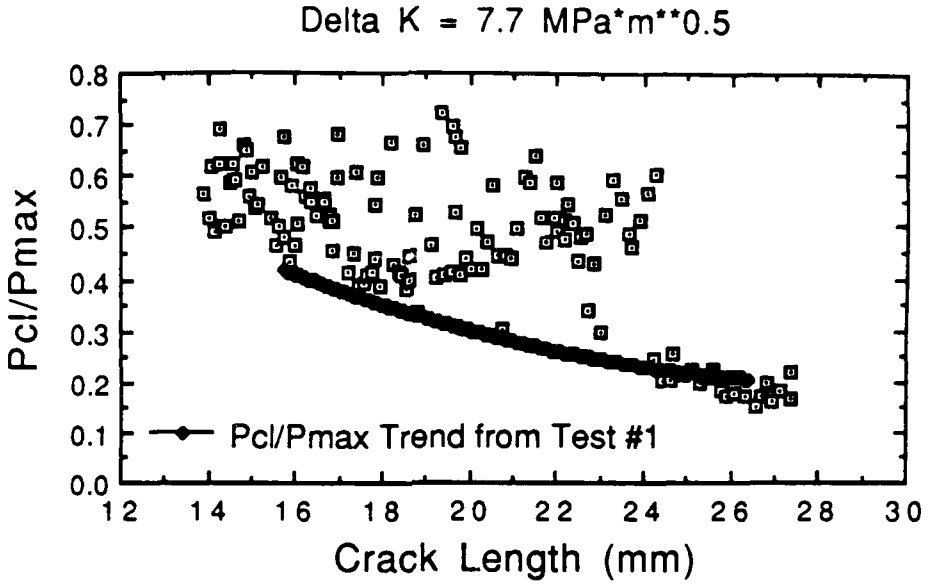

Figure 4-10. P_{cl}/P_{max} (as Measured by Clip Gage) vs Crack Length for Crack Growth Segments #2 - #6 of Test #4 (Constant Stress Intensity Range = 7.7 MPa$\sqrt{m}$)

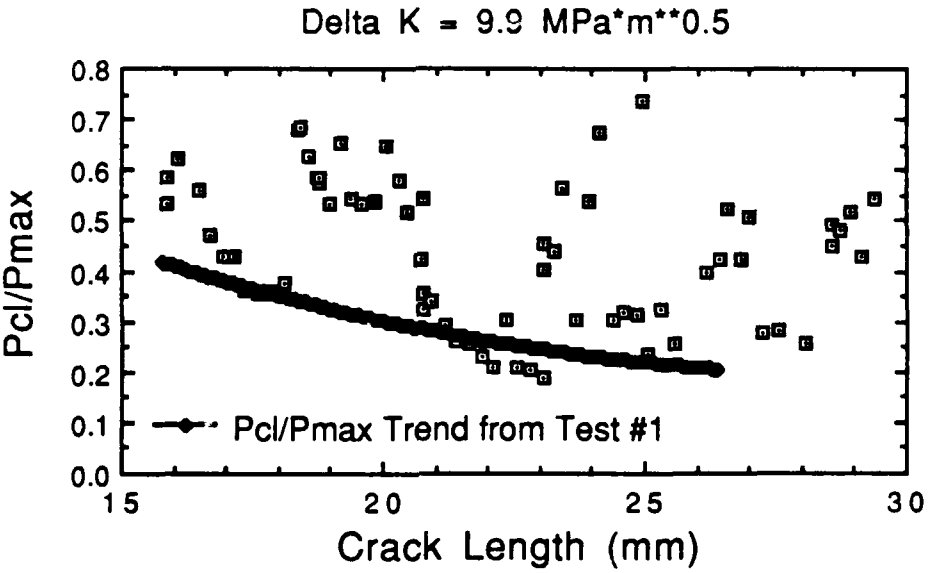

Figure 4-11. P_{cl}/P_{max} (as Measured by Clip Gage) vs Crack Length for Crack Growth Segments #2 - #6 of Test #5 (Constant Stress Intensity Range = 9.9 MPa$\sqrt{m}$)

From these figures we can see that the large amount of scatter in the P_{cl}/P_{max} data makes the data difficult to analyze. A slight downward trend can be discerned as crack length increases, but a regression fit to this data would not give a confident value of P_{cl}/P_{max} as a function of crack length. For this reason, a direct comparison between data obtained from the clip gage and the IDG was only possible for the constant maximum amplitude load test.

From the clip gage data obtained during the constant stress intensity range tests, we can conclude the following:

1. The P_{cl}/P_{max} data as measured by the clip gage for these tests display large amounts of scatter. The amount of scatter in the data is increased in the tests with higher stress intensity ranges.
2. The second order regression equation that was fit to the P_{cl}/P_{max} data from the constant maximum amplitude load test provides a trend which appears to be a lower bound of the P_{cl}/P_{max} data obtained from the constant stress intensity range tests.

c. Direct Comparison Between Clip Gage and IDG Measurements

Load-displacement plots were obtained from both the clip gage and the laser IDG during each data acquisition cycle.

Any data cycle in which either load-displacement plot was irregular was discarded. Two separate data files were constructed; one data file contained the closure loads as determined by the laser IDG and the other contained the closure loads as determined by the clip gage. The data records in these files were obtained at identical crack lengths. (Data from the first segment of crack growth was discarded, because P_{cl}/P_{max} data from both the clip gage and the IDG displayed a lot of scatter and showed no distinct trend.)

When incremental polynomial regressions are performed upon these data files, the only differences between the resulting data will be in the closure loads measured and in the effective stress intensity ranges. Figure 4-12 shows the comparison between the effective stress intensity ranges determined from the two different measurement techniques for the constant maximum amplitude load test; the applied stress intensity data for this test is shown as well.

As mentioned in the previous section, due to the large amount of scatter in the P_{cl}/P_{max} data obtained during the constant stress intensity range tests, a regression could not be fit to the data from these tests to provide a confident measurement of P_{cl}/P_{max} as a function of crack length. A direct comparison between the clip gage and the IDG is therefore possible only for the constant maximum amplitude load test.

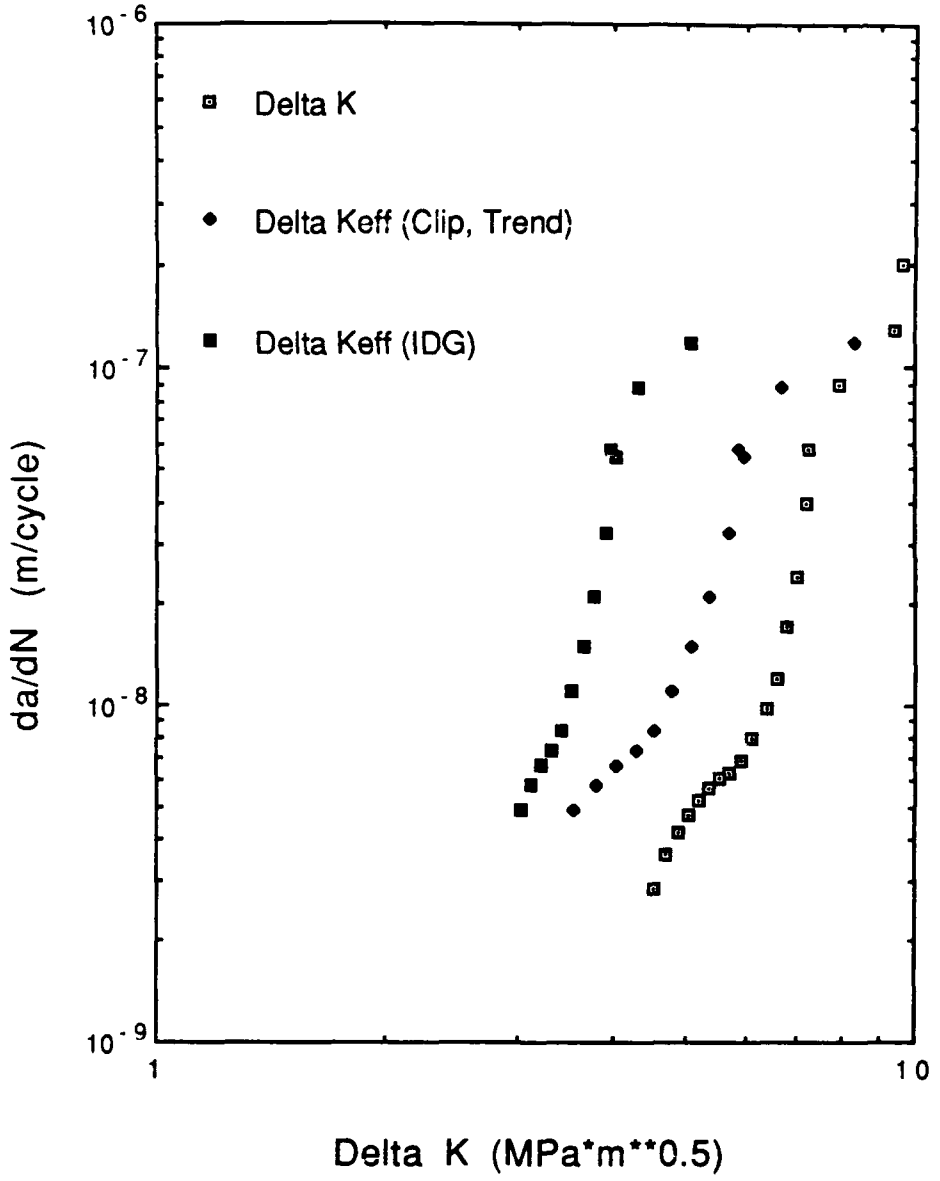

Figure 4-12. Comparison of Delta Keff from Clip Gage and IDG, Constant Maximum Amplitude Load Test

From the direct comparison of the two measurement techniques for the constant maximum amplitude load test, we can conclude that:

1. The laser IDG measures a higher closure load than the clip gage. This was found to be true for the range of crack lengths at which a value for P_{cl}/P_{max} could be confidently determined.
2. The higher closure load results in a lower value for effective stress intensity range.
3. The higher closure load measured by the laser IDG is due to the greater sensitivity, higher accuracy, and to the near-field nature of the IDG measurements.

Test #2. Constant Stress Intensity Range Test (With Overloads Applied)

A fatigue test was conducted with constant stress intensity range in order to produce a constant crack growth rate. To ascertain the effect of the various levels of overload upon the crack growth, several single overloads of different magnitude were applied to the specimen. This test was conducted at a constant stress intensity range of 5.5 $MPa\sqrt{m}$; overloads of 50%, 80%, and 100% were applied to the specimen.

After precracking was completed and before any overloads were applied to the specimen, the baseline constant stress intensity range of 5.5 $MPa\sqrt{m}$ was applied for one segment of crack growth (approximately 2.5 mm) to ensure that the crack growth rate prior to the overload was constant.

The 50% overload was applied at the crack length of 13.30 mm. This level of overload had hardly any effect upon the crack growth rate. The crack growth rate after the overload was only slightly retarded; it quickly recovered to pre-overload levels.

After further crack growth occurred at a constant crack growth rate, the 100% overload was applied at a crack length of 14.71 mm. This level of overload completely retarded the crack growth. The crack growth rate dropped to rates of about 10^{-9} meters per cycle. This was considered to be "noise", however; after the 100% overload, an additional 4 million load cycles were applied to the specimen with no further crack growth observed.

The 100% overload resulted in a large plastic zone in front of the crack tip. Another "precracking" was performed in order to extend the crack tip into a region of material unaffected by the overload. After this "precracking" was completed, the baseline stress intensity range of 5.5 $MPa\sqrt{m}$ was resumed. The test was monitored to ensure that a constant crack growth rate was observed and that the effect of the 100% overload had been removed.

The 80% overload was applied to the specimen at a crack length of 18.77 mm. It was expected that this level of overload would provide retardation larger than that observed after the 50% overload, but not completely retard the crack growth as did the 100% overload. The 80% overload significantly retarded the crack growth, but allowed the crack growth rate to recover to pre-overload levels after a significant but reasonable period of time.

Figure 4-13 shows the crack growth rate as a function of crack length for this test; the crack lengths at which overloads were applied are clearly marked.

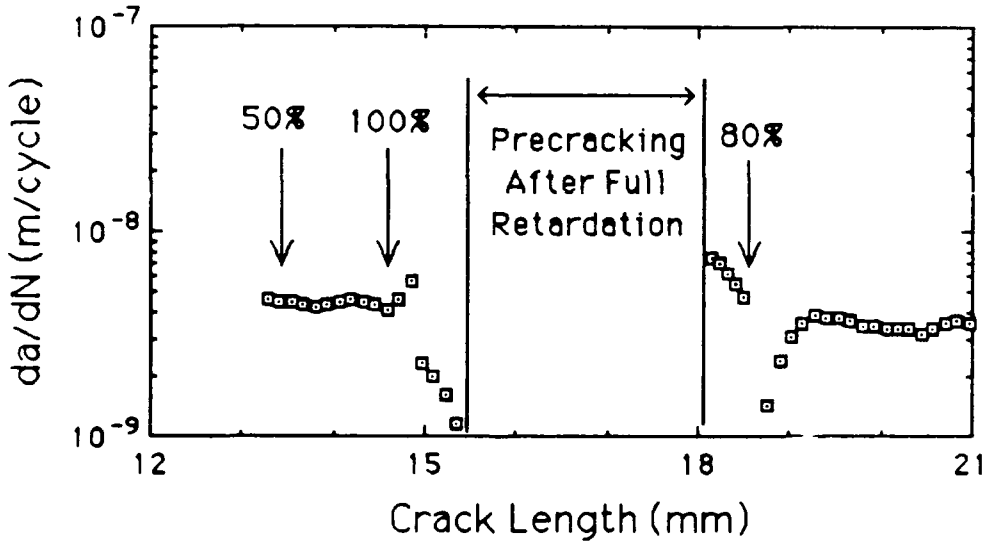

Figure 4-13. Crack Length vs Crack Growth Rate for Test #2 (Location and Level of Overloads are Shown)

The results of this constant stress intensity range test with single overloads can be summarized as follows:

1. The level of overload has a dramatic effect upon the post-overload crack growth. Low levels of overload may have no measurable effect upon crack growth rate, while higher levels of overload may result in complete retardation of crack growth.
2. For this material, specimen geometry and this constant stress intensity range of 5.5 MPa$\sqrt{m}$, the 50% level of overload had only a slight effect upon the post-overload crack growth rate. The 80% level of overload provides a significant (but not complete) retardation of crack growth. The 100% level of overload completely retarded the crack growth.

In light of these results, the 80% overload level was selected for use with subsequent tests that required overloads.

Constant Stress Intensity Range Tests, No Overloads Applied

Test #3. Constant Stress Intensity Range of 5.5 MPa$\sqrt{m}$

Test #4. Constant Stress Intensity Range of 7.7 MPa$\sqrt{m}$

Test #5. Constant Stress Intensity Range of 9 9 MPa$\sqrt{m}$

Figure 4-14 shows the crack growth rate data for Tests #3, #4, and #5 plotted against applied stress intensity range. These results are shown in relation to the baseline data obtained from the constant maximum amplitude load test (Test #1). These data, obtained from different tests, show a good agreement with the baseline data.

Figure 4-15 compares the effective stress intensity range (ΔK_{eff}) from these three constant stress intensity range tests with the ΔK_{eff} data obtained from the constant maximum amplitude load test. The effective stress intensity ranges shown in this figure were calculated from closure values obtained from the Pcl/Pmax profiles determined by adjusting the IDG closure measurements back to 0.2 mm behind the crack tip. (This technique was previously discussed in "Discussion of Closure Measurement Techniques, a. Laser IDG, page 4-9).

As previously seen in Figure 4-5, the closure load in the constant stress intensity range tests (Tests #3 through #5) was function of crack length. As a result of the high closure at the beginning of the fatigue tests, the effective stress intensity range is low at the shorter crack lengths. As the crack grows, the value for closure load drops and the

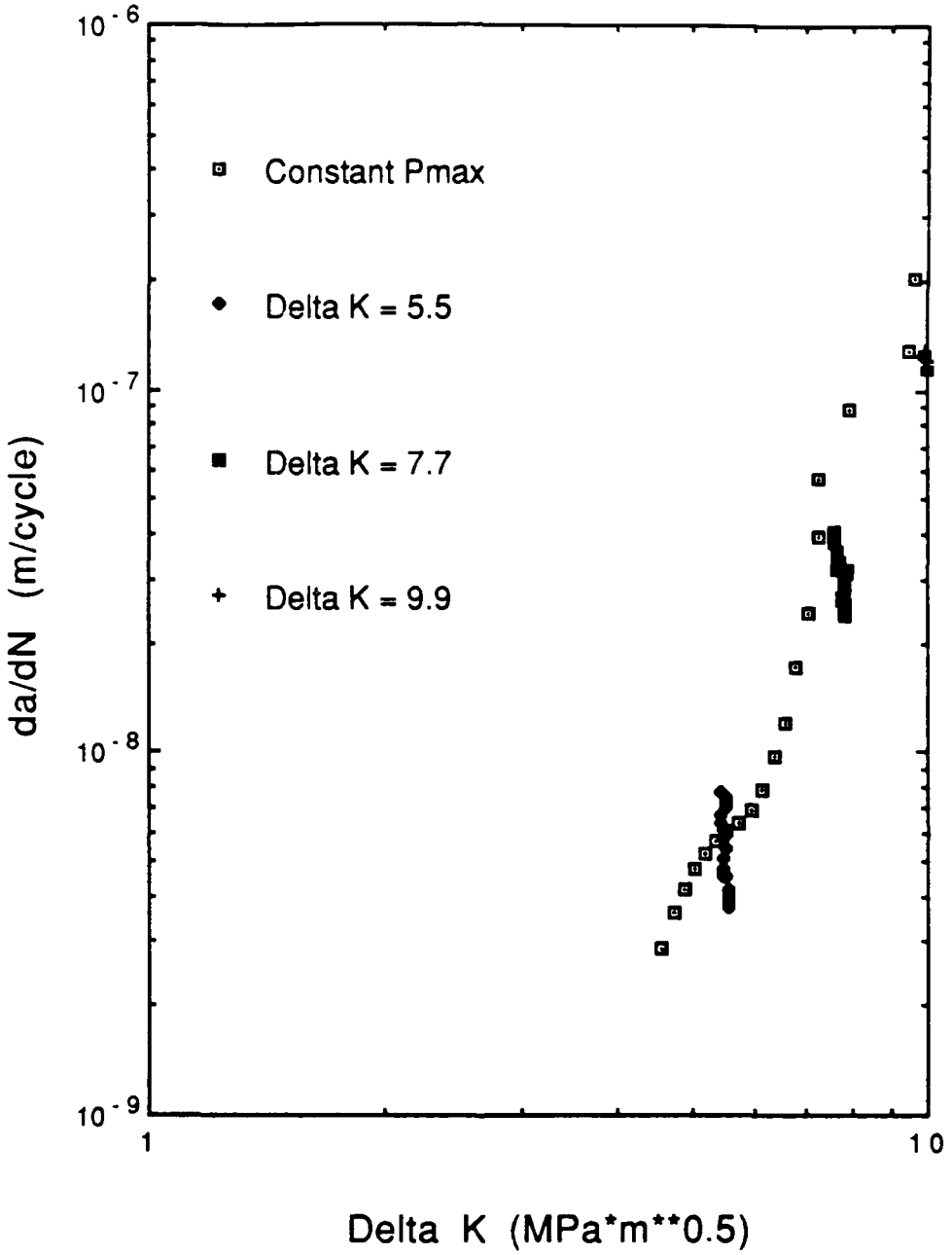

Figure 4-14. Comparison of Constant Stress Intensity Range Tests With Constant Maximum Amplitude Load Test Data

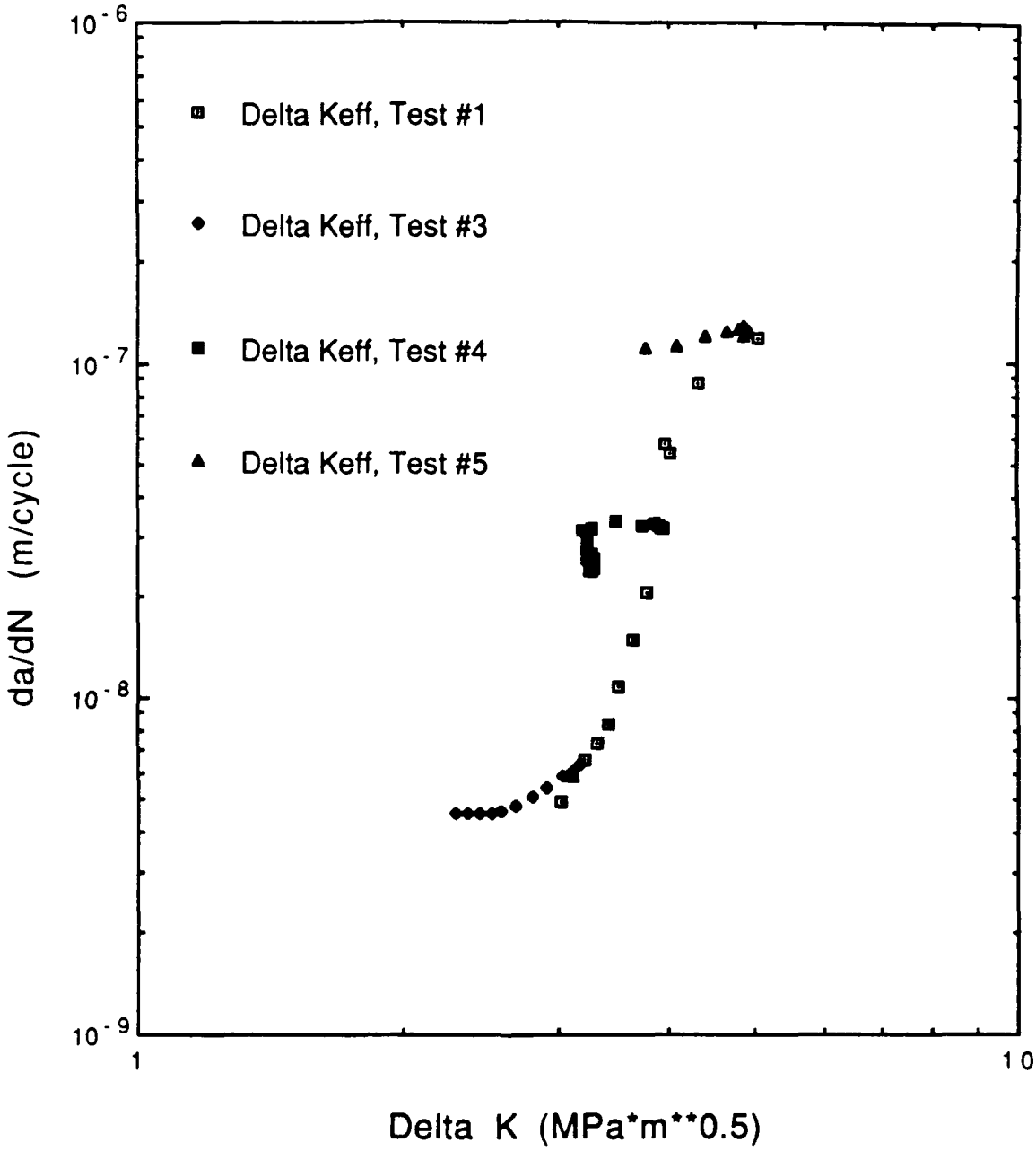

Figure 4-15. Comparison Between Delta Keff from Constant Stress Intensity Range Tests with Constant Pmax Test

values of effective stress intensity range approach the values of effective stress intensity range obtained for the baseline constant amplitude load case (Test #1). This is shown in Figure 4-15.

In general, the results of the constant stress intensity range tests (Tests #3 through #5) can be summarized as follows:

1. The closure load measured by the IDG, adjusted to a point 0.2 mm behind the crack tip, was a function of crack length when the applied stress intensity range was kept constant. This adjusted closure load decreased with an increase in crack length. Hence, the effective stress intensity range changed as the crack grew.
2. At the longer crack lengths, after the closure load had decreased from initially high levels, the effective stress intensity range vs crack growth rate data matched the data obtained from the baseline constant amplitude load test.

Constant Stress Intensity Range Tests, 80% Overloads Applied

Test #6. Constant Stress Intensity Range of 5.5 MPa$\sqrt{m}$

Test #7. Constant Stress Intensity Range of 7.7 MPa$\sqrt{m}$

Test #8. Constant Stress Intensity Range of 9.9 MPa$\sqrt{m}$

Test #9. Constant Stress Intensity Range of 9.9 MPa$\sqrt{m}$

Four different tests were conducted in which a single overload of 80% above the instantaneous baseline maximum load value was applied. In Test #6, two separate overloads were applied. In all, five separate instances of single overloads were applied to the compact tension specimens.

Delay Distances and Delay Cycles

Delay distances and delay cycles were obtained from the crack growth histories shown in Appendix C. (See Figure 4-16 for an example; the actual graphs used are included in Appendix G.) Two parallel lines were drawn through the data; one line was drawn through the data obtained prior to the overload, and the other was drawn through data obtained after the overload. These lines were extrapolated to the left; the difference in crack length between these two parallel lines is the delay distance.

The term "delay cycles" is defined as the number of cycles it took the crack growth rate to recover to normal pre-overload rates; this could be found by identifying the number of cycles that corresponded to the values where the parallel lines intersected the crack growth histories.

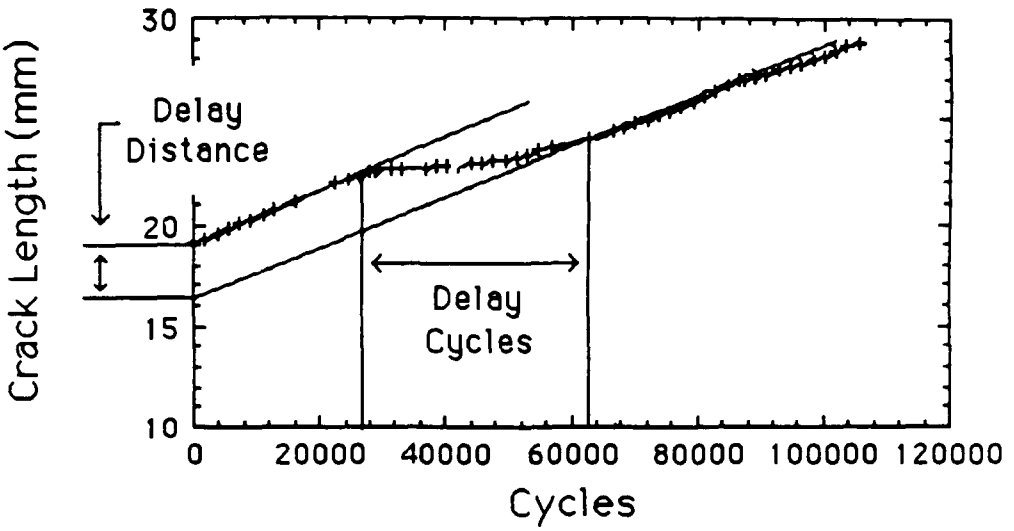

Figure 4-16. Determination of Delay Distance & Delay Cycles

Table 4-2 summarizes the results of the tests that involved overloads. Information from Table 4-2 is presented in Figures 4-17 and 4-18.

Table 4-2. Delay Distances & Delay Cycles for Tests #6 - #9

Test Number	Crack Length at which Overload is Applied (mm)	Delay Distance (mm)	Delay Cycles
6	14.47	0.5	70,000
6	20.22	0.6	75,000
7	14.51	2.2	130,000
8	13.88	2.3	56,000
9	21.96	2.5	38,000

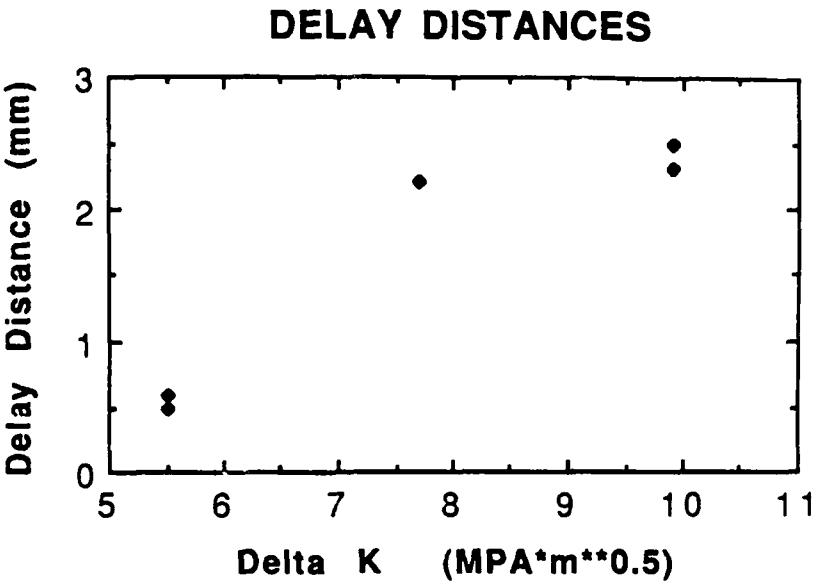

Figure 4-17. Delay Distances for Constant Stress Intensity Range Tests Involving Overloads (Tests #6 - #9)

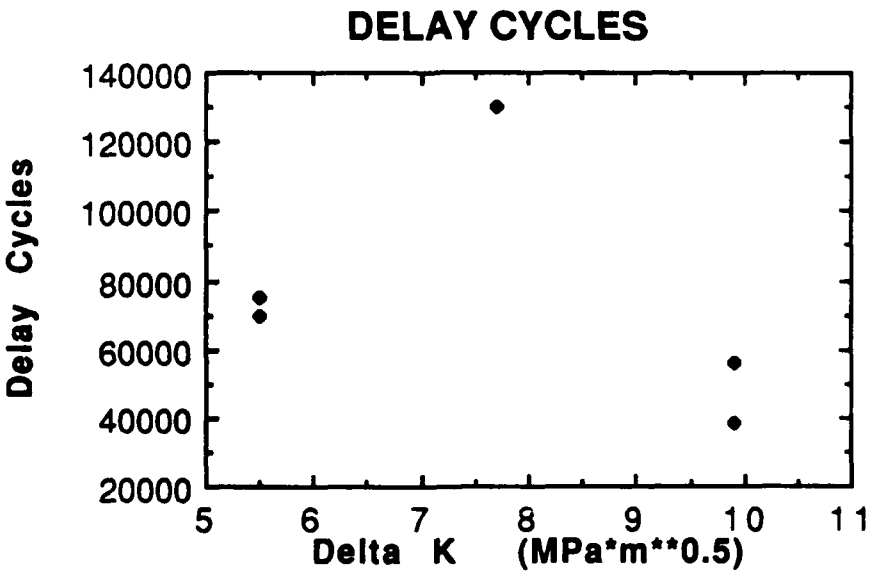

Figure 4-18. Delay Cycles for Constant Stress Intensity Range Tests Involving Overloads (Tests #6 - #9)

From Figures 4-17 and 4-18 we can conclude:

1. For a given level of overload, the delay distance depends upon the stress intensity range at which the overload is applied. For larger stress intensity ranges, the delay distance is larger.
2. Delay cycles are a function of stress intensity range at which the overload is applied.

Effective Stress Intensity Ranges (ΔK_{eff}) for Tests Involving Overloads

When the P_{cl}/P_{max} trends as measured by the IDG were analyzed for the segments of crack growth where overloads were applied, it was readily apparent that the overload had an effect upon closure. Before the overload was applied, the P_{cl}/P_{max} data showed the decreasing trend which is normal as the crack tip grows away from the indents. Data obtained after the application of the overload displays a large amount of scatter introduced into the data trend. (Figure 4-19 shows a typical plot of P_{cl}/P_{max} data for a crack growth segment that includes an 80% overload.) This scatter prevented an analytical treatment of the data to determine effective stress intensity ranges from the IDG closure data.

As discussed in Section III, the incremental polynomial regression used to determine smoothed values from raw data is very sensitive to the regression interval chosen. In the

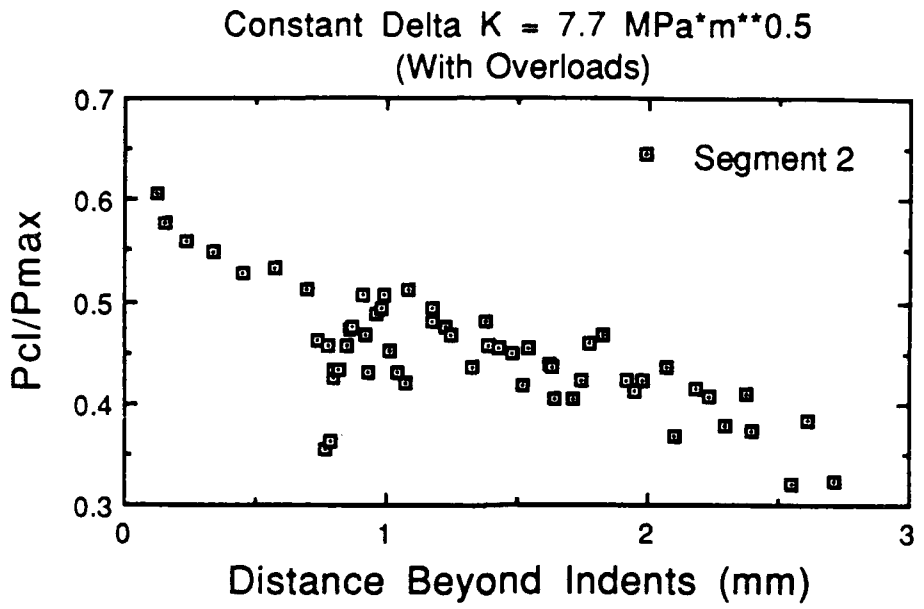

Figure 4-19. P_{cl}/P_{max} (as measured by laser IDG) vs Distance Beyond Indents for a Crack Growth Segment that Includes an Overload

tests which involved overloads, a small regression interval (0.005 in) was needed to provide the resolution necessary to display the crack growth retardation. Due to the large amount of scatter in the P_{cl}/P_{max} data after the overload, however, a regression interval of this size included only a few data points in each segment of regression interval, and did not provide smooth values for closure load from the regression. Therefore, only a comparison of the raw data for the IDG closure and the regression on the retardation was performed.

For the tests involving overloads, Figure 4-20 shows a typical comparison between the following as a function of crack length: crack growth rate (from incremental polynomial

regression), P_{cl}/P_{max} as measured by the laser IDG (raw data), and P_{cl}/P_{max} as measured by the clip gage (raw data). (The comparisons for all of the tests involving overloads are presented in the sets of graphs in Appendix F.)

The segment of crack growth which includes the overload region is shown, along with the P_{cl}/P_{max} data from both the clip gage and the laser IDG for the same segment of crack growth. For ease of comparison between the curves, the data are presented in a form such that the overload is shown at 0.0 mm for all three curves.

As seen in Figure 4-20, the application of the overload has a dramatic effect upon the crack growth rate. The simultaneous introduction of large amounts of scatter into the closure data as measured by both near-field (IDG) and far-field (clip gage) techniques of measurement is readily apparent.

Crack Surface Morphology

Examination of the crack behavior under the various conditions of crack growth provides an explanation for many of the experimental results observed in the course of this study. The polishing of the specimen surface for use with the laser IDG rendered the crack surface easily observable under a microscope; typical magnifications ranged from 100X to 400X.

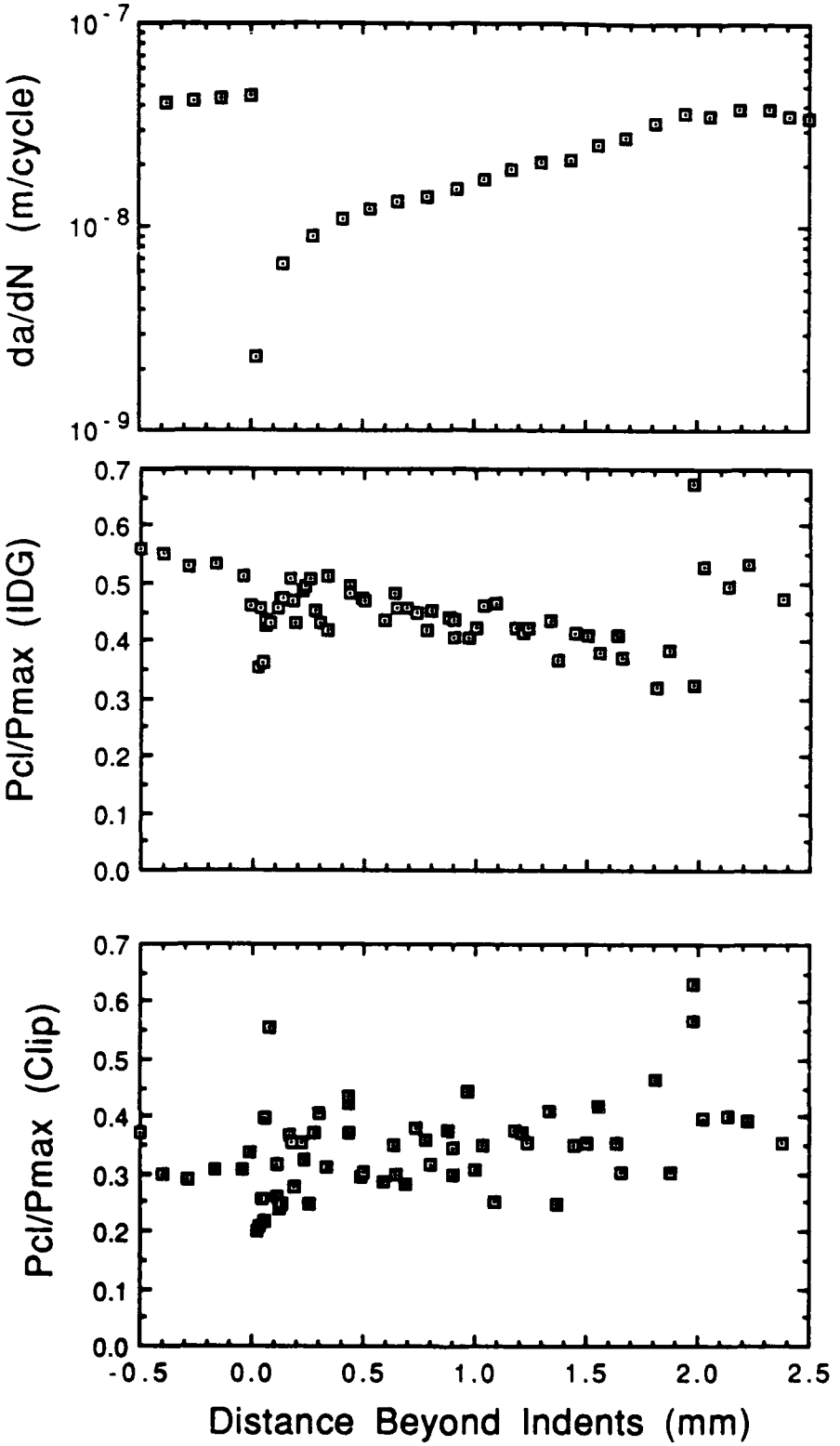

Figure 4-20. Comparison of Crack growth Data with Raw Closure Data (IDG and Clip Gage) for Overload Region

An observation of the crack growth during the constant stress intensity range tests without overloads (Tests #3 - #5) show no distinct differences in the crack behavior among any of the tests. In the constant stress intensity range tests, the load history contains no sudden changes; a gradual drop in load occurs as the crack grows in order to maintain the constant stress intensity range.

Photos in Figures 4-21, 4-22, and 4-23 show crack behavior for applied stress intensity ranges of 5.5, 7.7, and 9.9 MPa$\sqrt{m}$, respectively. The magnification in these photos is 200X. The crack growth in all three figures is from the left to the right side of the picture. The path of crack growth in specimens where the load history contained no sudden changes was almost linear in nature. Minor excursions from this linear trend, such as those shown at the left of Figure 4-20 and the central portion of Figure 4-21, were observed, but recovery to straight line crack growth was made after very small crack extensions in all cases.

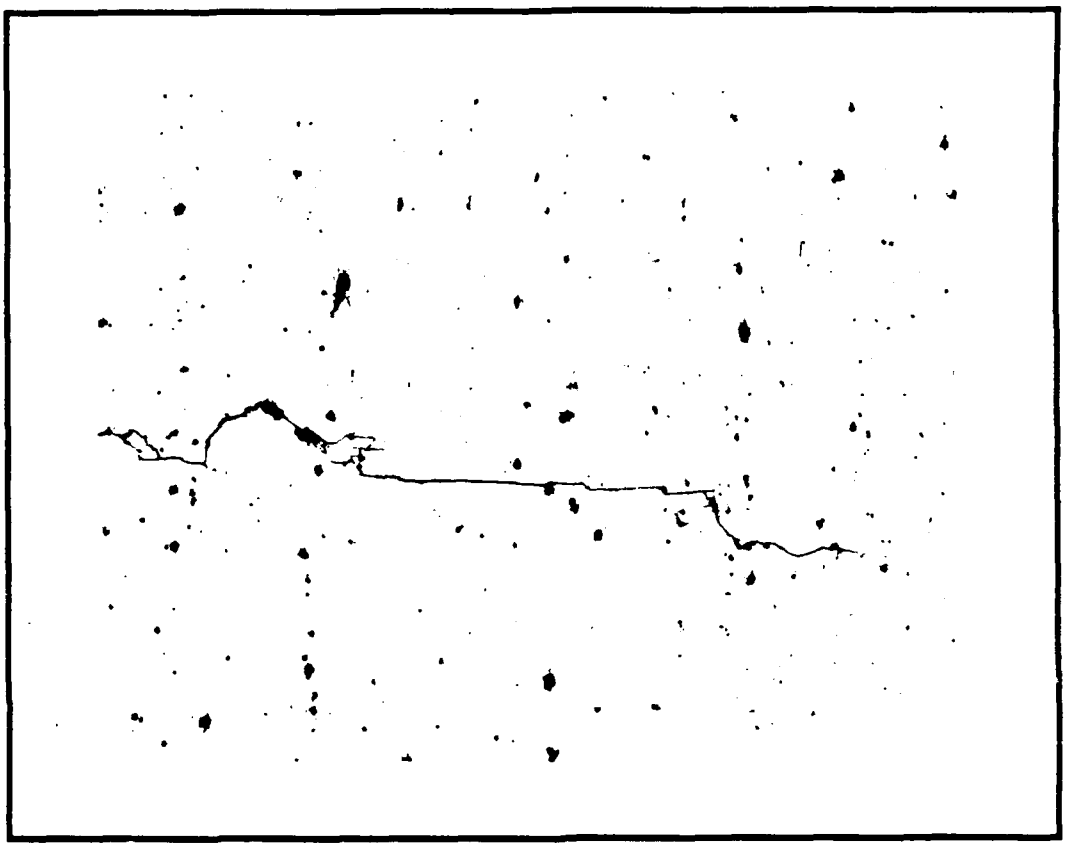

Figure 4-21. Crack Growth at Constant Stress Intensity Range of 5.5 MPa$\sqrt{m}$ (Magification = 200X)

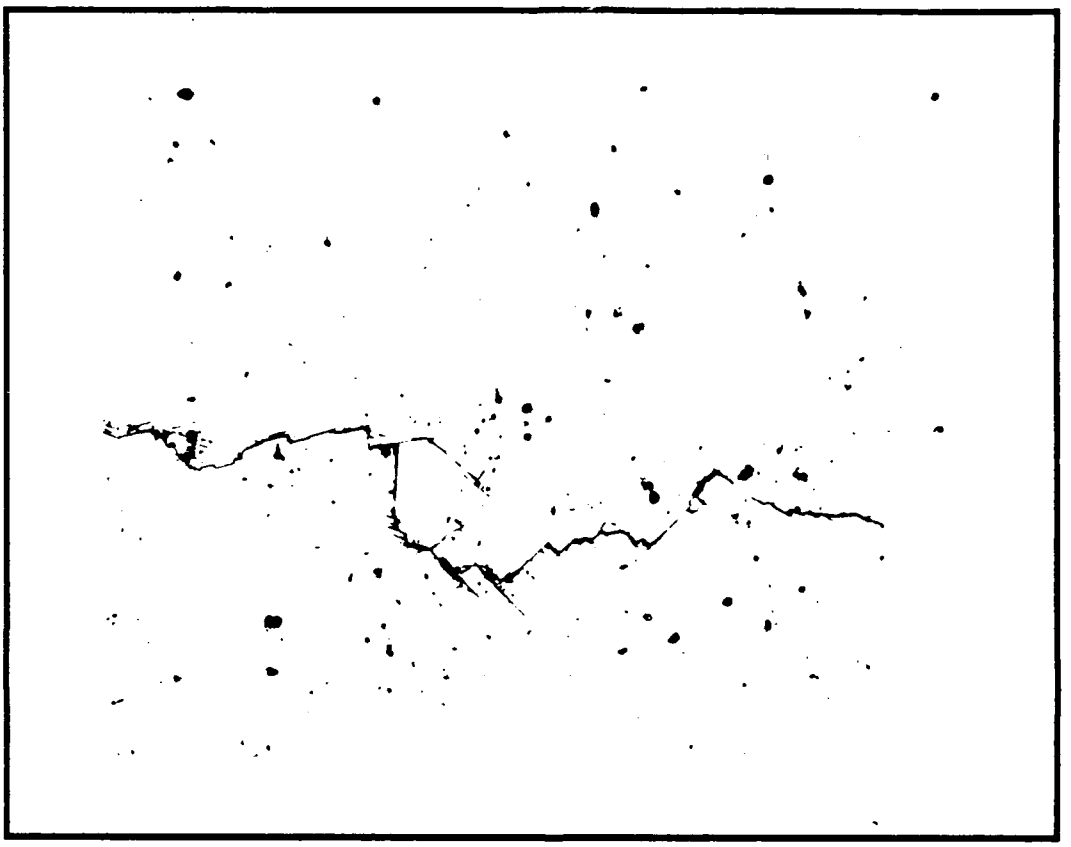

Figure 4-22. Crack Growth at Constant Stress Intensity Range of 7.7 MPa$\sqrt{m}$ (Magification = 200X)

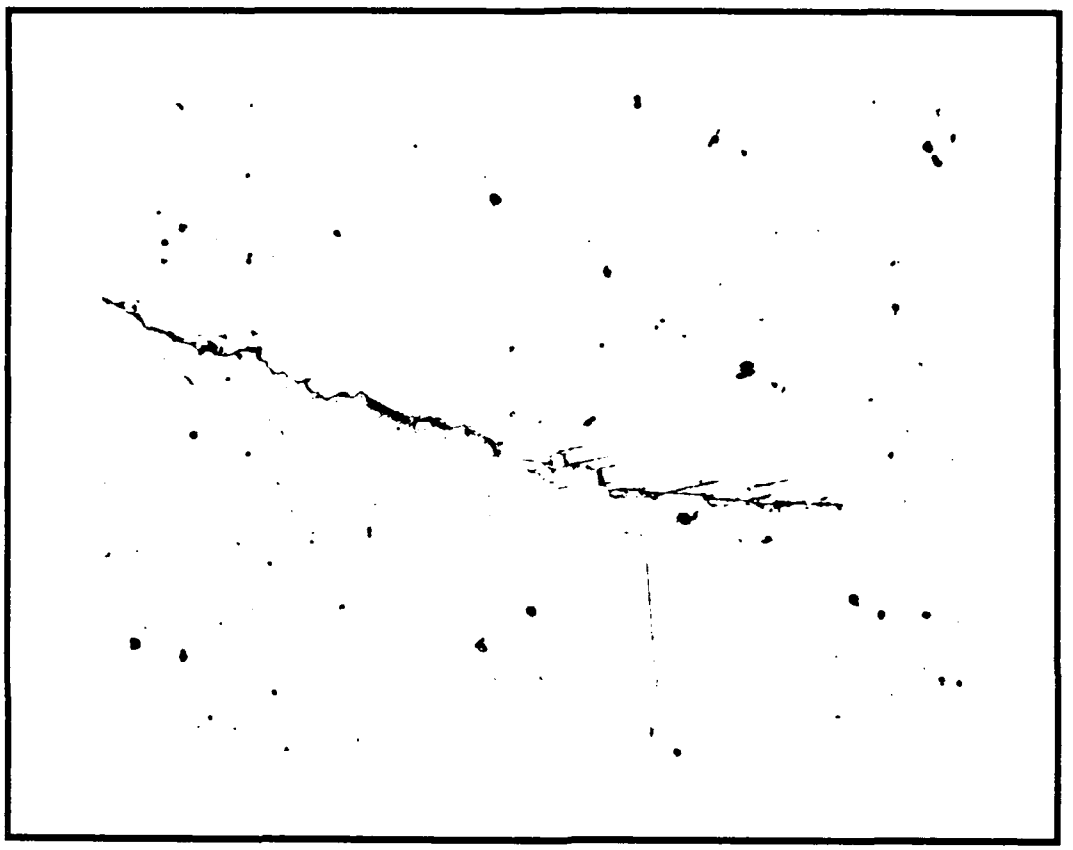

Figure 4-23. Crack Growth at Constant Stress Intensity Range of 9.9 MPa$\sqrt{m}$ (Magification = 200X)

Figures 4-24, 4-25, and 4-26 show representative regions where the tests transitioned from precracking to the fatigue test. Photos show crack behavior in these regions for applied stress intensity ranges of 5.5, 7.7, and 9.9 MPa$\sqrt{m}$, respectively. Each photo shows the first set of indents placed after the precracking had been completed; crack growth in these photos are toward the right side of the picture.

Specimens were precracked such that the final maximum stress intensity factor was 4.4 MPa$\sqrt{m}$ (4.0 ksi); this placed the final stress intensity range encountered during precracking to be 4.0 MPa$\sqrt{m}$ (3.6 ksi). These photos show that the more dramatic changes in load history (caused by the sudden change from precracking to fatigue test) caused noticeable change in the crack growth pattern.

In the constant stress intensity range tests of 7.7 MPa$\sqrt{m}$ (Test #4, Figure 4-25) and 9.9 MPa$\sqrt{m}$ (Test #5, Figure 4-26), however, distinct differences between the precracking portion and the fatigue test portions of the test are seen. When the fatigue test begins, significant changes in crack growth direction are noticed, and some secondary cracking has taken place at the point of crack deviation. However, these secondary cracks were not seen to propagate any significant distance. Not much difference was seen between the precracking portion and the fatigue test portion of the constant stress intensity range test of 5.5 MPa$\sqrt{m}$ (Test #3, Figure 4-24); no secondary cracking was noted in this particular test.

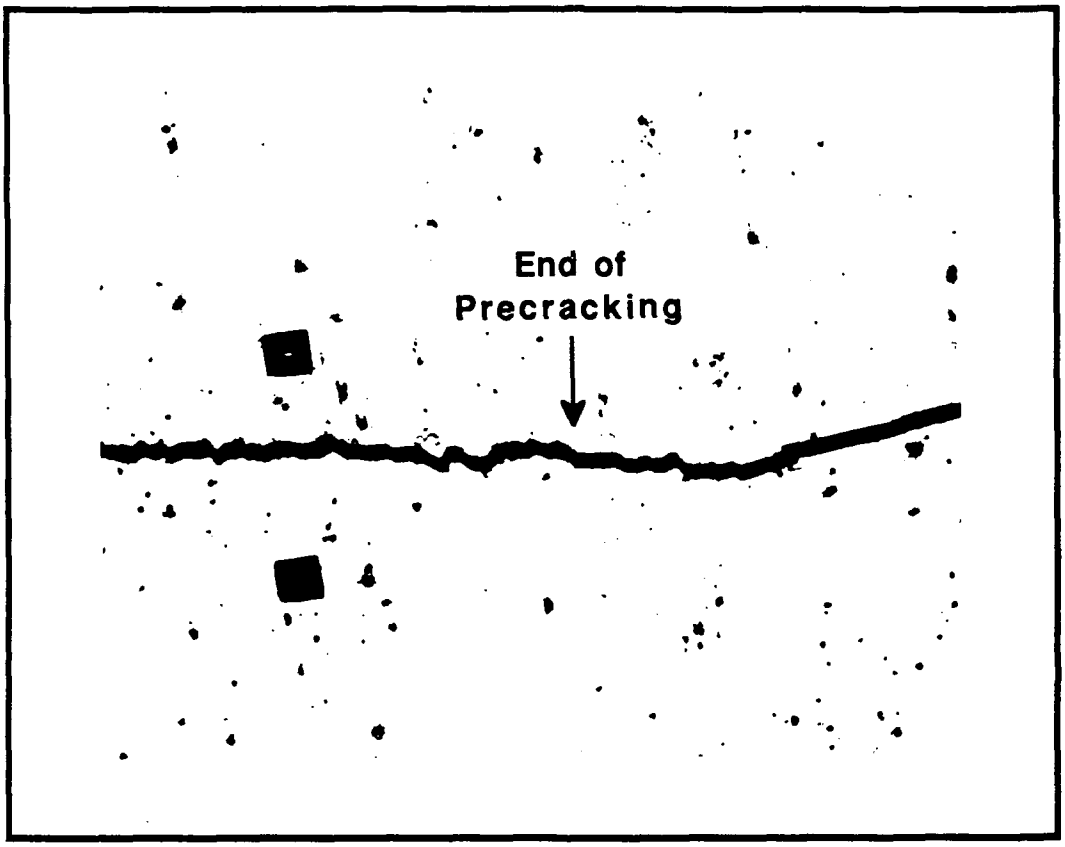

Figure 4-24. Transition from Precracking to Applied $\Delta K = 5.5$ MPa$\sqrt{m}$ (Magification = 200X)

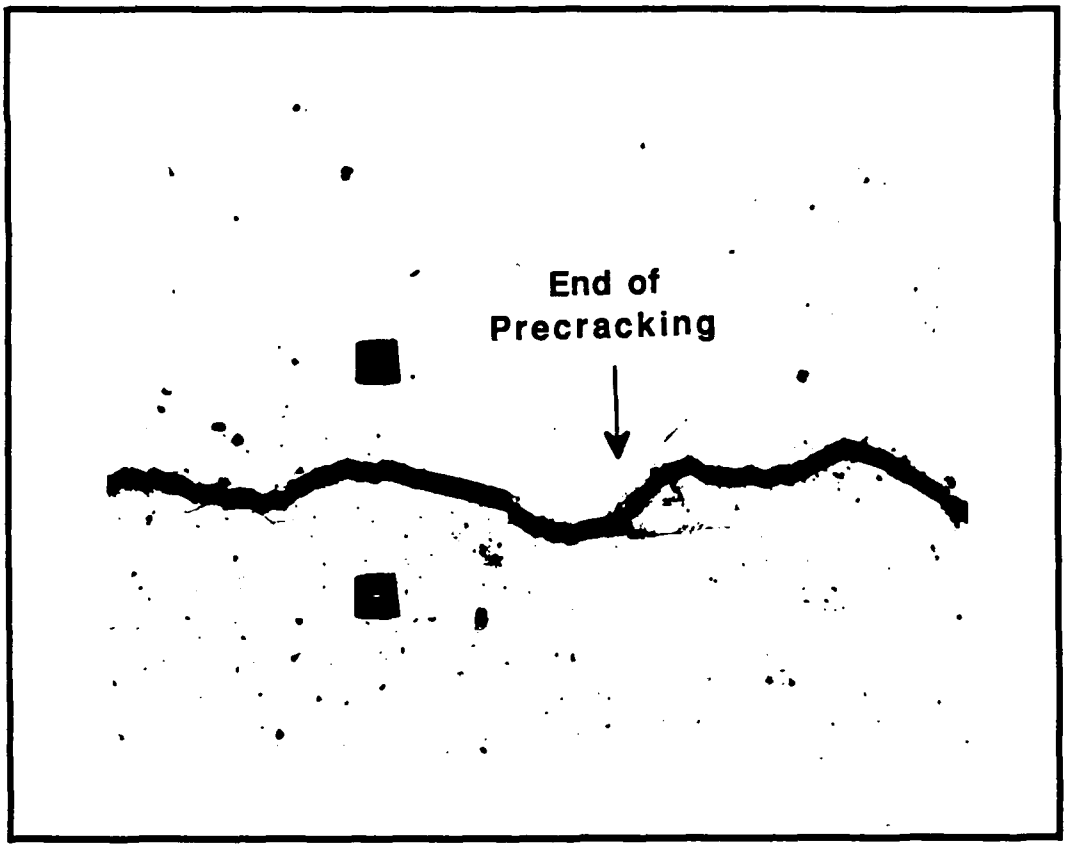

Figure 4-25. Transition from Precracking to Applied $\Delta K = 7.7\ MPa\sqrt{m}$ (Magification = 200X)

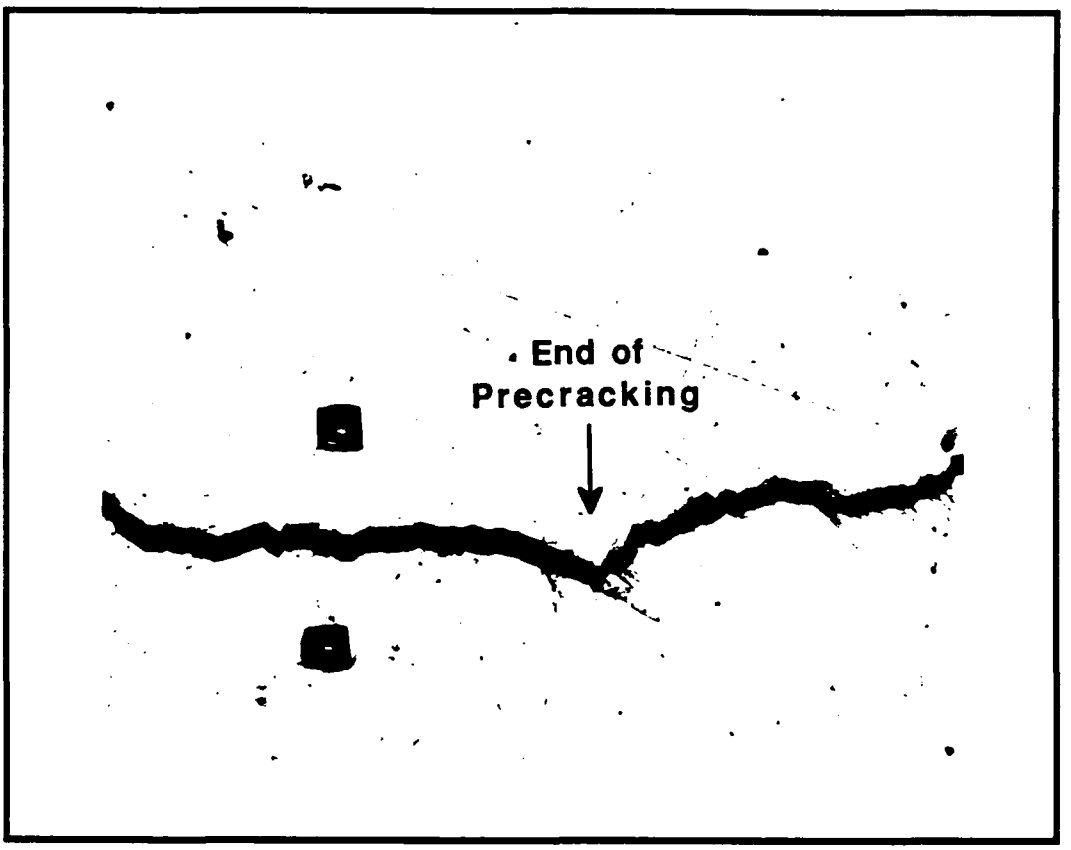

Figure 4-26. Transition from Precracking to Applied $\Delta K = 9.9\ MPa\sqrt{m}$ (Magification = 200X)

These deviations in crack growth direction introduce a Mode II component into the crack growth behavior; this, in turn, increases the amount of asperity-induced closure. Therefore, closure after a sudden significant change in loading history is no longer a primarily plasticity-induced phenomenon. This temporary deviation from linear behavior in the crack growth and the corresponding introduction of Mode II behavior are the cause of the transition zone for closure behavior observed for the first segment of each crack growth test after precracking.

Figures 4-27, 4-28, and 4-29 show representative regions where 80% overloads were applied. Photos show crack behavior in these regions for applied stress intensity ranges of 5.5, 7.7, and 9.9 $MPa\sqrt{m}$, respectively. The same behavior as seen in the transition zone from precracking to fatigue test, is also seen here, but the behavior is much more pronounced in the instances involving an overload.

In the cases involving overload, significant amounts of secondary cracking are seen to occur; these secondary cracks actually develop and propagate for a distance along with the primary crack. In this region where the secondary cracks are propagating, significant amounts of Mode II behavior will be developed (in addition to the applied Mode I loading) and the closure phenomenon will be affected by this change. This change in closure behavior is probably the cause of the large amounts of scatter and lack of distinct trend for closure data that was encountered after an overload.

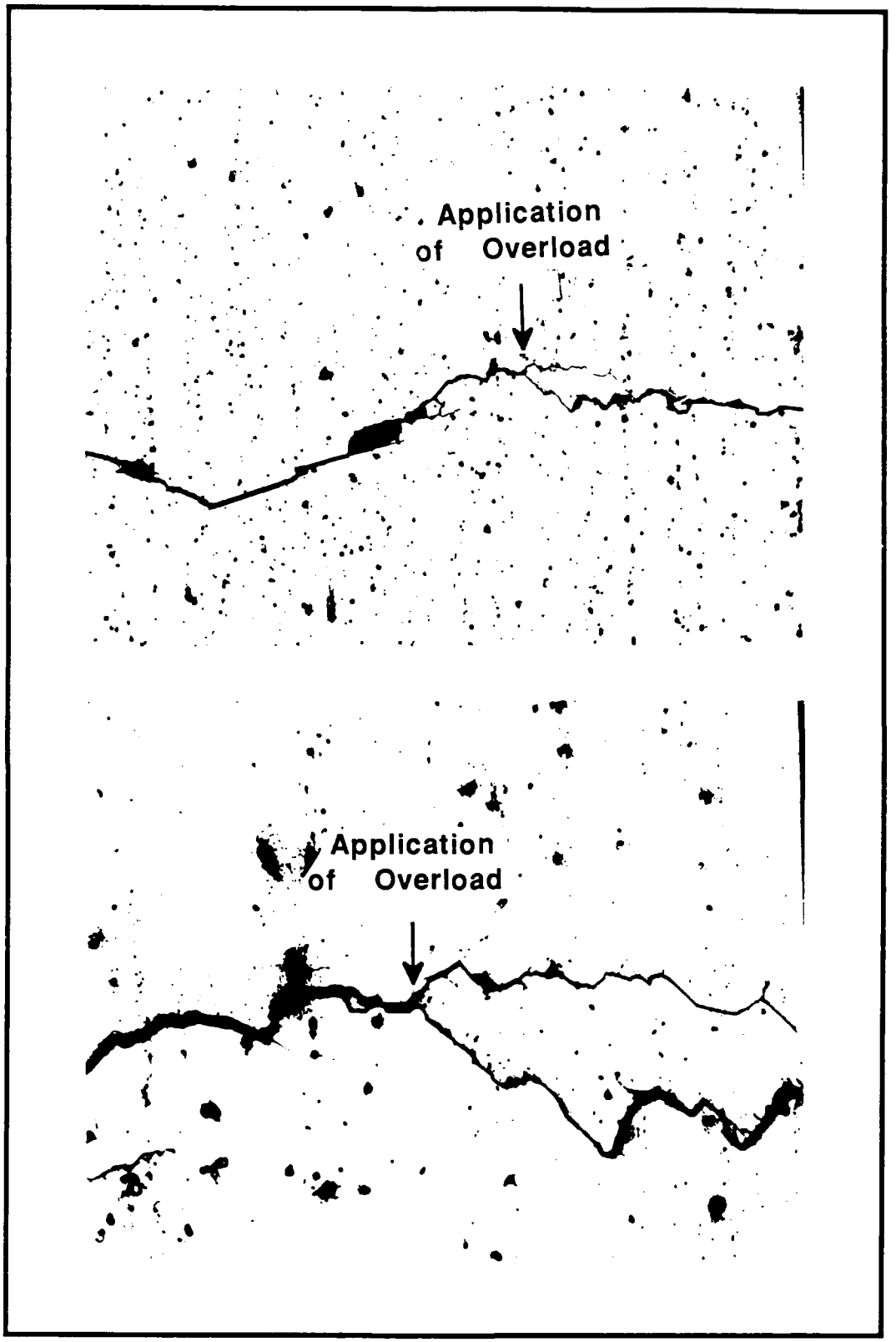

Figure 4-27. Region of 80% Overload at $\Delta K = 5.5$ MPa$\sqrt{m}$
(Top Photo = 100X, Lower Photo = 400X)

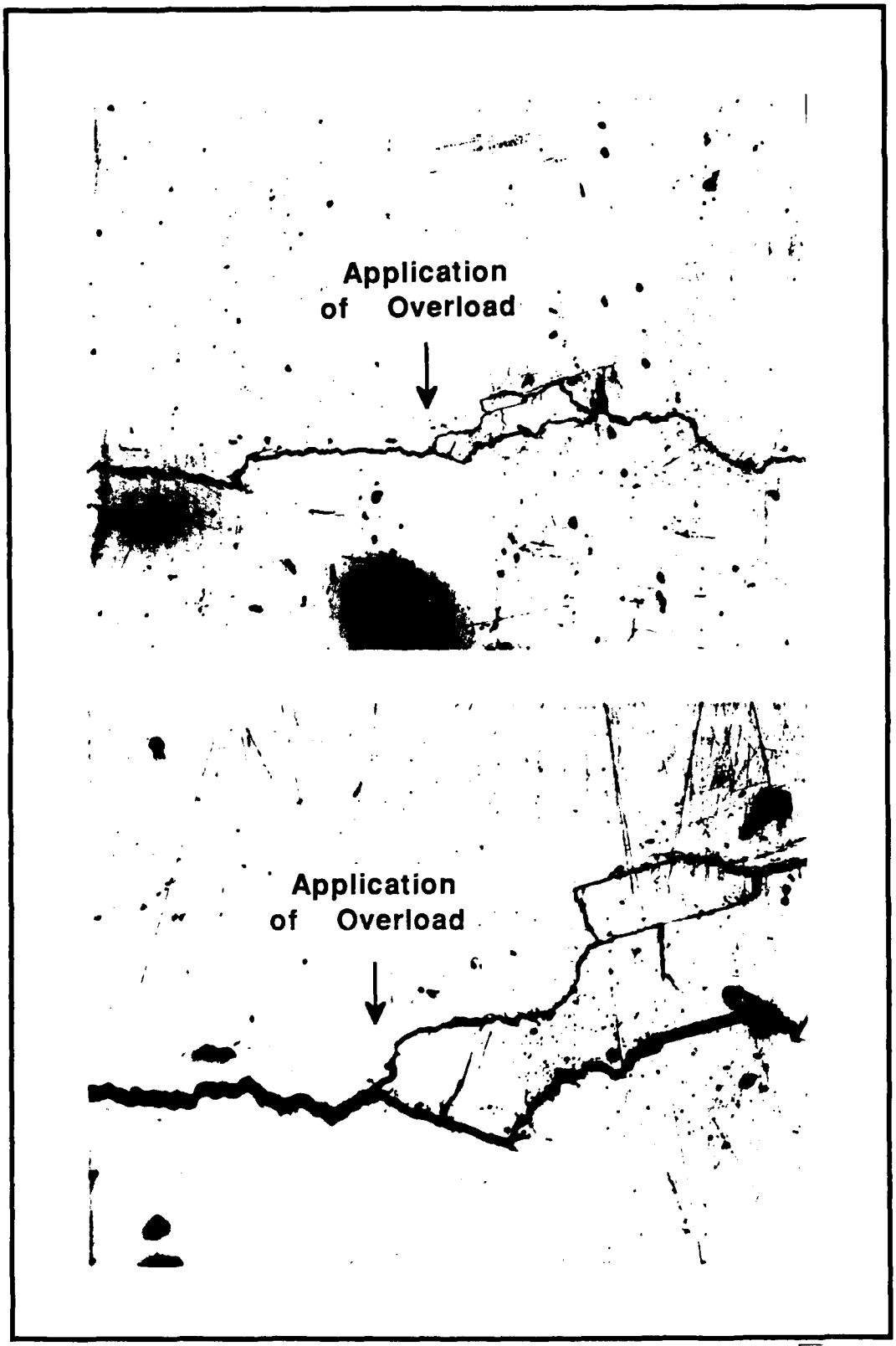

Figure 4-28. Region of 80% Overload at $\Delta K = 7.7$ MPa$\sqrt{m}$
(Top Photo = 100X, Lower Photo = 400X)

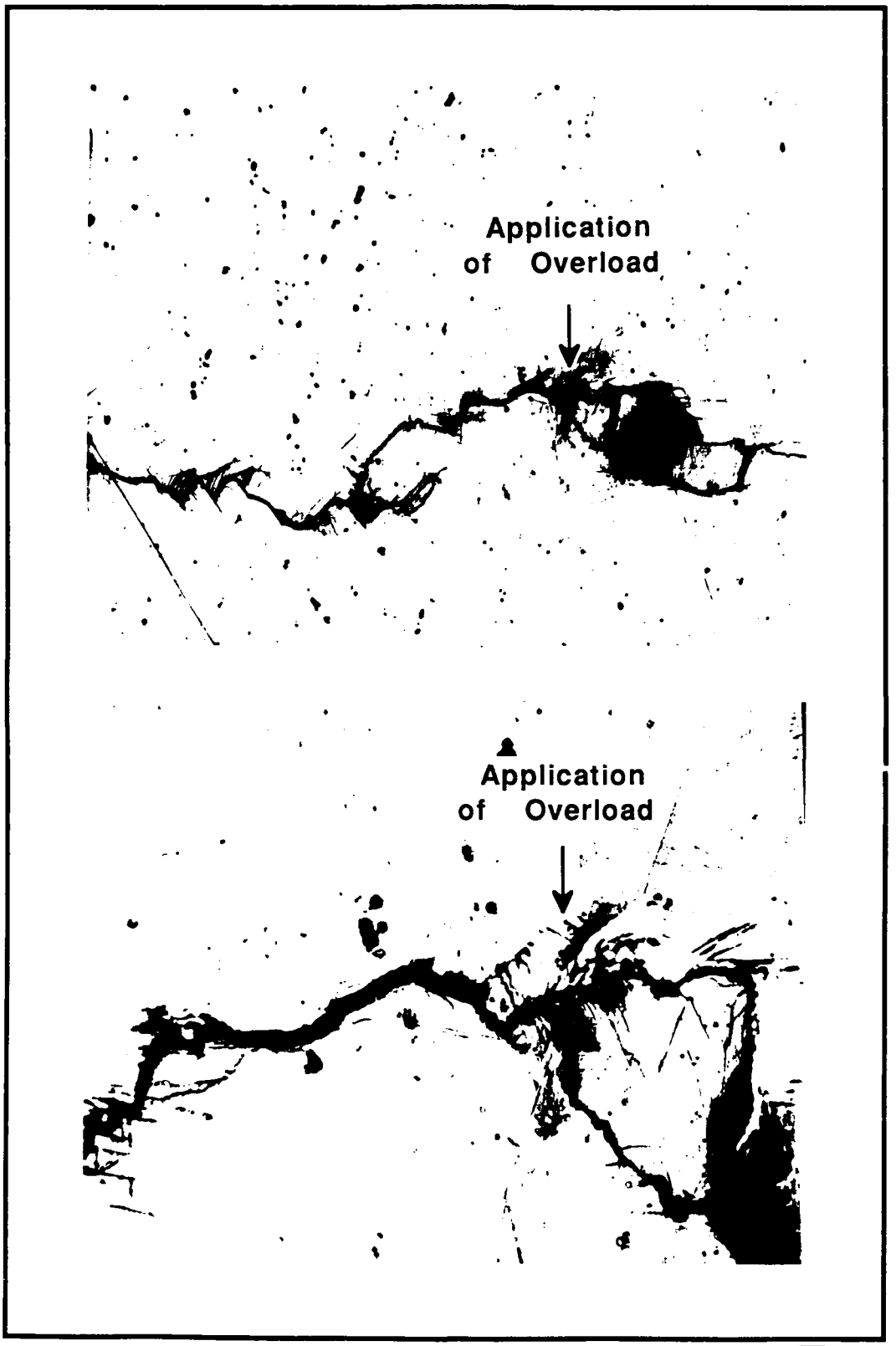

Figure 4-29. Region of 80% Overload at ΔK = 9.9 MPa$\sqrt{m}$
(Top Photo = 100X, Lower Photo = 400X)

From microscopic analysis of the crack growth trends, we can conclude that:

1. There are no distinct differences seen between the crack growth behavior at different applied stress intensity ranges.
2. A sudden and significant change in load history will induce changes in crack growth direction and cause secondary cracking.
3. In the cases involving 80% overload, the secondary cracking developed and propagated for some distance along with the primary crack before it was left behind by the primary crack.
4. The sudden changes in crack direction and secondary cracking had significant effects upon the closure measured by both the clip gage and the IDG. Large amounts of scatter was introduced into the closure data, and no distinct trend among the tests involving overloads was seen.

V. Conclusions

This study was conducted to determine the effects of single overloads upon crack growth in aluminum-lithium 2091. Two different measurement techniques were used to record load-displacement data; a clip gage was used for far-field measurements, and a laser interferometric displacement gage (IDG) was used to measure displacements in the near-field.

Several types of fatigue tests were performed upon compact tension specimens. A constant maximum amplitude load test was conducted in order to establish baseline crack growth rate vs. effective stress intensity range data for this material for the two methods of measuring closure used in this study. Fatigue tests were also conducted at three different constant stress intensity ranges. These constant stress intensity range tests were conducted with and without overloads; tests involving overloads had the overloads applied at two different crack lengths.

Based on the results of the tests, the following conclusions were made:

1. The laser IDG measured a higher closure load than the clip gage over crack lengths where a direct comparison between the two measurement techniques could be made.

2. The ratio of closure load to maximum load (P_{cl}/P_{max}) in the crack growth segment immediately following precracking showed no distinct trend. For the remaining segments of crack growth that included no sudden changes in loading, P_{cl}/P_{max} as measured by the IDG displayed distinct trends.

3. P_{cl}/P_{max} as measured by the IDG showed a dependence upon the distance from the microhardness indents (where measurements were taking place) and the crack tip. Using a second-order regression to fit the P_{cl}/P_{max} data measured by the IDG, the closure load measured could be normalized to a point 0.2 mm behind the crack tip.

4. When normalized, the closure load measured was dependent upon the crack length. Because the closure load was found to be a function of crack length, the effective stress intensity ranges calculated from the closure load were dependent on crack length as well.

   When effective stress intensity ranges vs crack growth rates for the constant stress intensity range tests were compared to the baseline data obtained from the constant maximum amplitude

load test, the data from the constant stress intensity range tests fell away from the baseline data for the shorter crack lengths (where the closure was high), but as the crack grew and closure decreased the data approached and coincided with the baseline data.

5. For a specific level of overload, the delay distance and delay cycles were functions of the applied stress intensity range.

6. No distinct difference is seen in the crack growth trends for different constant stress intensity ranges.

7. Sudden and significant changes in load behavior (such as an overload) cause a change in the direction of crack growth, and also result in secondary cracking. These, in turn, cause significant amounts of Mode II behavior in the crack loading, which adds an asperity-induced component of closure until the crack growth returns to a normal linear trend.

VI. Recommendations

The tests for this study were conducted at a low stress ratio (0.1). The sensitivity of the laser IDG makes an accurate determination of closure in the region near the crack tip possible. At higher stress ratios, the closure has been found to have a smaller effect; therefore, the laser IDG would be an ideal tool for measuring any closure that might be present at high stress ratios. In the future, the laser IDG should be used with tests conducted at different stress ratios.

In this study, the P_{cl}/P_{max} as measured by the laser IDG was used to determine profiles for P_{cl}/P_{max} as a function of crack length; this was done by using regressions for P_{cl}/P_{max} trends to determine the P_{cl}/P_{max} value for a specific distance beyond the indents. To obtain better resolution in the profiles of P_{cl}/P_{max} as a function of crack length, the segments of crack growth could be shortened; this would yield more data points per specimen by obtaining more segments of crack growth per specimen.

Through the use of a more accurate and more sensitive measurement device (such as the laser IDG) to measure displacements of a fatigue specimen, the effect of closure on crack growth rates can be more effectively studied.

Appendix A: Clip Gage Construction

A non-conducting clip gage used in this study was constructed as per dimensions found in ASTM 399, Annex A1 (32:695-696). The cantilever arms of the clip gage were titanium alloy; the spacer block between the arms was machined from nylon. Nylon was the material of choice for the spacer block for two primary reasons: its non-conducting properties electrically insulated the arms of the clip gage from each other, and its resistance to compression minimized hysteresis effects and other errors that could affect the measurement of crack mouth displacement.

Initial attempts to use this gage were unsuccessful; the nylon did not have enough resistance in tension to keep the screws which attached the arms to the block from stripping the threads out of the tapped hole. Attempts to hold the clip gage arms in place with cyanoacrylate adhesive also failed.

After several trials, a clamping fixture was used in combination with the cyanoacrylate adhesive; this clamping fixture was insulated from the arms of the clip gage by Teflon cloth. This final configuration held the cantilever arms rigidly in place and simultaneously satisfied the condition that the gage be non-conducting. Resistance between the arms of the clip gage was measured to be in excess of 90,000 ohms.

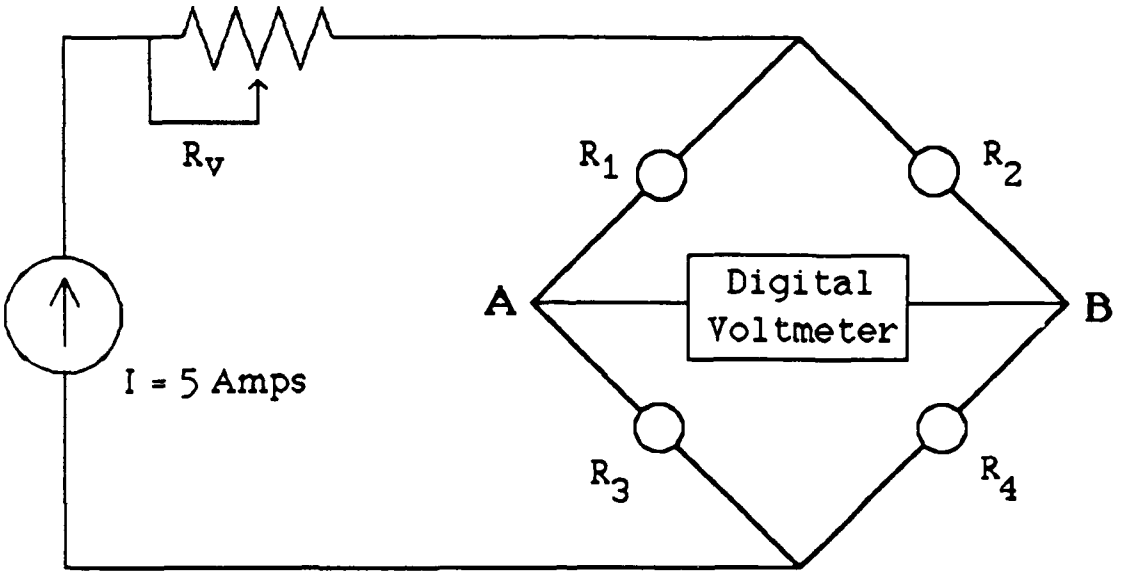

Figure A-1. Wheatstone Bridge Circuit for Clip Gage

Each arm of the clip gage was instrumented with two strain gages, one on the inner side of the arm and one on the outer side of the arm. These strain gages were wired into the circuit shown in Figure A-1.

This configuration, commonly known as a Wheatstone bridge, is very sensitive to changes in resistance in any branch of the circuit (R_1, R_2, R_3, or R_4); this makes it an ideal circuit for detecting the small changes in resistance experienced by strain gages experiencing deformation.

When inserted into the notch at the mouth of the CT specimen, the strain gages on the inner surfaces of the clip gage arms experience compression and those on the outer surfaces of the arms undergo ɔnsion. As a tensile load is applied to the specimen, the mouth of the specimen opens and

the arms of the clip gage spread wider. This bending causes a change in resistance in each of the strain gages; these changes in resistance cause voltage changes between Point A and Point B of the Wheatstone bridge.

A constant excitation current of 5.0 amps was used for the clip gage circuit. Due to software constraints of the data acquisition software, the voltage between Point A and Point B of the clip gage circuit had to be kept between +10.0 and -10.0 volts. The variable resistor R_V was used to adjust the current flowing through the bridge so that this condition was satisfied during all parts of the data acquisition cycle.

Prior to testing, a standard calibration fixture was used to establish the relation between displacement of the specimen mouth and the voltage measured across the bridge. Input from the load cell and from the digital voltmeter in the clip gage circuit during data acquisition provided a load-displacement relation at the mouth of the compact tension specimen under cyclic fatigue conditions.

Strain Gage Specifications

The strain gages used in the construction of the clip gage had the following specifications:

Manufacturer: Measurements Group, Inc.
Micro-Measurement Division
Raleigh, North Carolina

Gage Type: CEA-06-187UW-350

Resistance: 350.0 ohms ± 0.3% (at 24° C)

Appendix B: Generalized Electric Potential Solution (36)

As mentioned in Section II, measurement of the changes in voltage measured across potential leads spot-welded to a compact tension specimen can be used to track the growth of a crack in the specimen during fatigue tests.

The voltage difference across the potential leads, V, is a function of the following parameters:

$$V = f(B, \kappa, I, \frac{a}{W}) \qquad \text{(B-1)}$$

where B is the specimen thickness, κ is the electrical conductivity of the material, I is current passed through the specimen, a is the crack length and W is the specimen width.

For a given compact tension specimen with a constant current passed through it, the only parameter that will change during a fatigue test will be the crack length. Therefore, the voltage measured across the potential leads will be a function of a/W only. The relation between voltage and crack length will be of the form:

$$V = \frac{I}{B\kappa} * g(\frac{a}{W}) . \qquad \text{(B-2)}$$

An inverse relation will hold as well; for each compact tension specimen, there will be a unique value of crack length that corresponds to each value of voltage measured across the potential leads. This relation will be of the form:

$$\frac{a}{W} = \frac{B\kappa}{I} * h(V) . \qquad \text{(B-3)}$$

The relations in Eqs B-2 and B-3 must be the inverse of each other. In other words, any value for voltage generated by the substitution of a crack length into Eq B-2 must regenerate the original crack length when that voltage is substituted into Eq B-3.

When a constant current is passed through the specimen, the form of the distribution of electric potential in the specimen can be found using a finite element analysis. This analysis will generate the formulas relating crack length and voltage measured between any two specified points on the specimen. For this study, the finite element analysis was performed by George Hartman, University of Dayton Research Institute (UDRI), Dayton OH, for the configuration of electrical connections previously depicted in Figure 2-3. The resulting equations are:

$$V = \frac{I}{B\kappa} * (2.83766 - 15.2224*A + 106.67*A^2 - 312.903*A^3 + 496.84*A^4 - 405.065*A^5 + 134.265*A^6) \qquad \text{(B-4)}$$

$$A = \frac{B\kappa}{I} * (-0.424816 + 0.183053*V + 0.0768966*V^2 - 0.0172752*V^3 + 0.00094126*V^4) \qquad \text{(B-5)}$$

where the parameter A is the non-dimensionalized crack length (a/W) and κ, B, and I are the parameters previously defined in Eq B-1.

The value of κ, the material conductivity, is usually not known to a precision sufficient enough to allow accurate values of voltage or crack length to be calculated from Eqs B-4 or B-5, respectively.

This difficulty can be avoided by using a combination of crack length and voltage measurement that is known to be correct. For any given compact tension specimen, the material conductivity (κ) and specimen thickness (B) would not change. If the electric current passing through the specimen was kept at a constant value during fatigue testing, Eq B-2 takes the form:

$$V = C * f(\frac{a}{W}) \qquad \text{(B-6)}$$

where C is a constant, given by the parameter $\frac{I}{B\kappa}$.

If we obtain correct values for V and a/W by an independent means and substitute them into Eq B-6, we get:

$$Vo = C * f(\frac{a_o}{W}) \qquad \text{(B-7)}$$

Rearranging this equation, we find that:

$$C = Vo \; / \; f(\frac{a_o}{W}) \qquad \text{(B-8)}$$

Substituting into Eq B-7, we get:

$$V = V_o * \frac{f(a/W)}{f(a_o/W)} \qquad \text{(B-9)}$$

We can rearrange Eq B-9 to get:

$$f(\frac{a}{W}) = \frac{V}{V_o} * f(\frac{a_o}{W}) . \qquad \text{(B-10)}$$

Applying the inverse function g(V) to Eq B-10, we get obtain:

$$g(f(\frac{a}{W})) = \frac{a}{W} = g(\frac{V}{V_o} * f(\frac{a}{W})) \qquad \text{(B-11)}$$

Note that Eq B-11 is independent of material conductivity (K), specimen thickness (B), and the amount of electric current passed through the specimen (I). This equation is therefore valid for any compact tension specimen that has been geometrically scaled from the dimensions used to derive the original relationships between crack length and voltage across the potential leads; this scaling must include a scaling of the dimensions for the placement of potential leads and current input.

Initialization Procedure for the Electric Potential Relation

For this study, the compact tension specimen was periodically removed from the testing machine in order to place microhardness indents upon the face of the specimen (for use with the laser IDG). At these times, optical measurements of the crack length on the front and back of the specimen were made. From these measurements a thickness-averaged value for crack length was calculated. When the specimen was returned to the testing machine, the clip gage was mounted in the mouth of the specimen, the laser IDG was aligned, and the electrical connections on the front face of the specimen were reestablished.

The resistance of the specimen to the electric current passing through it caused the specimen to heat up slightly. Because the material conductivity is a function of temperature, thermal equilibrium in the specimen was necessary for a proper reinitialization of the crack length; a non-equilibrium value for voltage would improperly calibrate Eq B-11 and cause errors in the tracking of crack growth.

With the constant current of 10.0 amps used in this study, it took approximately five minutes for the electric field in the specimen (and therefore the voltage reading across the potential leads) to stabilize.

While the specimen was reaching thermal equilibrium, the optically-determined value for crack length would be input into the program which controlled the loading in the test machine. Once thermal equilibrium was achieved, fatigue cycling and data acquisition were resumed. The software that controlled the testing would immediately take a data sample; among other data, the voltage across the potential leads was taken. This value for voltage, along with the optically determined crack length, calibrated Eq B-11. Readings from a digital voltmeter during each data acquisition cycle allowed the tracking of subsequent crack growth in the specimen.

SPECIAL NOTES ABOUT EQUATIONS B-4 AND B-5:

As the value of a/W approaches 1.0, the voltage must approach infinity. (When the crack length equals the

specimen width, there is no remaining ligament in the specimen to conduct electricity; therefore, the voltage measured across the potential leads should be infinite.)

As discussed above, the relations in Eqs B-4 and B-5 must be the inverse of each other. The equations, however, are of different polynomial order. When plots of the relations in Eqs B-4 and B-5 are generated (Figures B-1 and B-2, respectively), it is noted that a plot of the relation expressed in Eq B-4 has a vertical asymptote, while the plot of the relation expressed in Eq B-5 displays a horizontal asymptote. A function with a horizontal asymptote can be represented with fewer terms of a polynomial expansion (when calculated to the same degree of accuracy) than a function with a vertical asymptote.

A check was made to ensure that Eqs B-4 and B-5 were inverses over the range of non-dimensional crack lengths ($0.25 \leq a/W \leq 0.8$) observed in this study. Typical values for specimen thickness, material conductivity, and current were used in this check. A value for crack length was substituted into Eq B-4 to obtain a theoretical value for voltage; this value of voltage was then substituted into Eq B-5 to generate a value for crack length. If these equations are truly inverses of one another, the crack length obtained from Eq B-5 should match the crack length originally substituted into Eq B-4. The results of this test, shown in Figure B-3, verify the inverse relationship between the two equations.

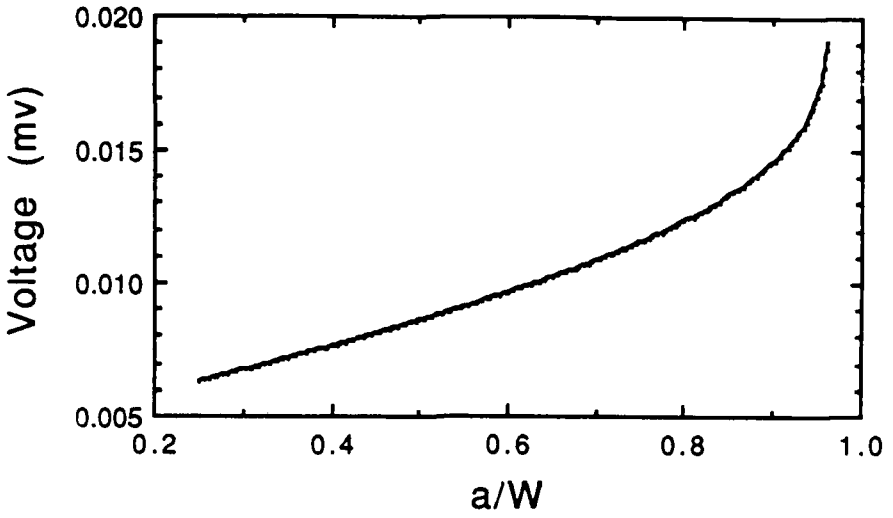

Figure B-1. Plot of Voltage as f(a/W), as related in Equation B-4

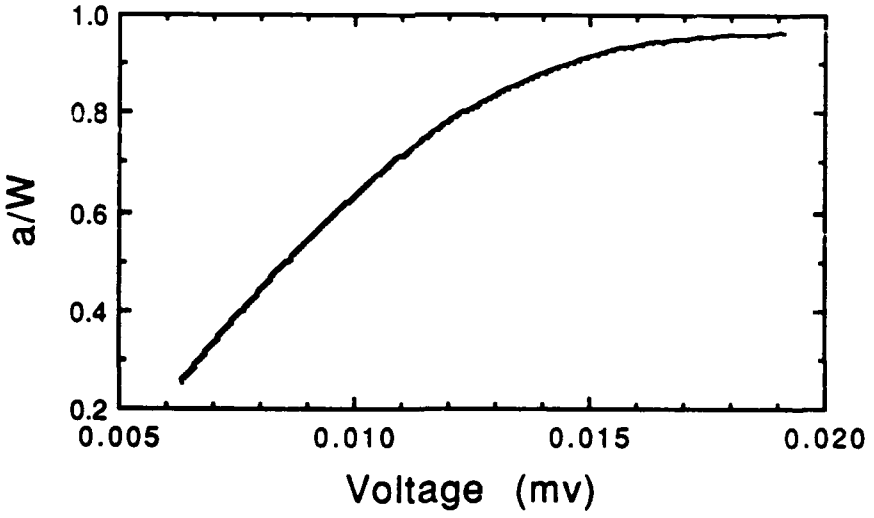

Figure B-2. Plot of a/W as f(Voltage), as related in Equation B-5

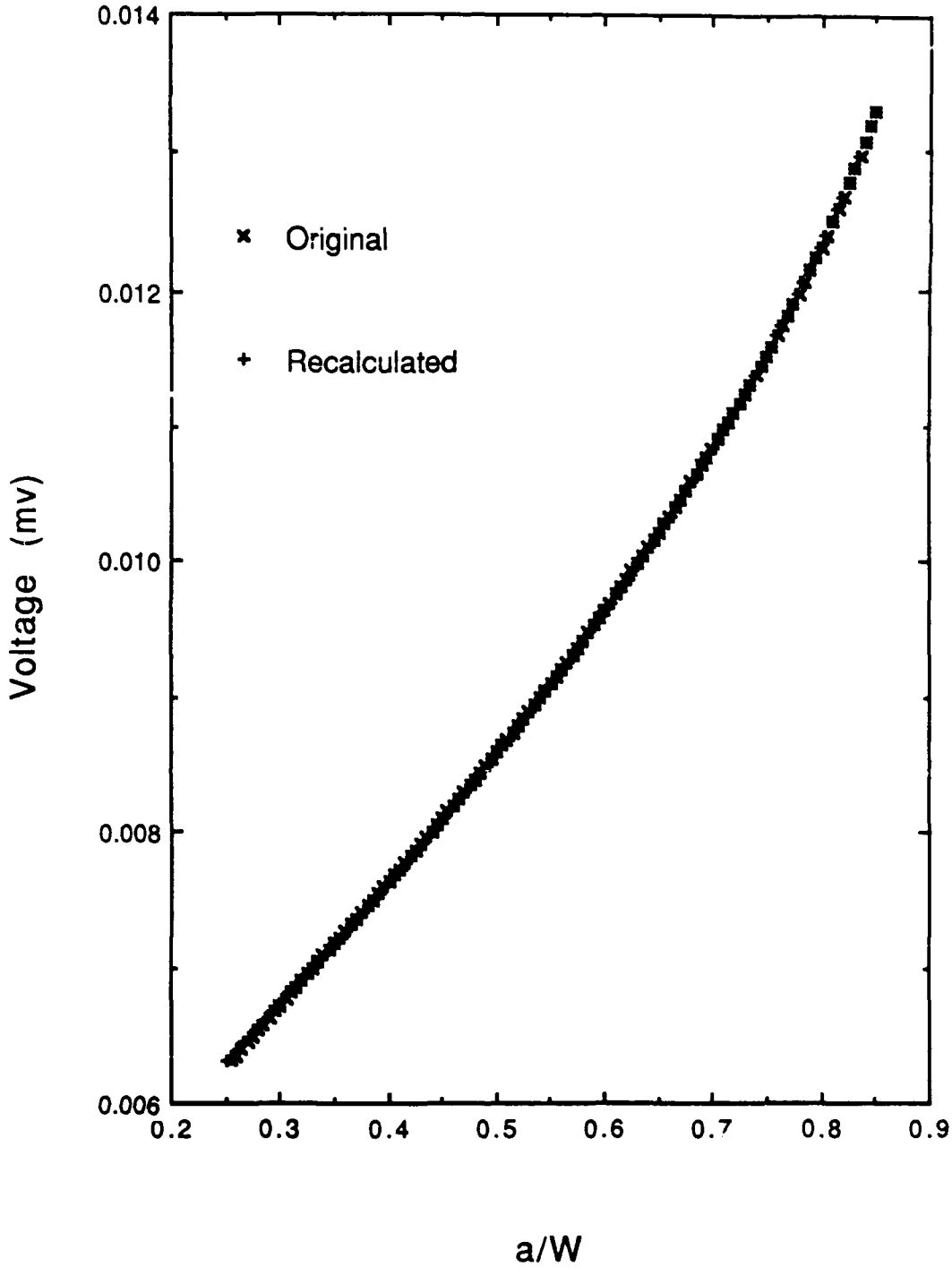

Figure B-3. Inverse Test of Eqs B-4 and B-5

The coefficients represented in Eqs B-4 and B-5 came from the latest iteration of the finite element analysis used to generate the relations between crack length and voltage; this latest iteration of the analysis provides only a slight improvement over the original analysis. Alternate coefficients for these equations were used in the electric potential solution that tracked the crack length in this study. Differences between the coefficients shown in Eqs B-4 and B-5 and those actually used are negligible.

Figure B-4 shows the results of calibrating the electric potential solution to experimental data obtained during one of the baseline tests. For the data in this figure, the values of crack length and voltage obtained immediately after the completion of precracking were used to calibrate the curve.

The curve need not be calibrated with initial values of crack length and voltage, however, and then "grown" forward from this point. The electric potential solution can be calibrated using data obtained at any time during the fatigue test. The only requirements
for the calibration data are that the crack length be accurately measured and that the corresponding value for voltage be obtained when the specimen is in thermal equilibrium with its surroundings.

For example, fatigue striations from individual load cycles are often evident on the crack surfaces of some alloys. In such alloys, an overload cycle can be used to

provide a "marker". This distinctive striation can be easily located on the crack surface, thereby yielding an accurate measurement of crack length; a corresponding voltage reading taken at the time of the overload can be used as a calibration point for the curve.

For many alloys the crack length at failure can be determined by examination of the crack surfaces after specimen failure. Crack length at failure, in combination witn a correct voltage reading, can be used to calibrate the crack growth that preceded failure.

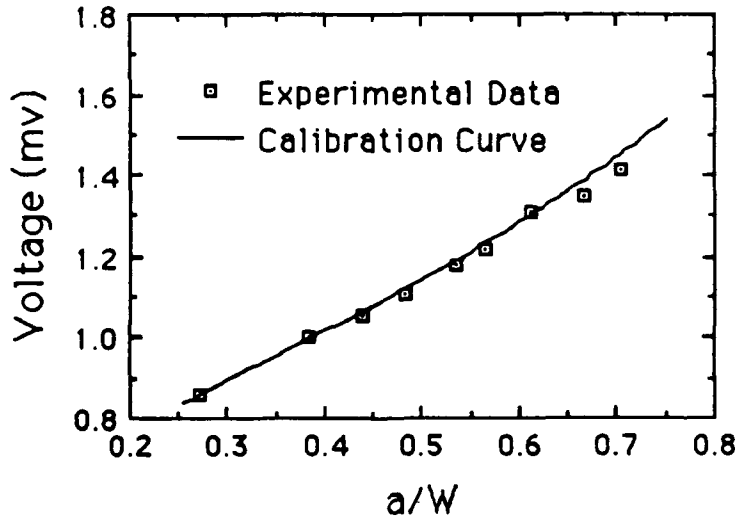

Figure B-4. Comparison of Calibration Curve and Experimental Data

Appendix C: Crack Growth Histories

The graphs in this appendix depict the crack length as a function of the number of load cycles applied to the specimen. The crack lengths shown are measured by the electric potential method and corrected with the linear interpolation technique discussed in Section III. For clarity, the number of cycles has been adjusted so that the end of the precracking and beginning of the fatigue test are designated by load cycle number one.

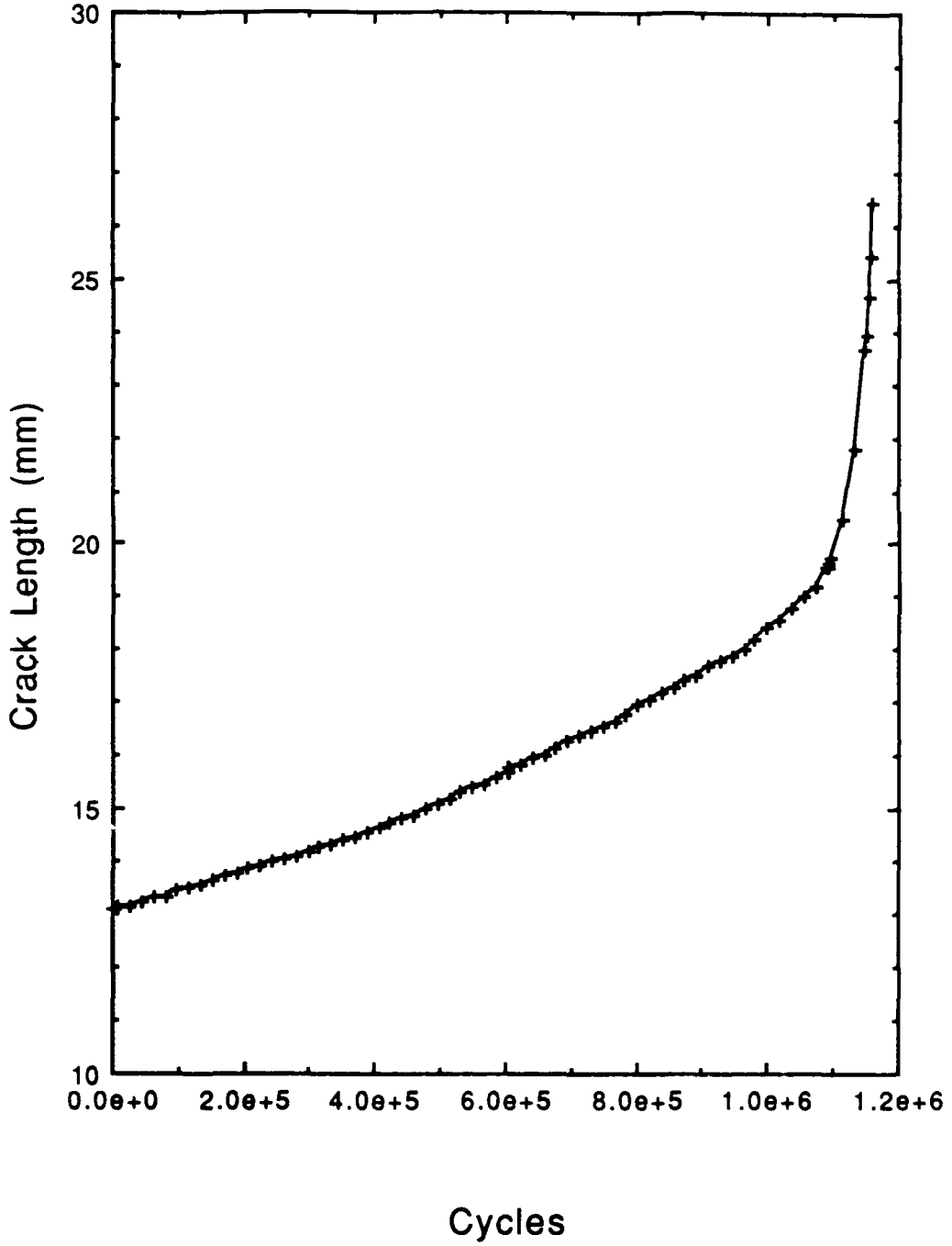

Figure C-1. Crack Length vs Cycles: Test #1

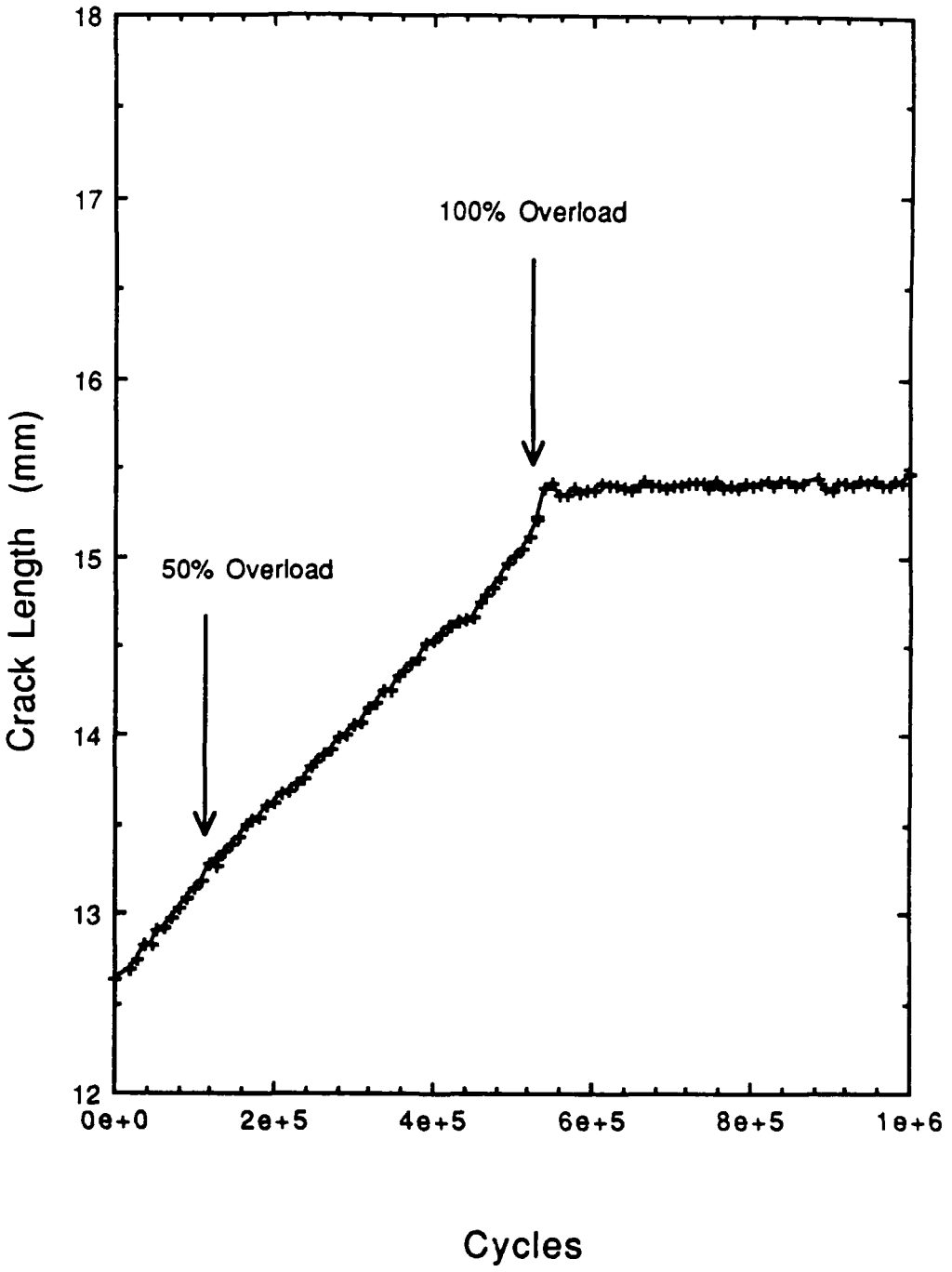

Figure C-2a. Crack Length vs Cycles: Test #2 (Section 1)

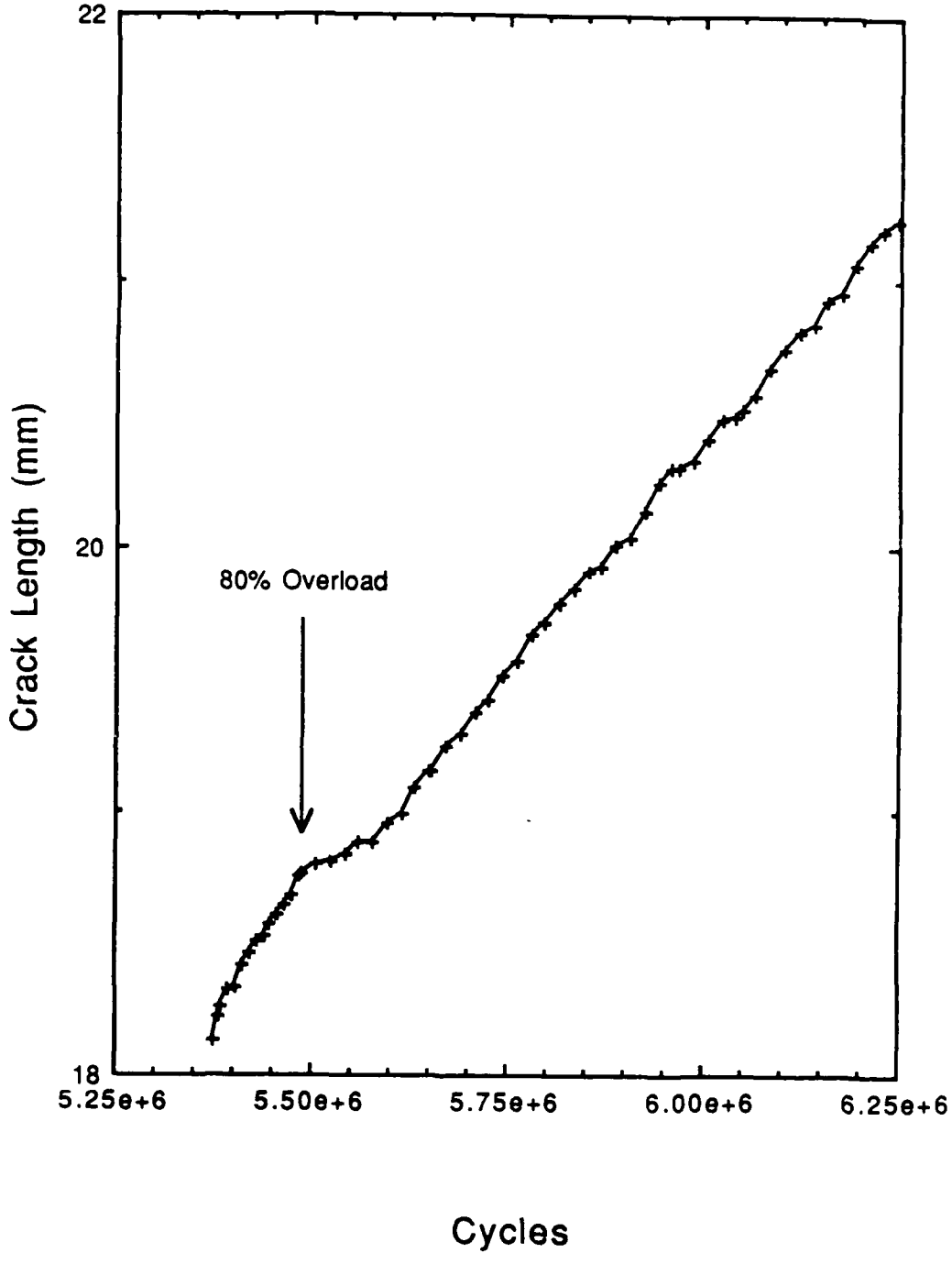

Figure C-2b. Crack Length vs Cycles: Test #2 (Section 2)

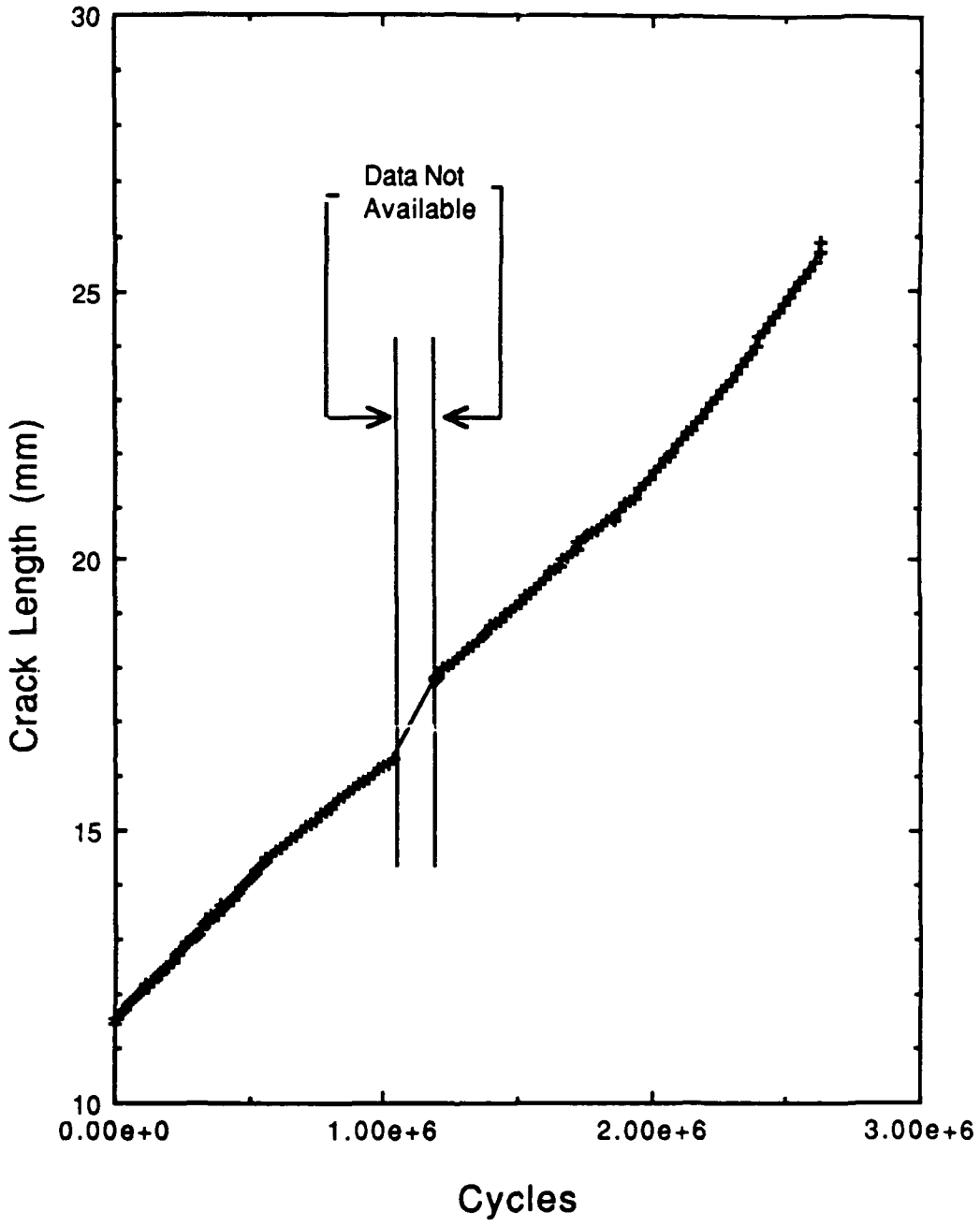

Figure C-3. Crack Length vs Cycles: Test #3

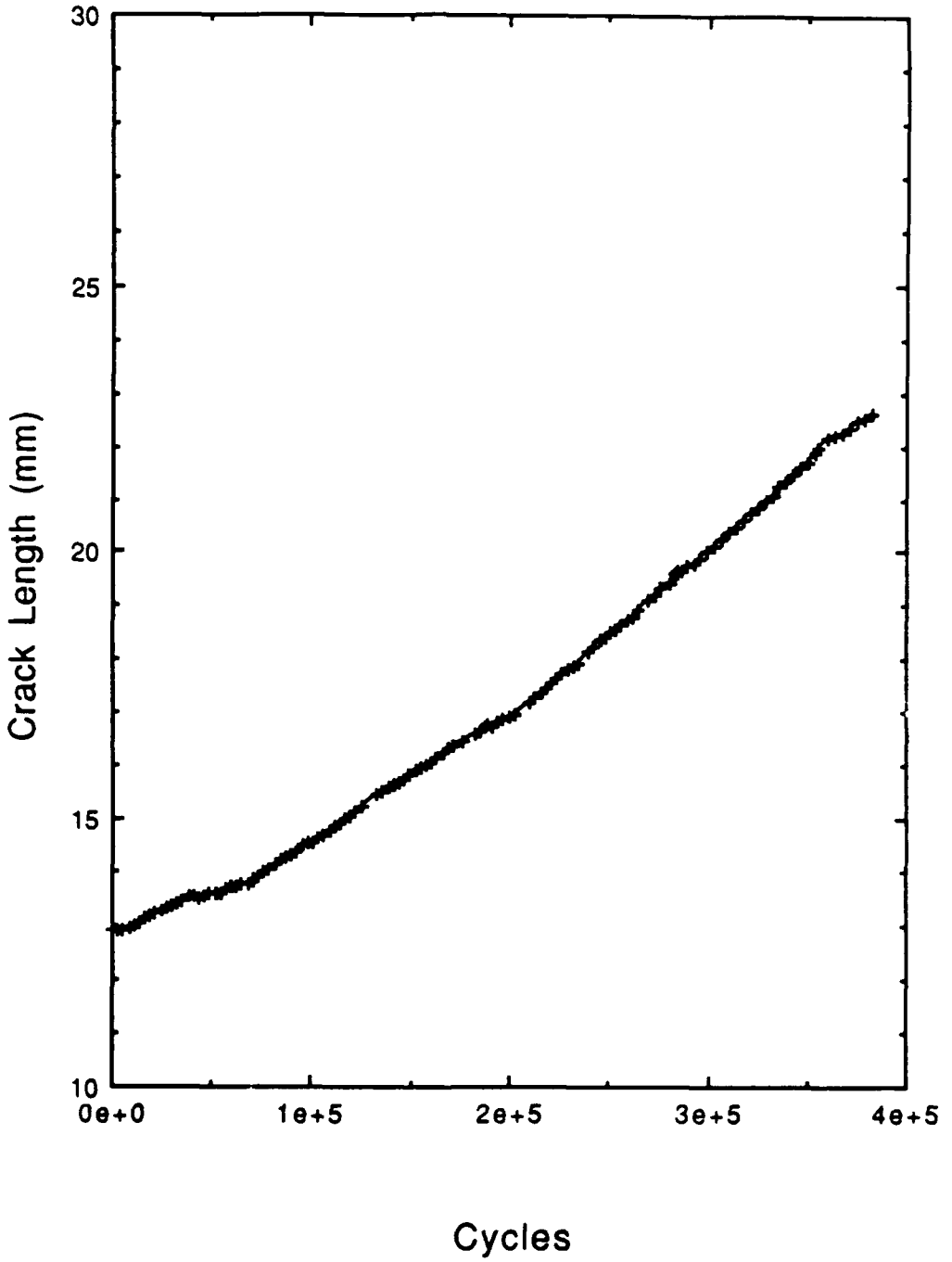

Figure C-4. Crack Length vs Cycles: Test #4

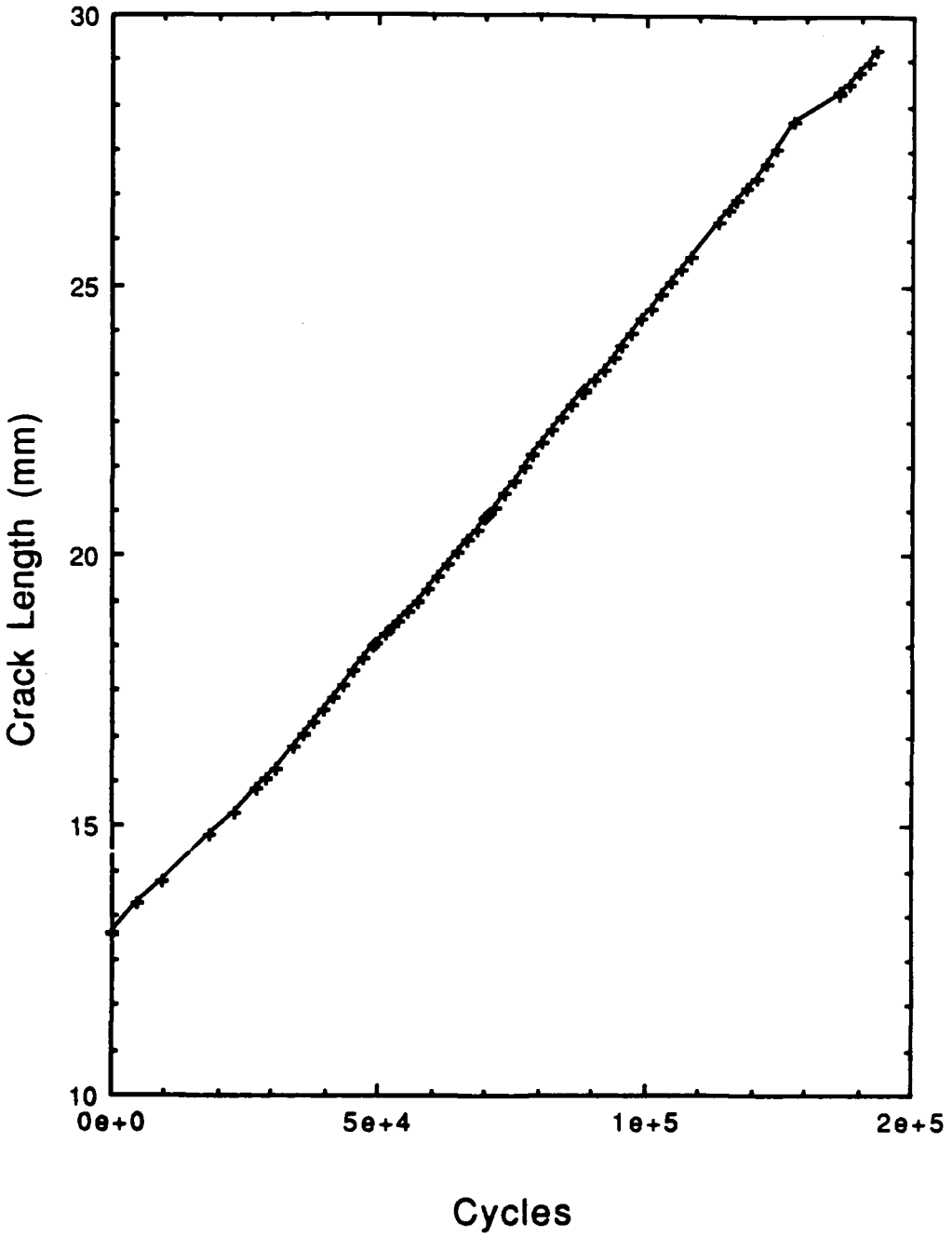

Figure C-5. Crack Length vs Cycles: Test #5

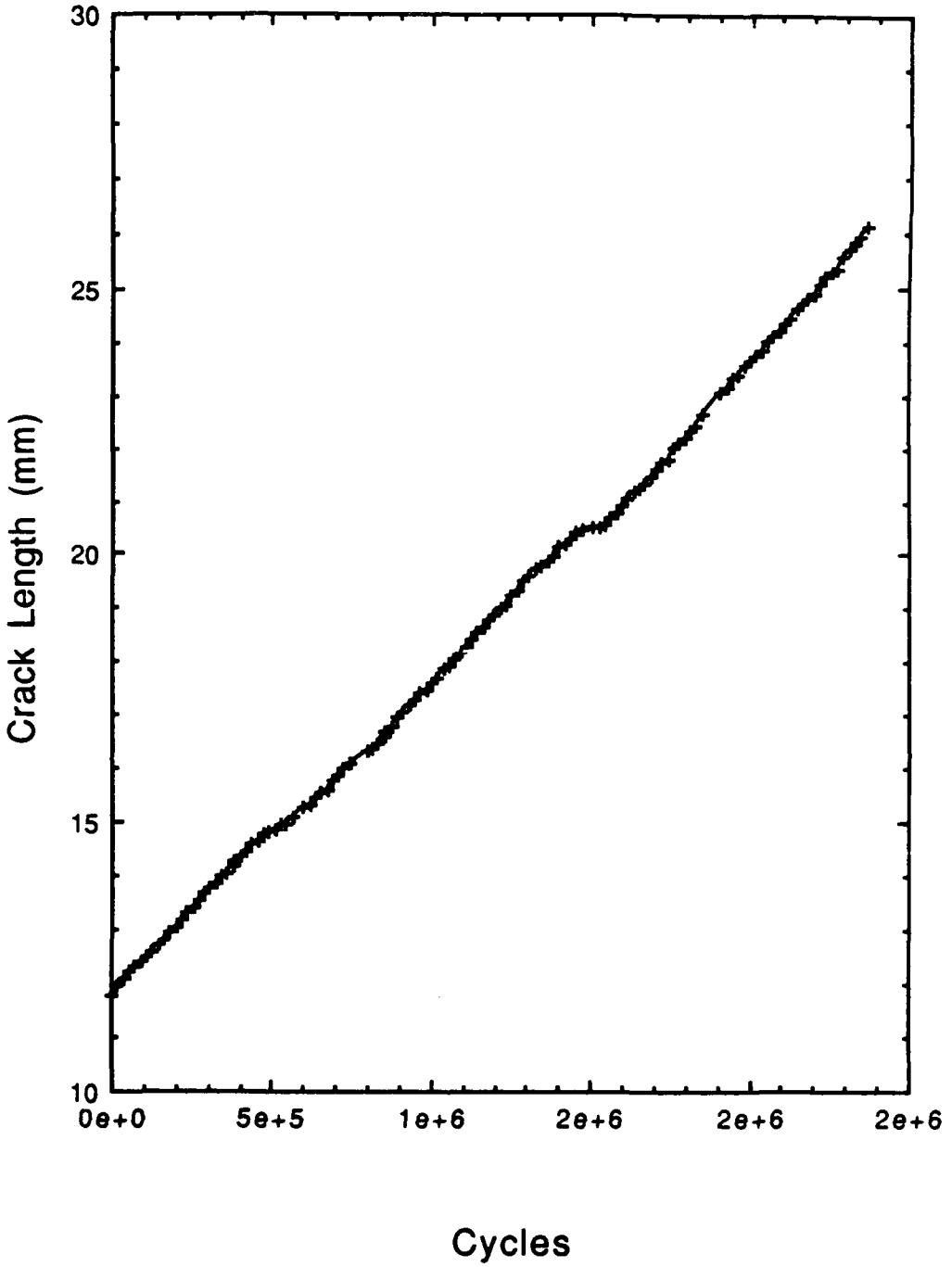

Figure C-6. Crack Length vs Cycles: Test #6

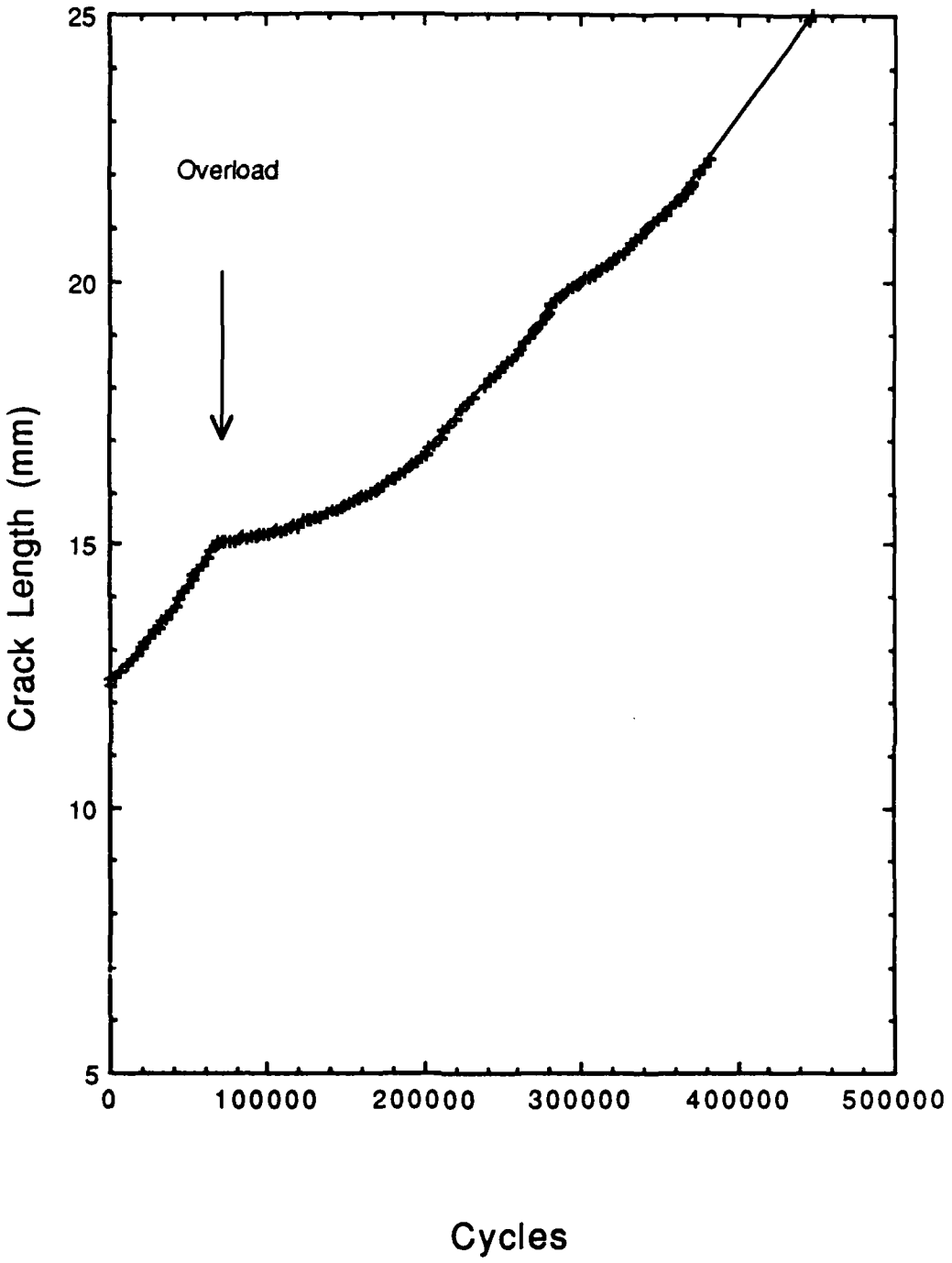

Figure C-7. Crack Length vs Cycles: Test #7

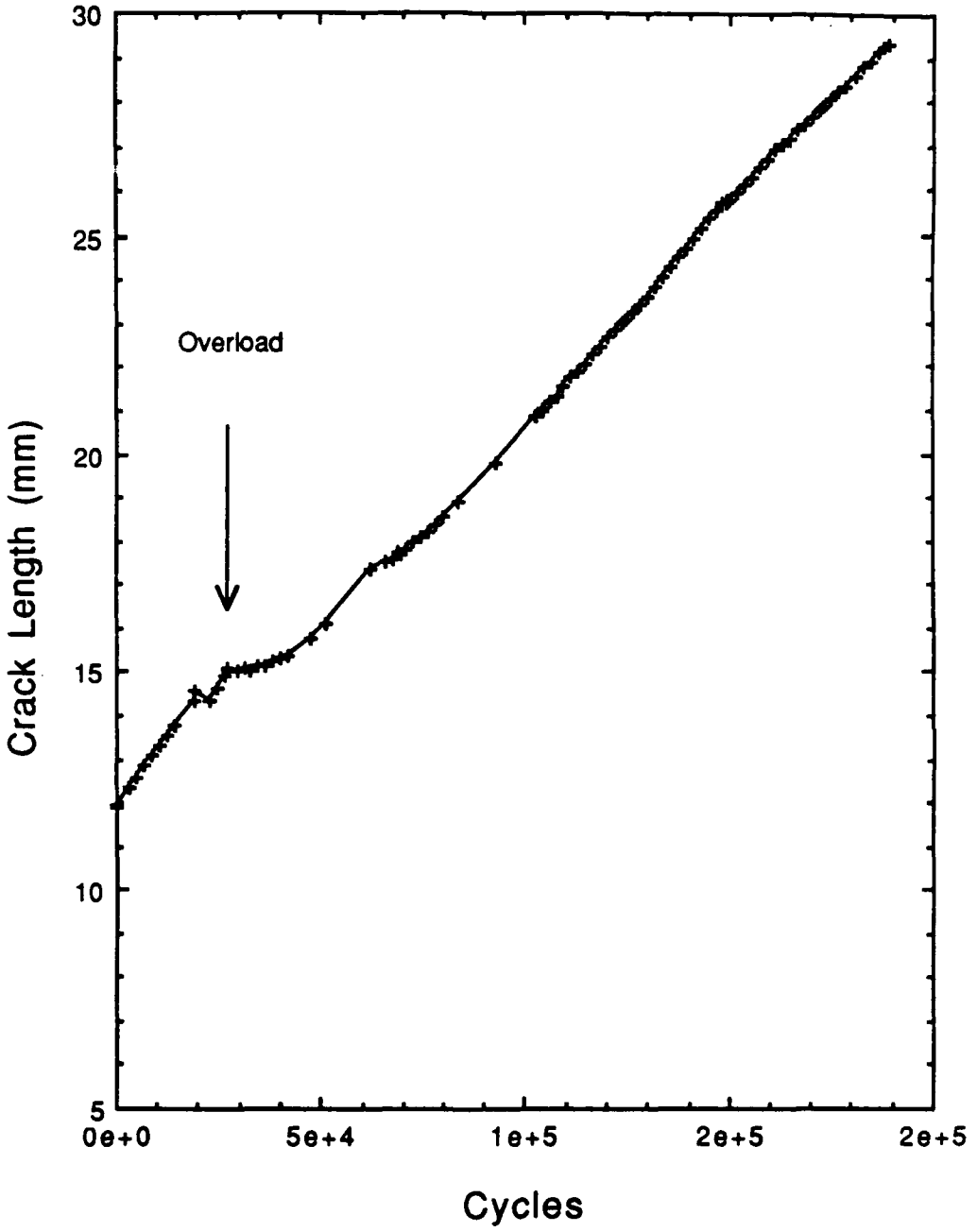

Figure C-8. Crack Length vs Cycles: Test #8

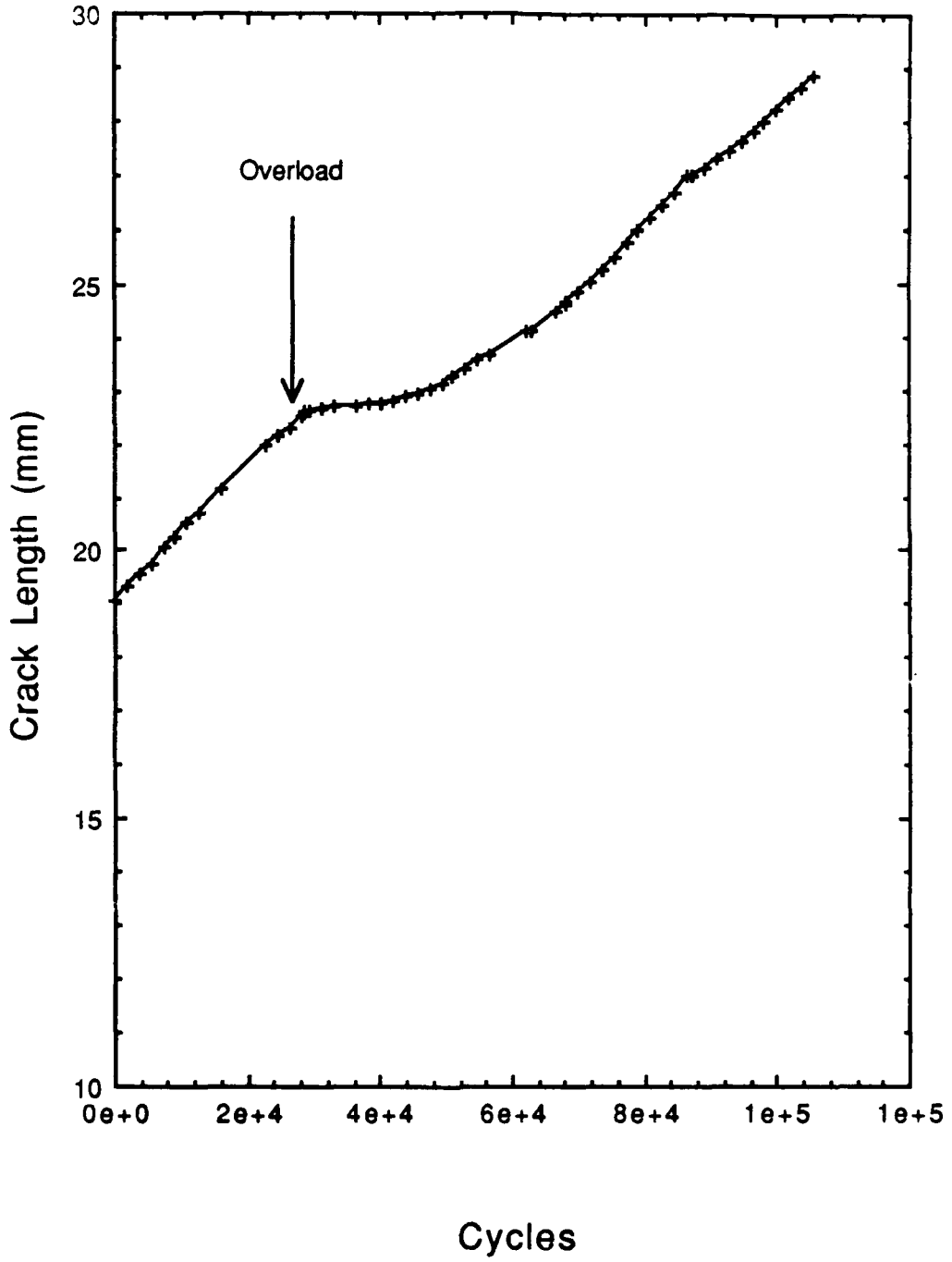

Figure C-9. Crack Length vs Cycles: Test #9

Appendix D: Crack Growth Rates for Tests Involving Overloads

The graphs in this appendix depict the crack growth rates as a function of crack length for the tests that involved overloads. For clarity, the distance has been adjusted so that the overload occurs at 0.0 mm. The title of the graph contains the information about the crack length at which the overload was applied.

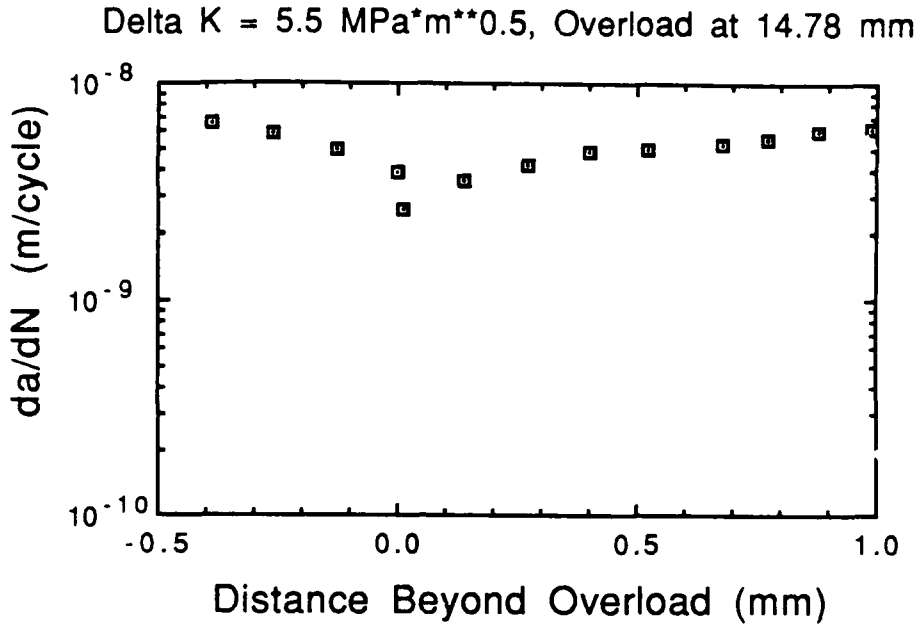

Figure D-1a. Crack Growth Rate vs. Crack Length, Test #6 (ΔK = 5.5 MPa$\sqrt{m}$, Overload at 14.78 mm)

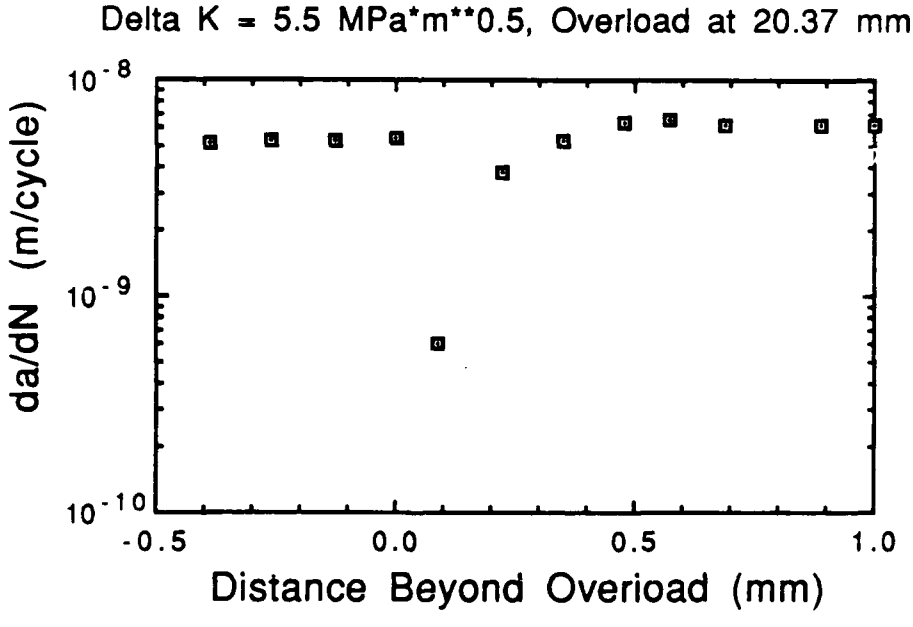

Figure D-1b. Crack Growth Rate vs. Crack Length, Test #6 (ΔK = 5.5 MPa$\sqrt{m}$, Overload at 20.37 mm)

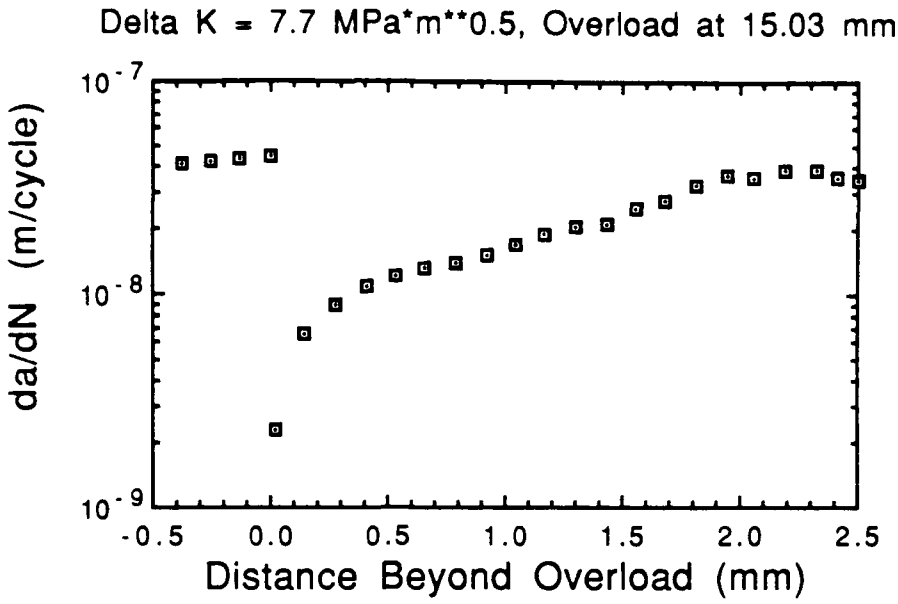

Figure D-2. Crack Growth Rate vs. Crack Length, Test #7 (ΔK = 7.7 MPa$\sqrt{m}$, Overload at 15.03 mm)

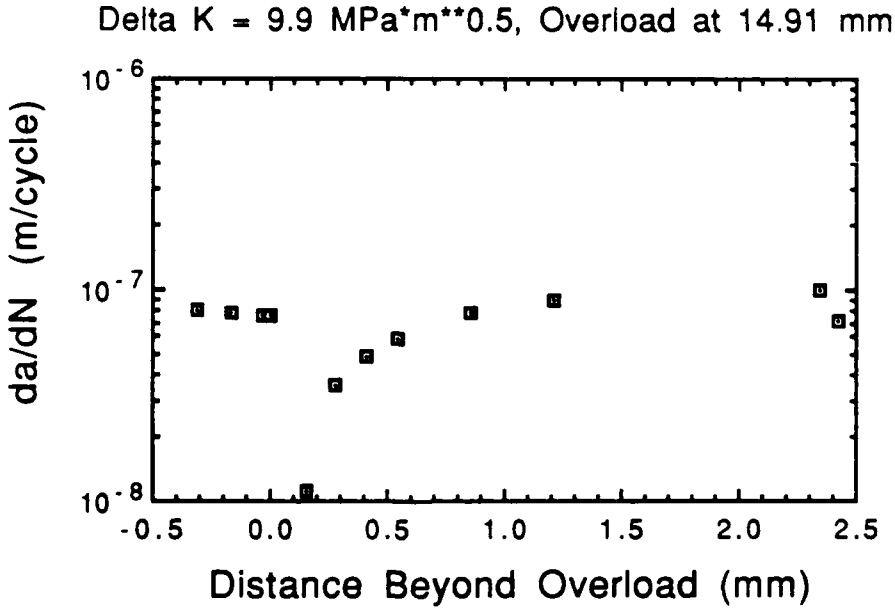

Figure D-3. Crack Growth Rate vs. Crack Length, Test #8 (ΔK = 9.9 MPa$\sqrt{m}$, Overload at 14.91 mm)

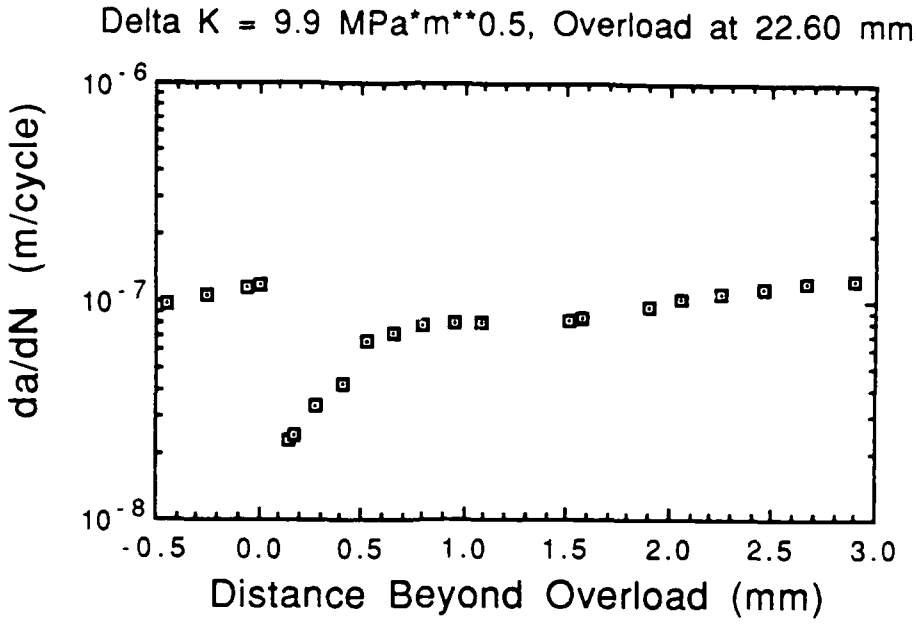

Figure D-4. Crack Growth Rate vs. Crack Length, Test #9 (ΔK = 9.9 MPa$\sqrt{m}$, Overload at 22.60 mm)

Appendix E: P_{cl}/P_{max} (IDG) Vs Distance Beyond Indents

The graphs in this appendix depict the P_{cl}/P_{max} value for closure measured by the laser IDG plotted against the distance beyond the microhardness indents at which the measurement was taken.

In the baseline fatigue tests, identifiable trends in P_{cl}/P_{max} were evident for most segments of crack growth. In the fatigue tests that involved overloads, some segments of crack growth prior to and after the segment involving the overload showed distinct trends in P_{cl}/P_{max} as well.

In cases where possible, a second order regression was fit to the data; the equation of the regression is shown underneath the graph.

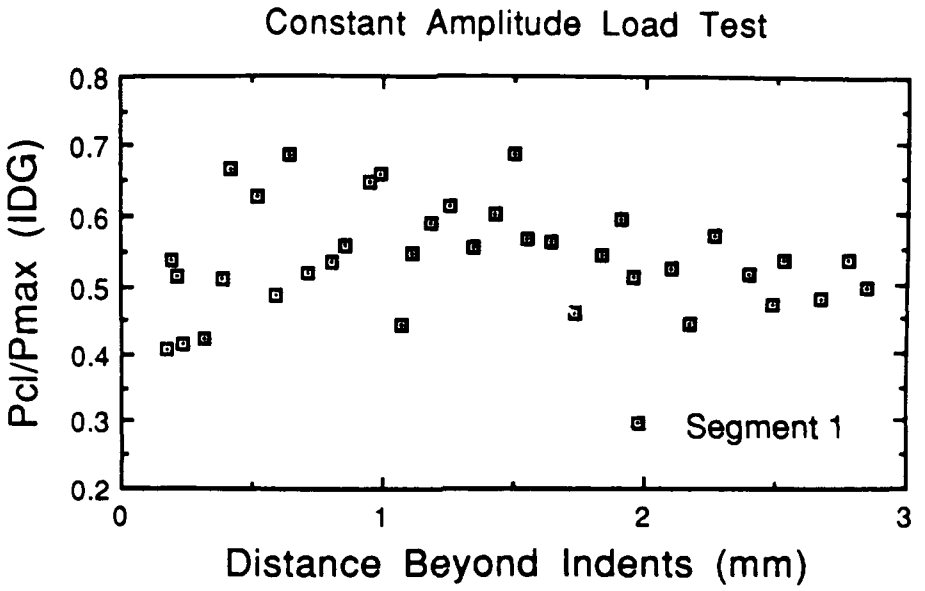

Figure E-1. Test #1, Constant Maximum Amplitude Load Test, Crack Growth Segment 1

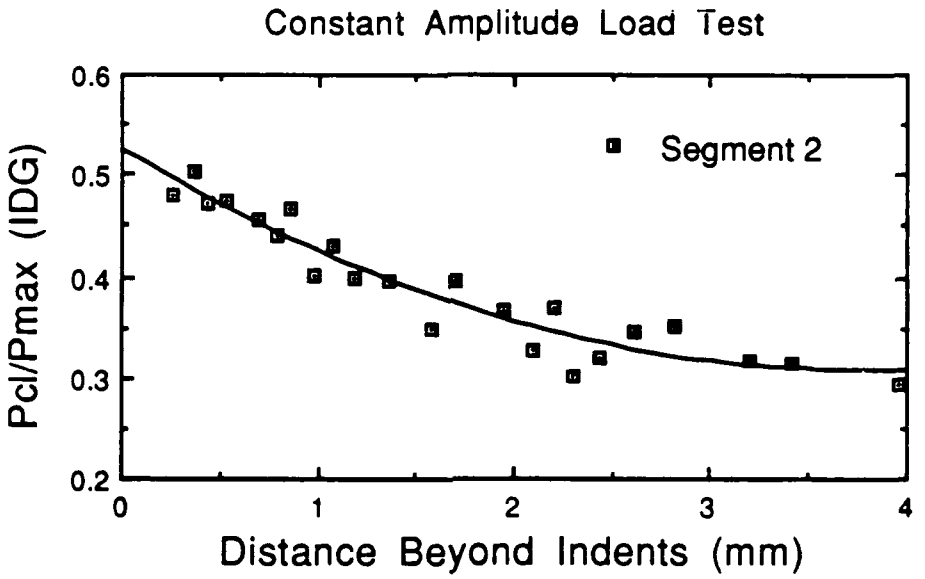

$y = 0.52526 - 0.11522x + 1.5219e\text{-}2x^2 \quad R^2 = 0.906$

Figure E-2. Test #1, Constant Maximum Amplitude Load Test, Crack Growth Segment 2

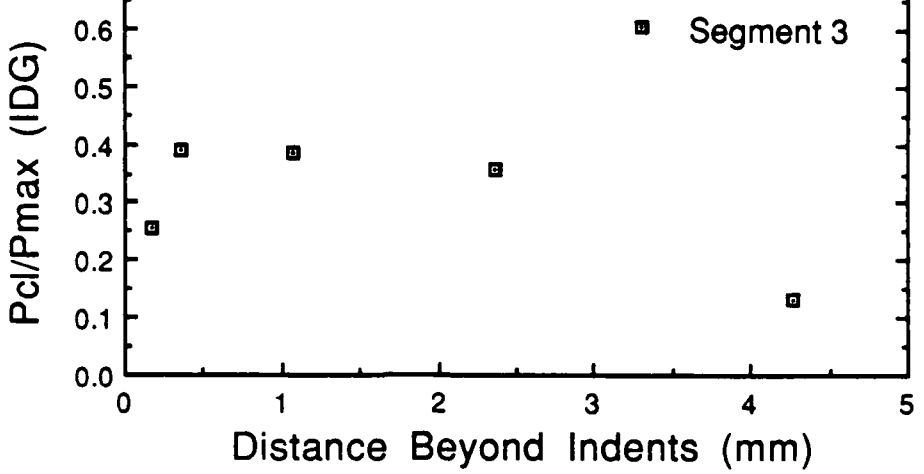

Figure E-3. Test #1, Constant Maximum Amplitude Load Test, Crack Growth Segment 3

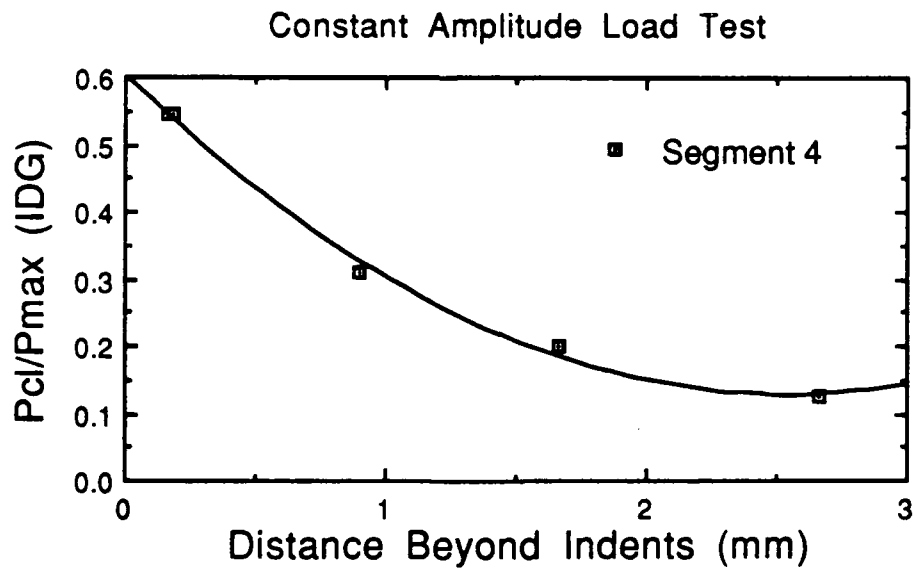

$y = 0.60457 - 0.37589x + 7.3971e\text{-}2x^2 \quad R^2 = 0.995$

Figure E-4. Test #1, Constant Maximum Amplitude Load Test, Crack Growth Segment 4

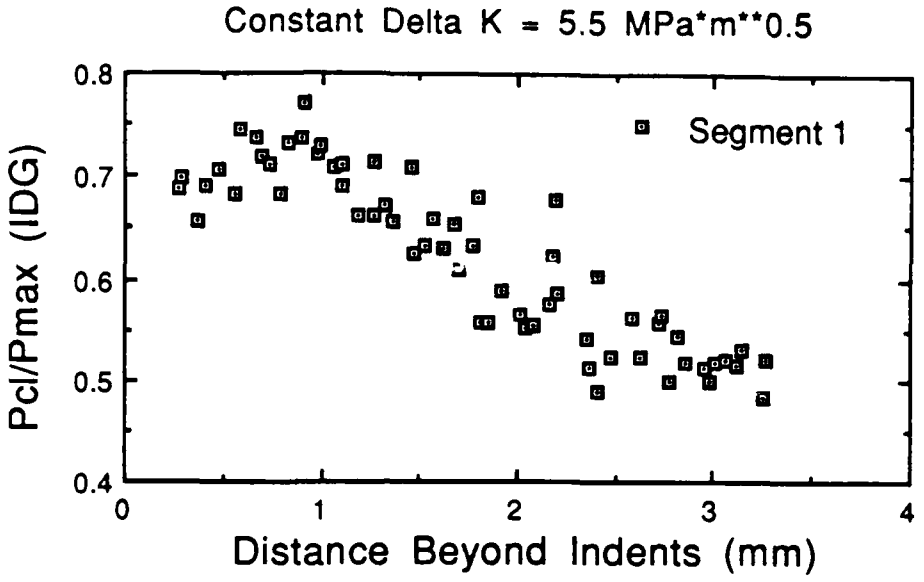

Figure E-5. Test #3, ΔK = 5.5 MPa$\sqrt{m}$, Crack Growth Segment 1

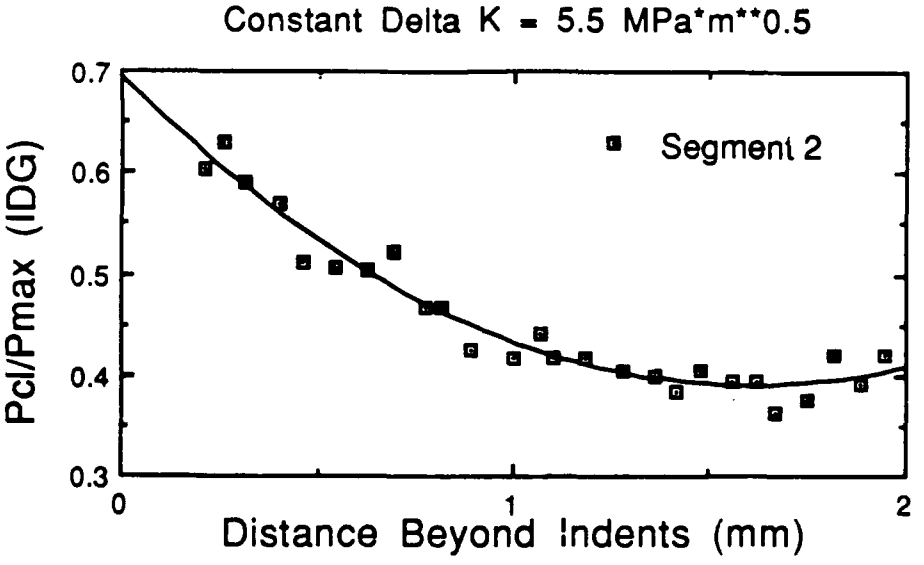

y = 0.69375 - 0.37967x + 0.11833x^2 R^2 = 0.951

Figure E-6. Test #3, ΔK = 5.5 MPa$\sqrt{m}$, Crack Growth Segment 2

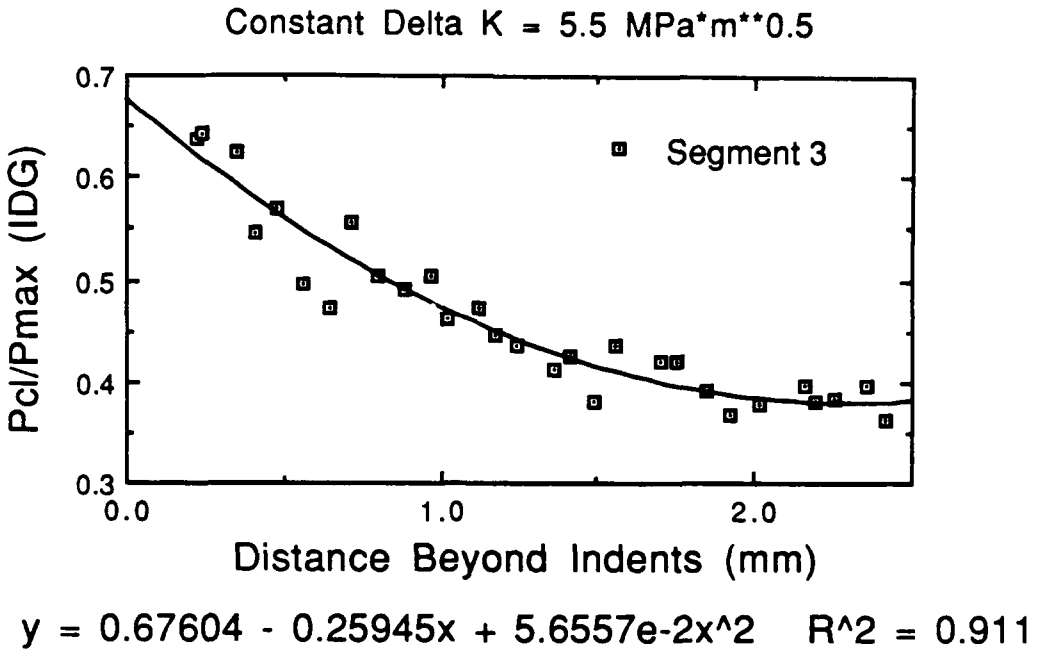

Figure E-7. Test #3, ΔK = 5.5 MPa$\sqrt{m}$, Crack Growth Segment 3

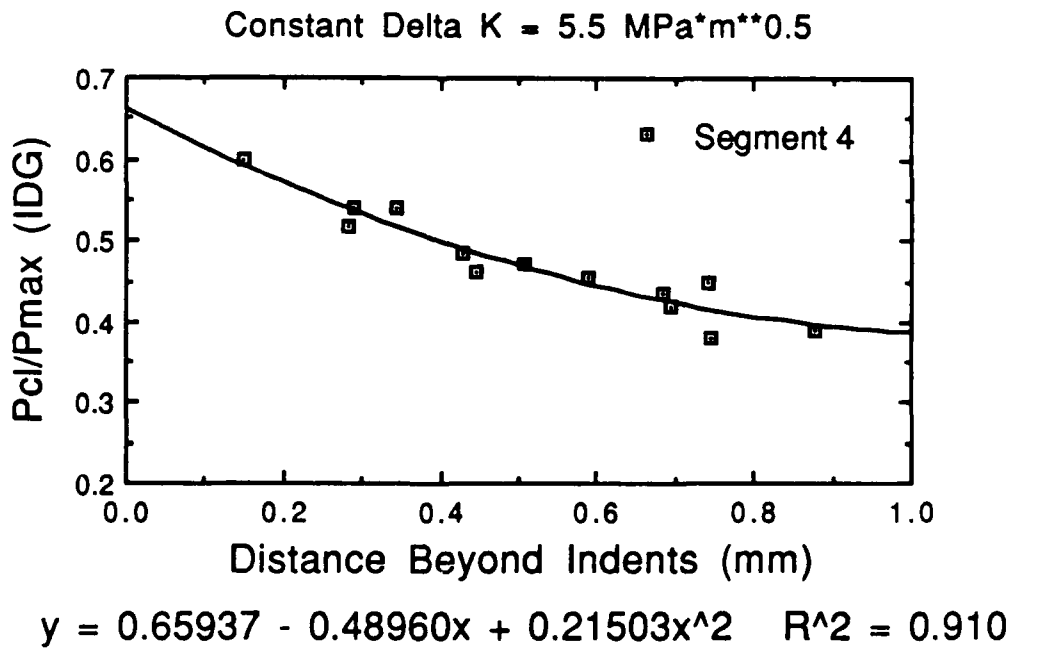

Figure E-8. Test #3, ΔK = 5.5 MPa$\sqrt{m}$, Crack Growth Segment 4

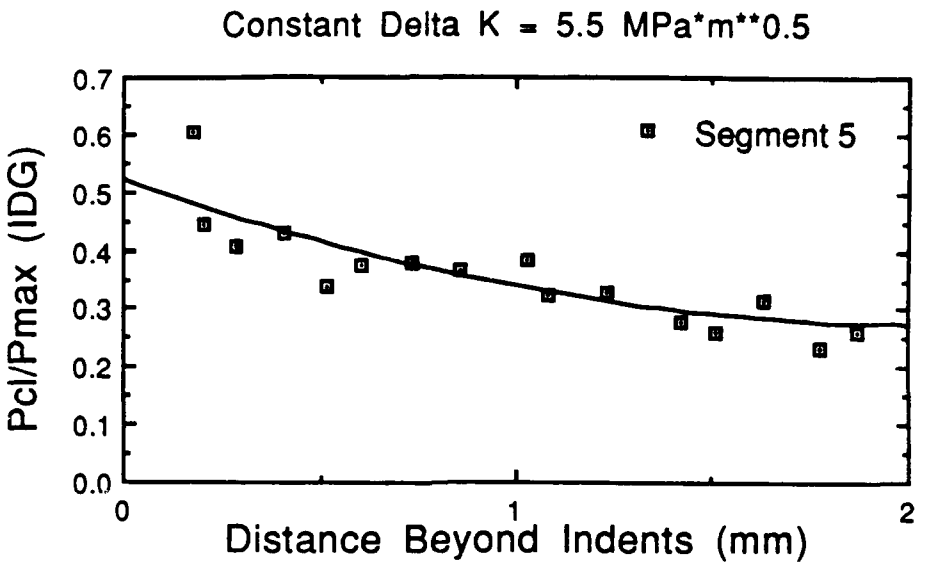

Figure E-9. Test #3, ΔK = 5.5 MPa$\sqrt{m}$, Crack Growth Segment 5

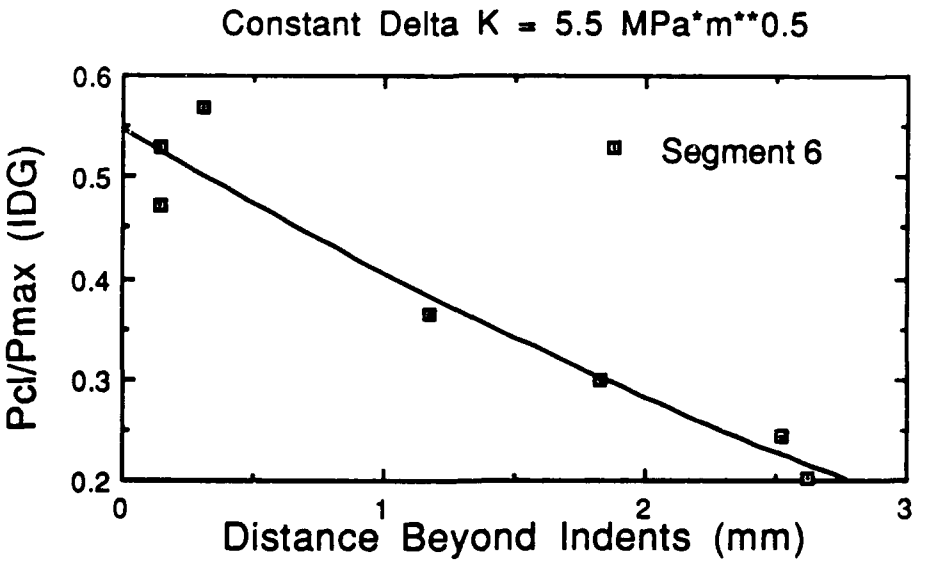

Figure E-10. Test #3, ΔK = 5.5 MPa$\sqrt{m}$, Crack Growth Segment 6

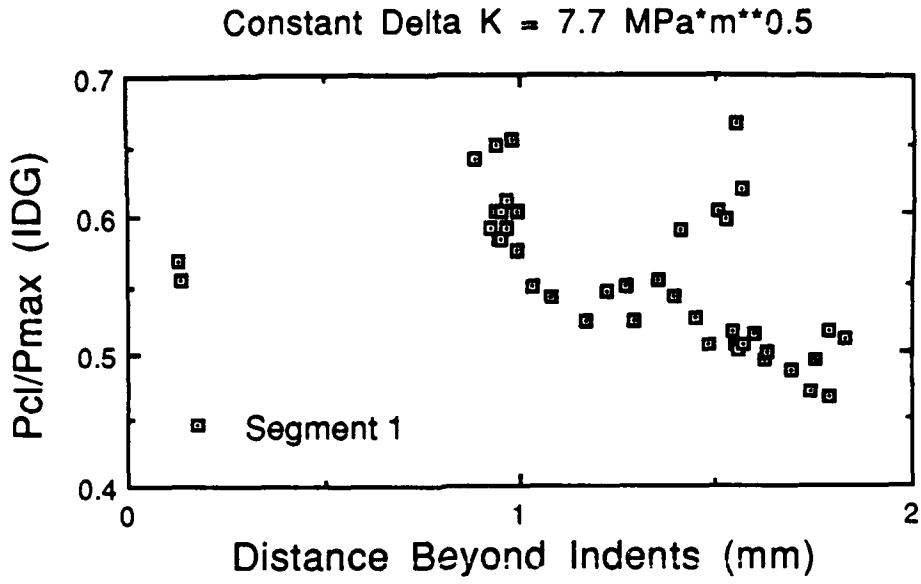

Figure E-11. Test #4, ΔK = 7.7 MPa$\sqrt{m}$, Crack Growth Segment 1

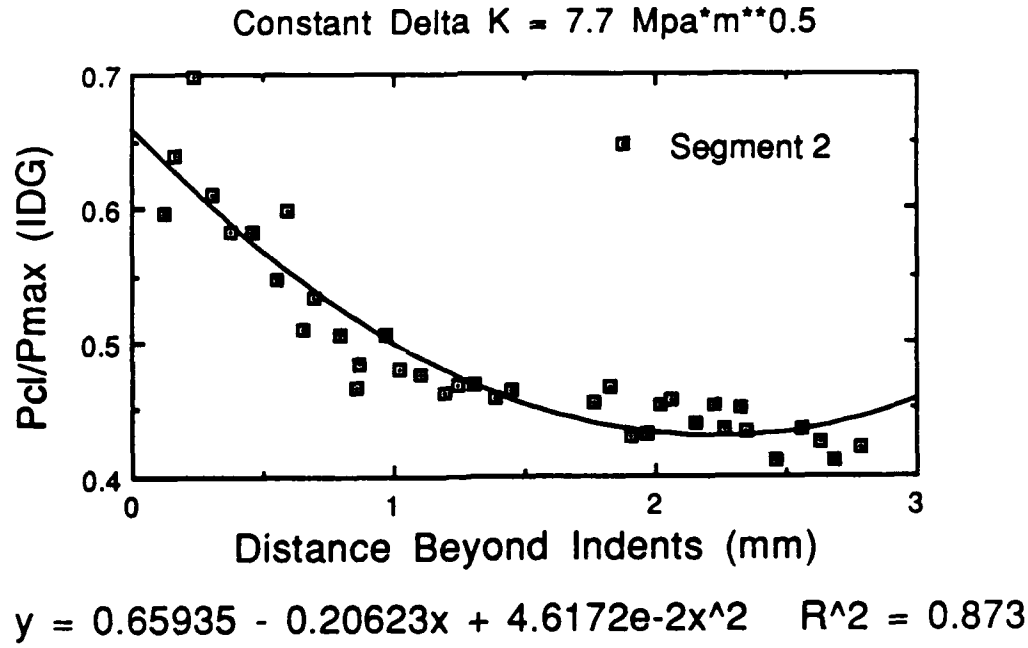

Figure E-12. Test #4, ΔK = 7.7 MPa$\sqrt{m}$, Crack Growth Segment 2

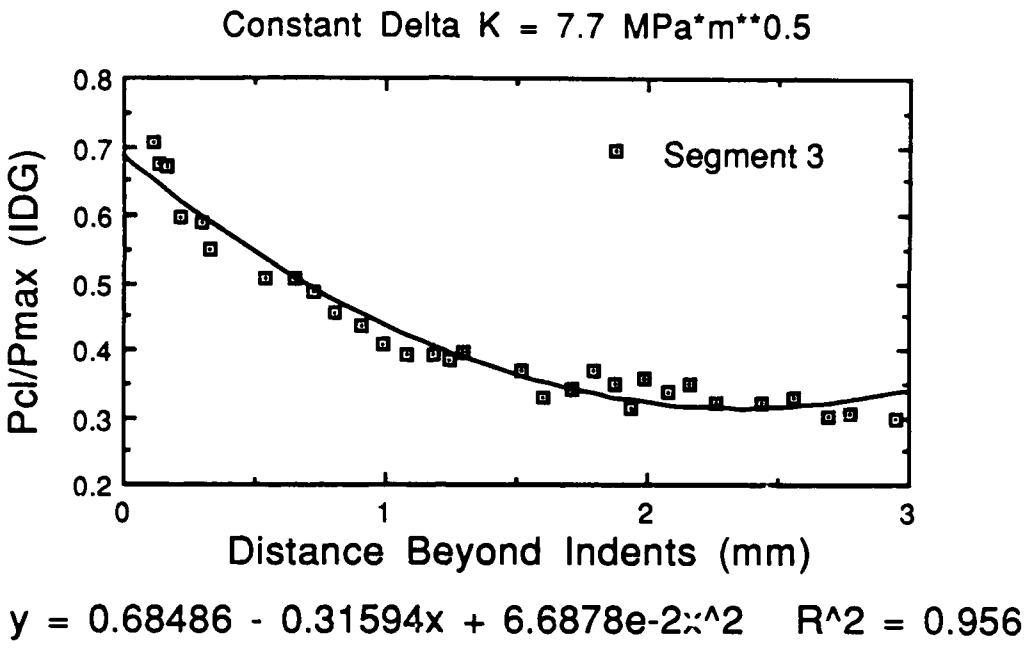

Figure E-13. Test #4, ΔK = 7.7 MPa$\sqrt{m}$, Crack Growth Segment 3

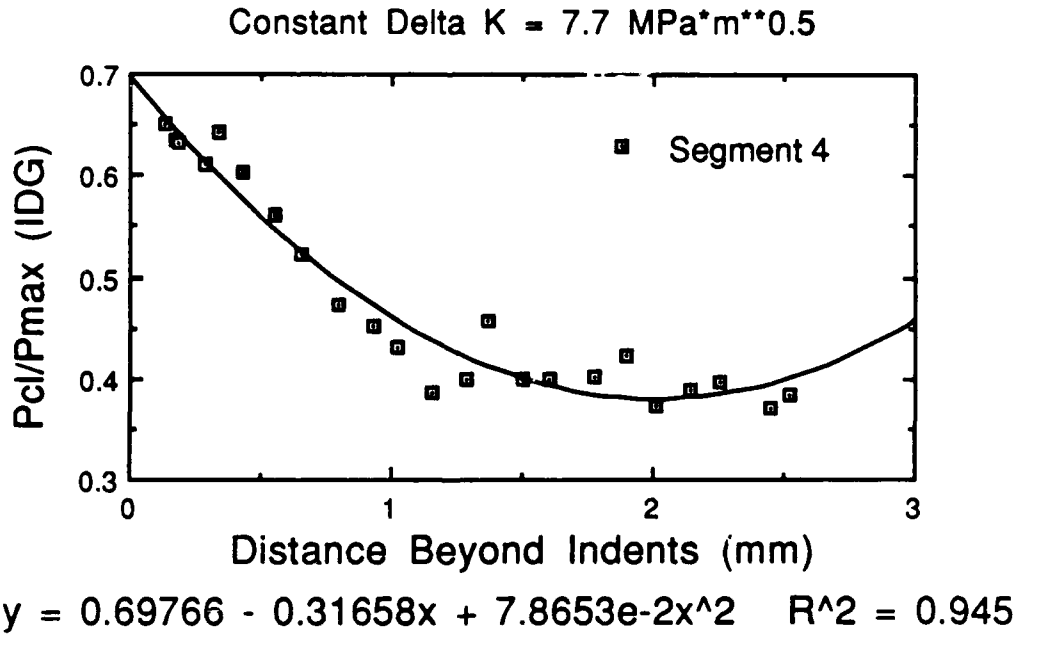

Figure E-14. Test #4, ΔK = 7.7 MPa$\sqrt{m}$, Crack Growth Segment 4

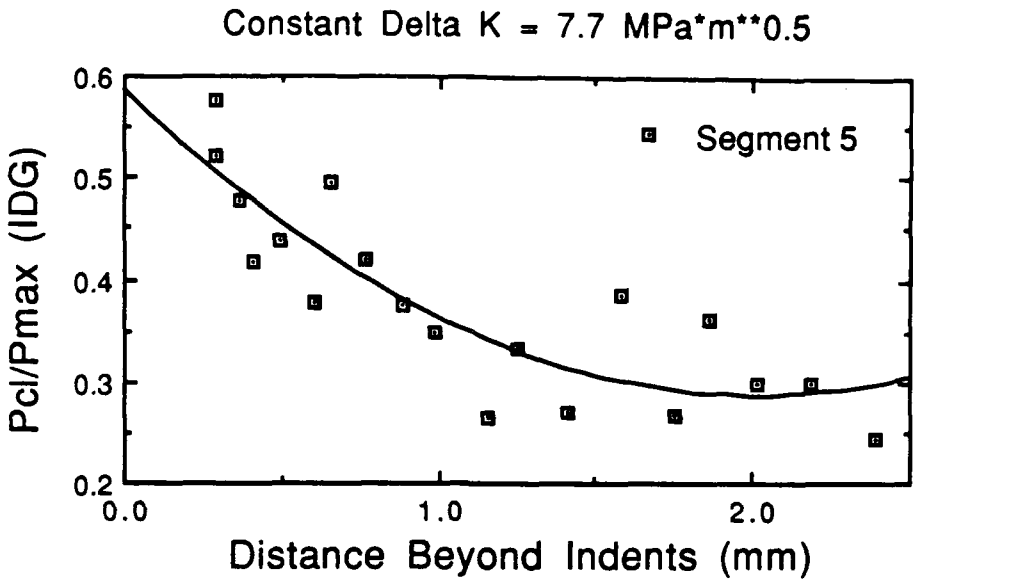

$y = 0.58602 - 0.29722x + 7.3889e\text{-}2x^2 \quad R^2 = 0.735$

Figure E-15. Test #4, $\Delta K = 7.7$ MPa$\sqrt{m}$, Crack Growth Segment 5

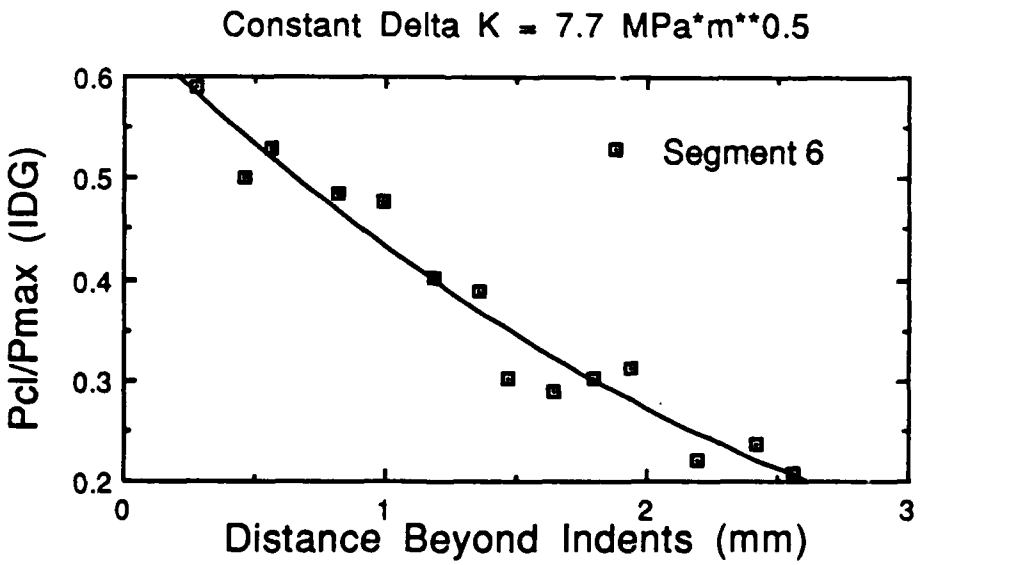

$y = 0.64812 - 0.24350x + 2.7599e\text{-}2x^2 \quad R^2 = 0.952$

Figure E-16. Test #4, $\Delta K = 7.7$ MPa$\sqrt{m}$, Crack Growth Segment 6

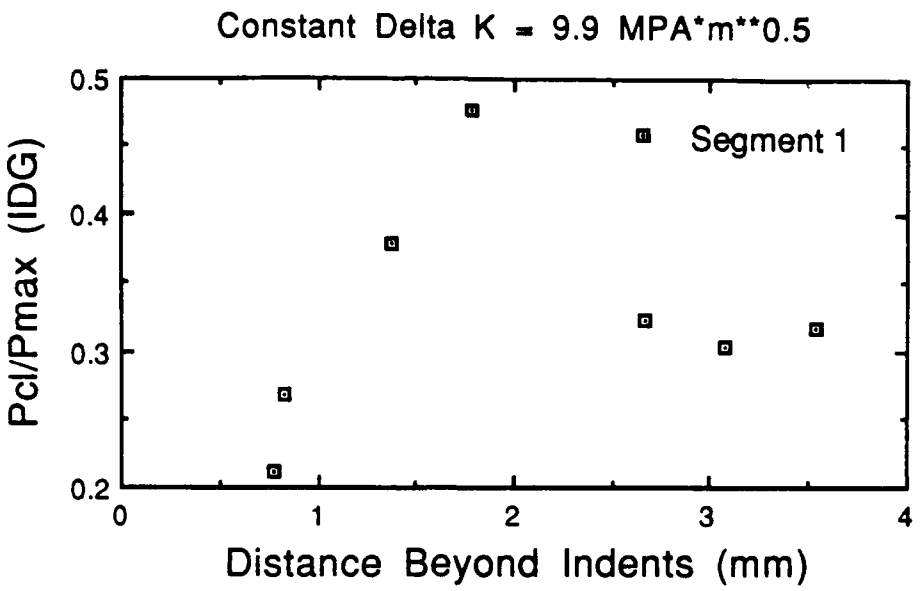

Figure E-17. Test #5, ΔK = 9.9 MPa$\sqrt{m}$, Crack Growth Segment 1

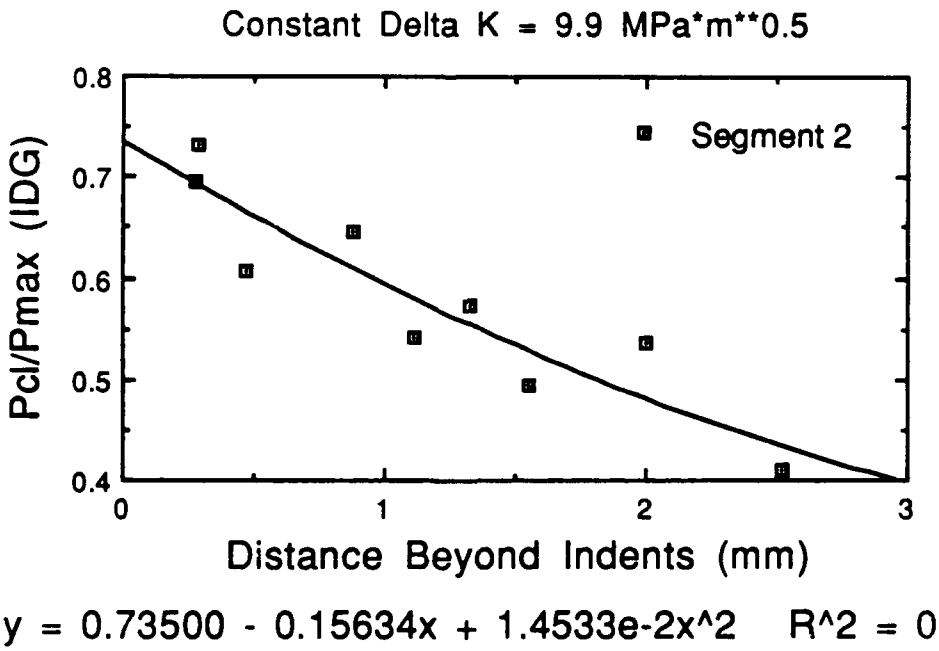

y = 0.73500 - 0.15634x + 1.4533e-2x^2 R^2 = 0.844

Figure E-18. Test #5, ΔK = 9.9 MPa$\sqrt{m}$, Crack Growth Segment 2

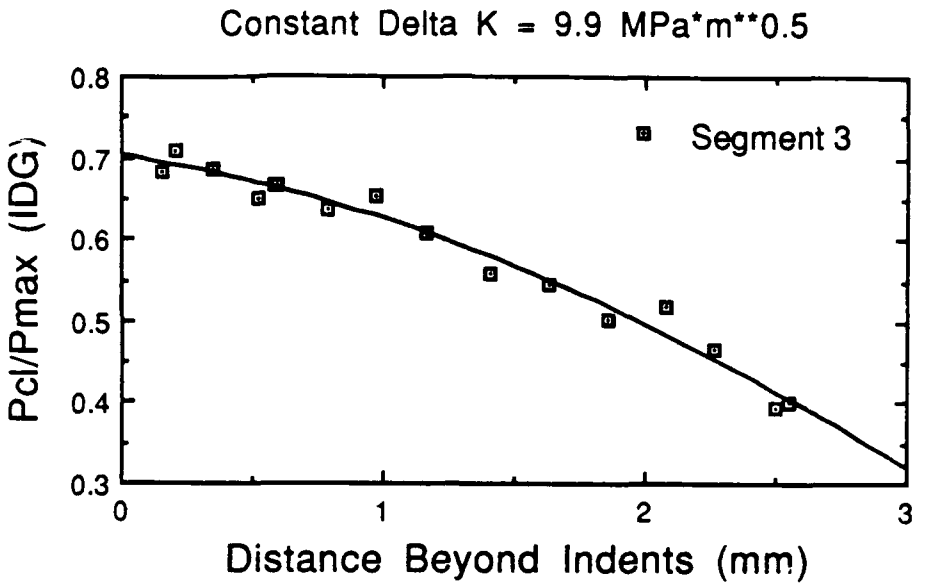

$y = 0.70262 - 5.2925e\text{-}2x - 2.5031e\text{-}2x^2 \quad R^2 = 0.975$

Figure E-19. Test #5, $\Delta K = 9.9$ MPa$\sqrt{m}$, Crack Growth Segment 3

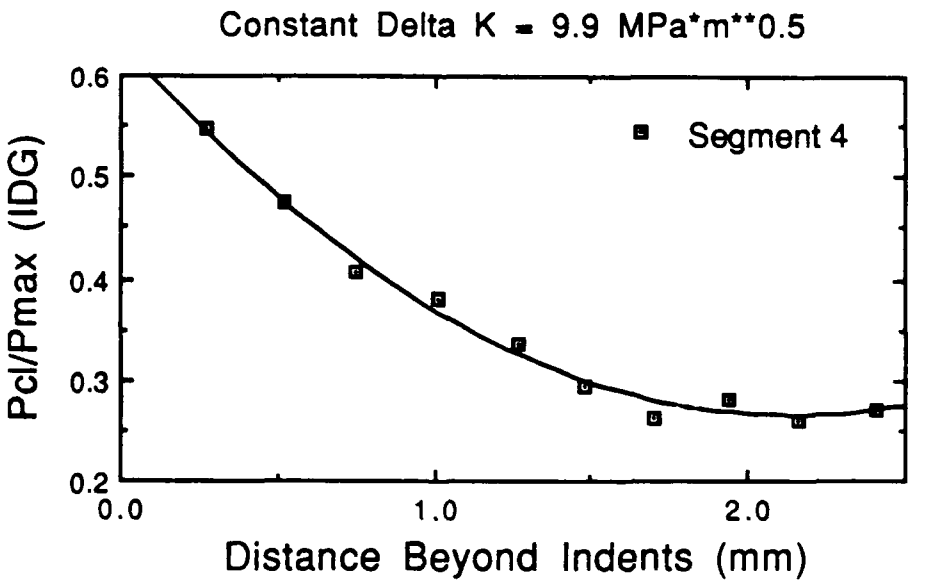

$y = 0.63177 - 0.34312x + 8.0024e\text{-}2x^2 \quad R^2 = 0.988$

Figure E-20. Test #5, $\Delta K = 9.9$ MPa$\sqrt{m}$, Crack Growth Segment 4

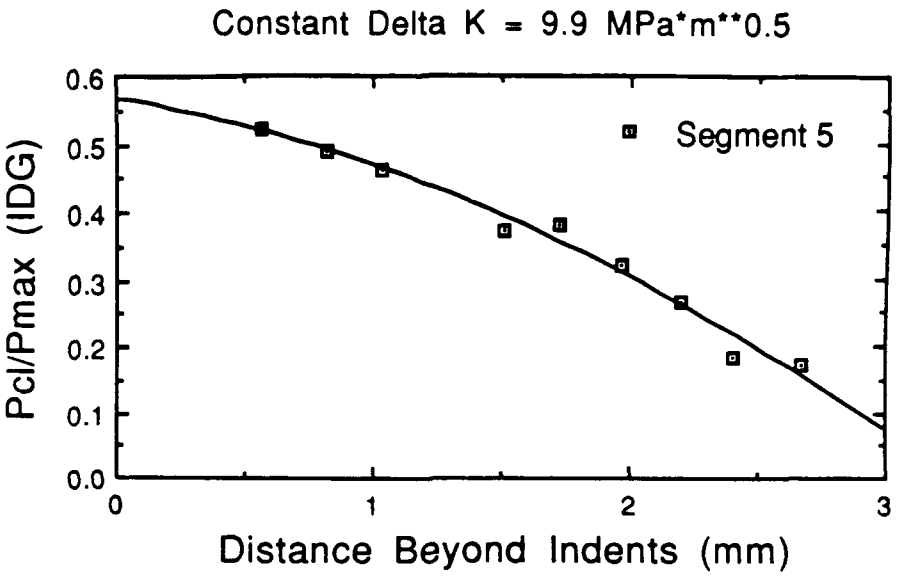

y = 0.56641 - 6.4383e-2x - 3.3277e-2x^2 R^2 = 0.980

Figure E-21. Test #5, ΔK = 9.9 MPa$\sqrt{m}$, Crack Growth Segment 5

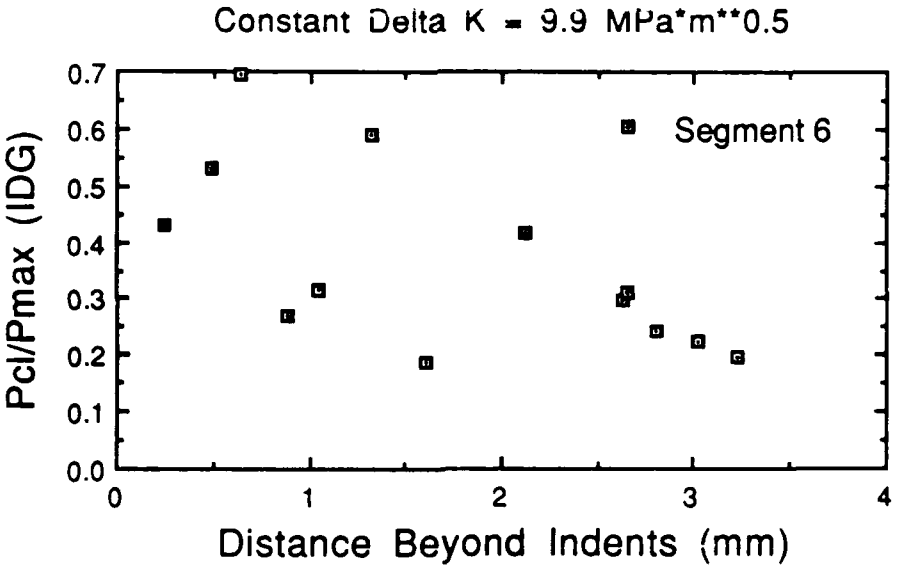

Figure E-22. Test #5, ΔK = 9.9 MPa$\sqrt{m}$, Crack Growth Segment 6

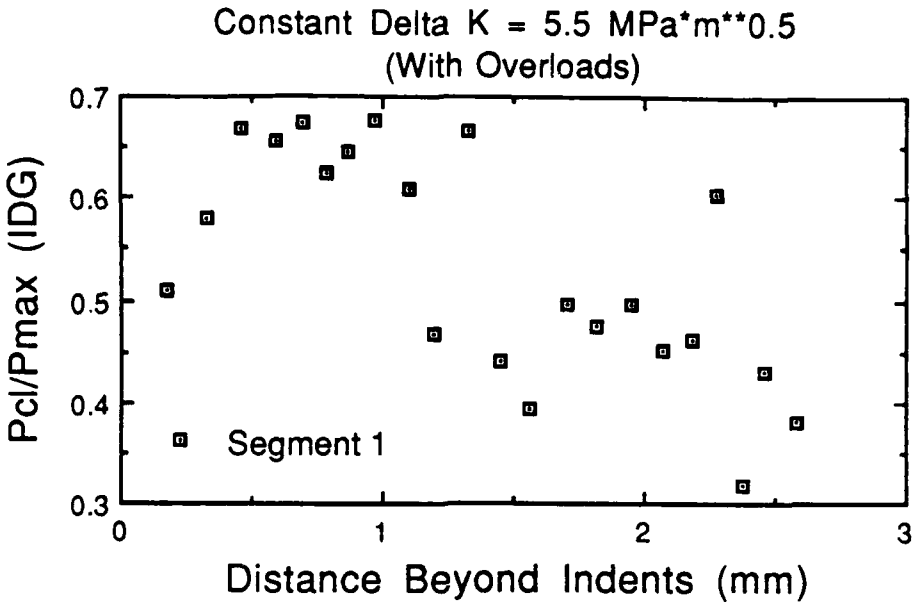

Figure E-23. Test #6, ΔK = 5.5 MPa$\sqrt{m}$, Crack Growth Segment 1

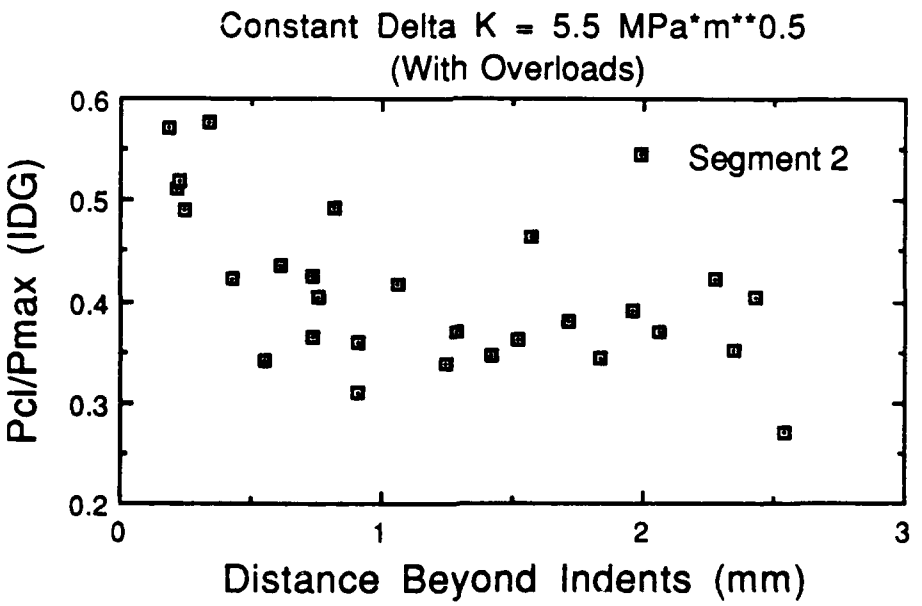

Figure E-24. Test #6, ΔK = 5.5 MPa$\sqrt{m}$, Crack Growth Segment 2

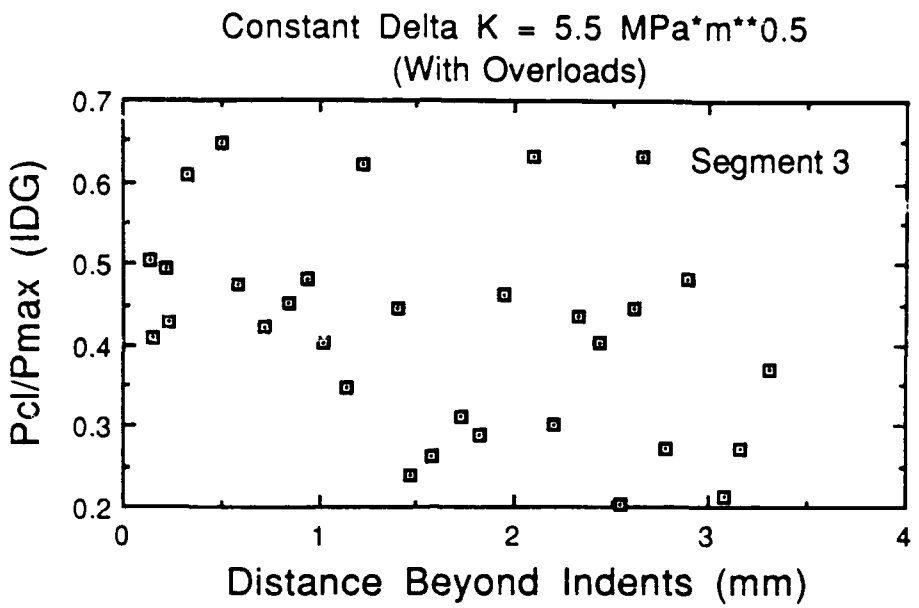

Figure E-25. Test #6, ΔK = 5.5 MPa$\sqrt{m}$, Crack Growth Segment 3

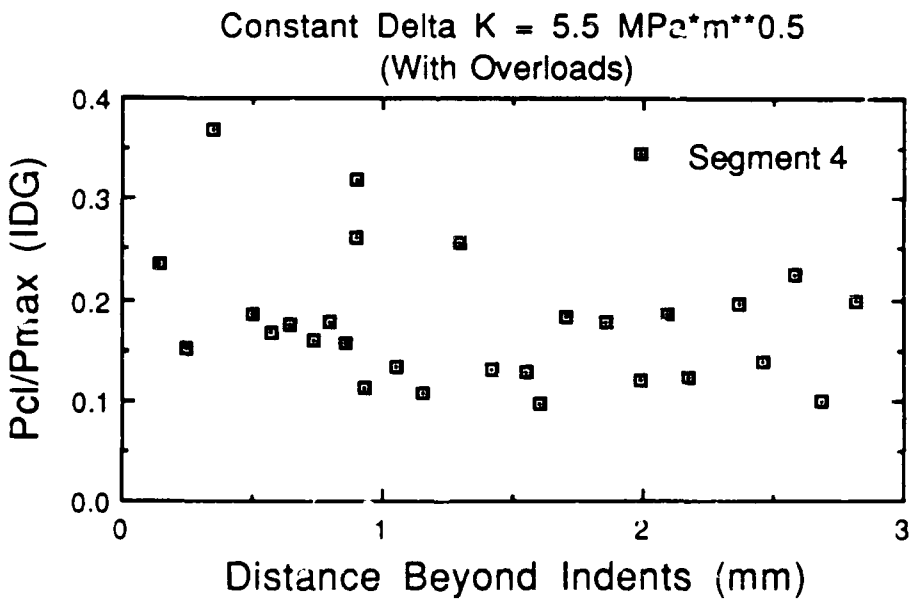

Figure E-26. Test #6, ΔK = 5.5 MPa$\sqrt{m}$, Crack Growth Segment 4

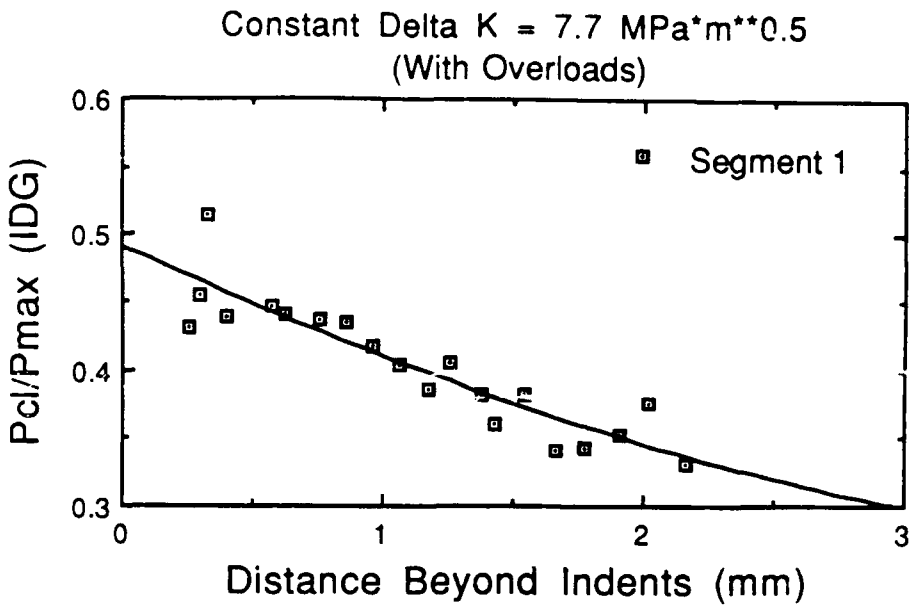

$y = 0.49072 - 8.9092e\text{-}2x + 8.2434e\text{-}3x^2 \quad R^2 = 0.825$

Figure E-27. Test #7, $\Delta K = 7.7$ MPa$\sqrt{m}$, Crack Growth Segment 1

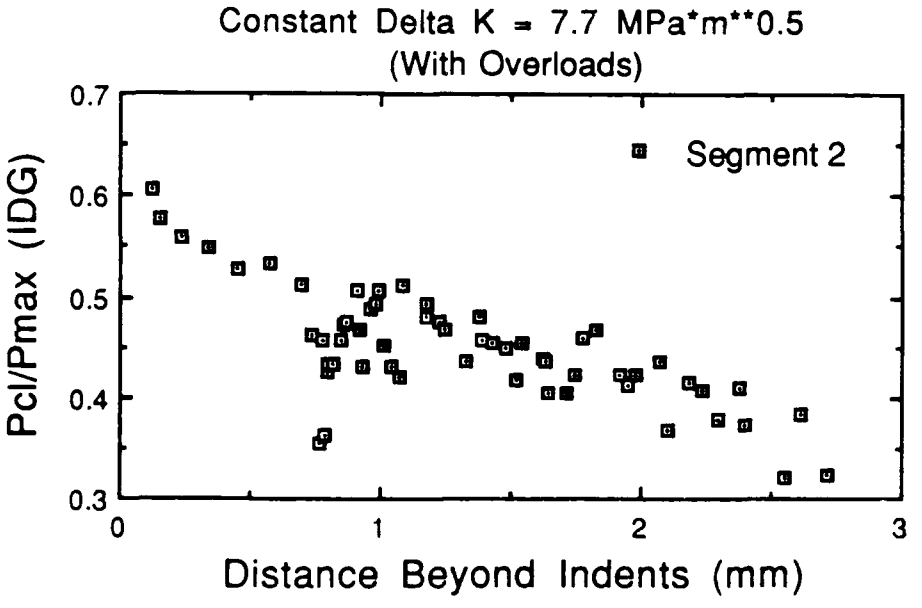

Figure E-28. Test #7, $\Delta K = 7.7$ MPa$\sqrt{m}$, Crack Growth Segment 2

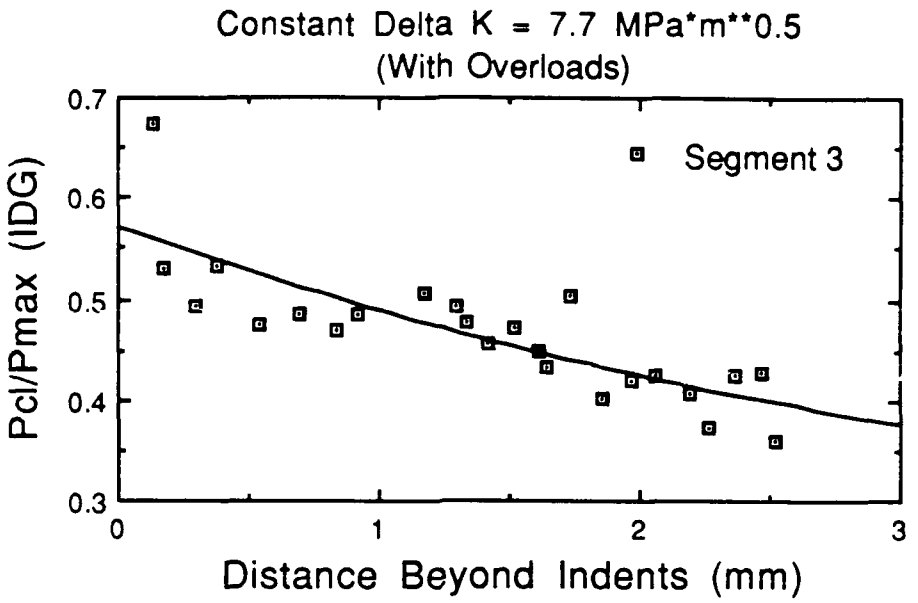

Figure E-29. Test #7, ΔK = 7.7 MPa$\sqrt{m}$, Crack Growth Segment 3

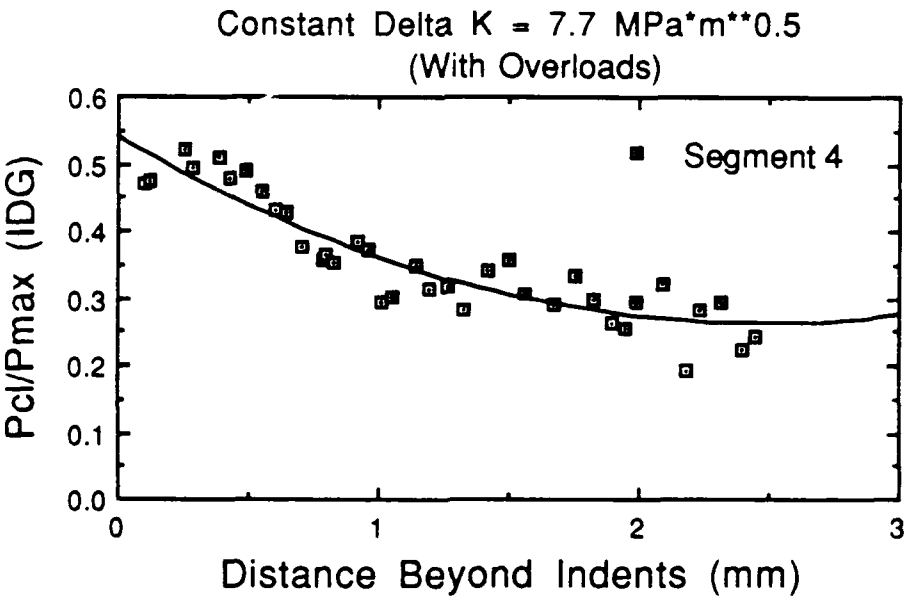

Figure E-30. Test #7, ΔK = 7.7 MPa$\sqrt{m}$, Crack Growth Segment 4

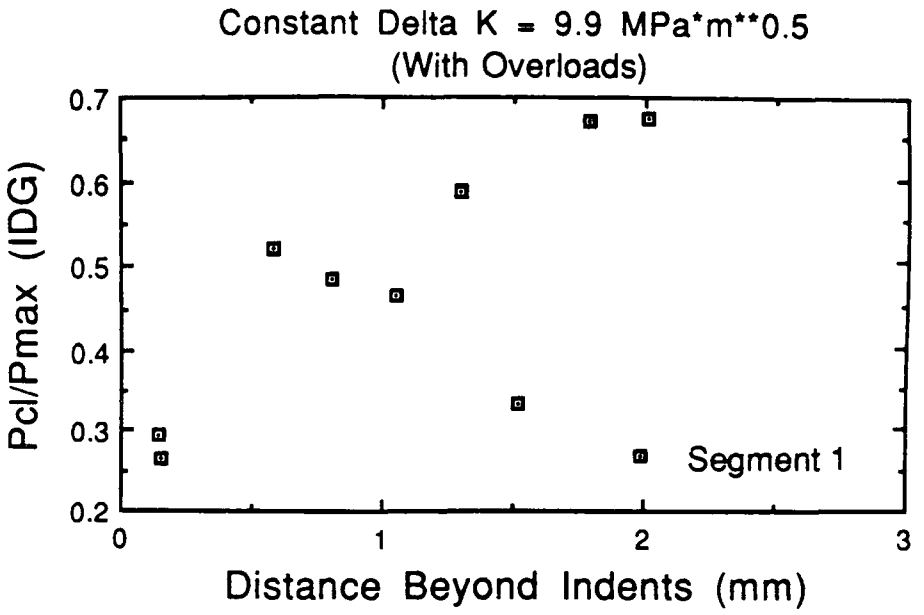

Figure E-31. Test #8, ΔK = 9.9 MPa$\sqrt{m}$, Crack Growth Segment 1

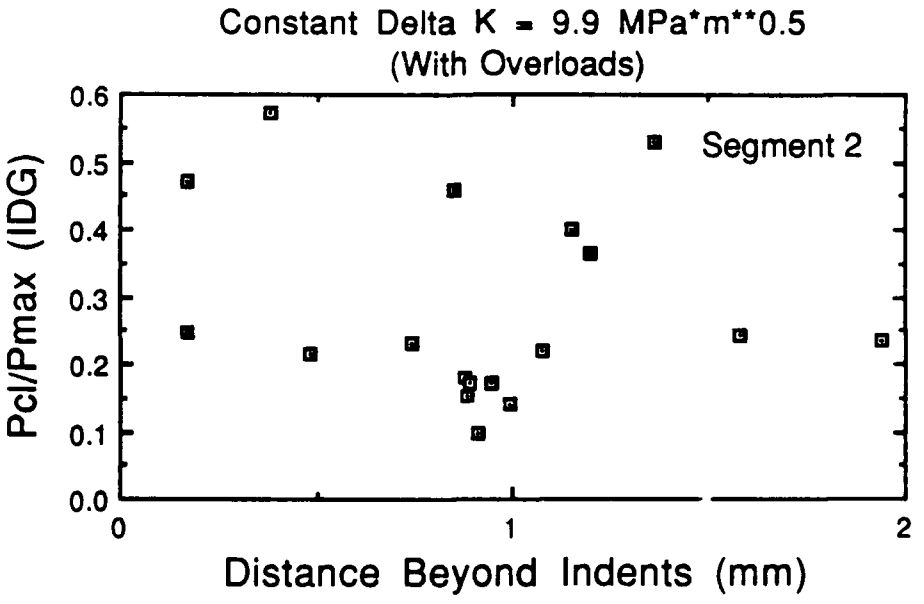

Figure E-32. Test #8, ΔK = 9.9 MPa$\sqrt{m}$, Crack Growth Segment 2

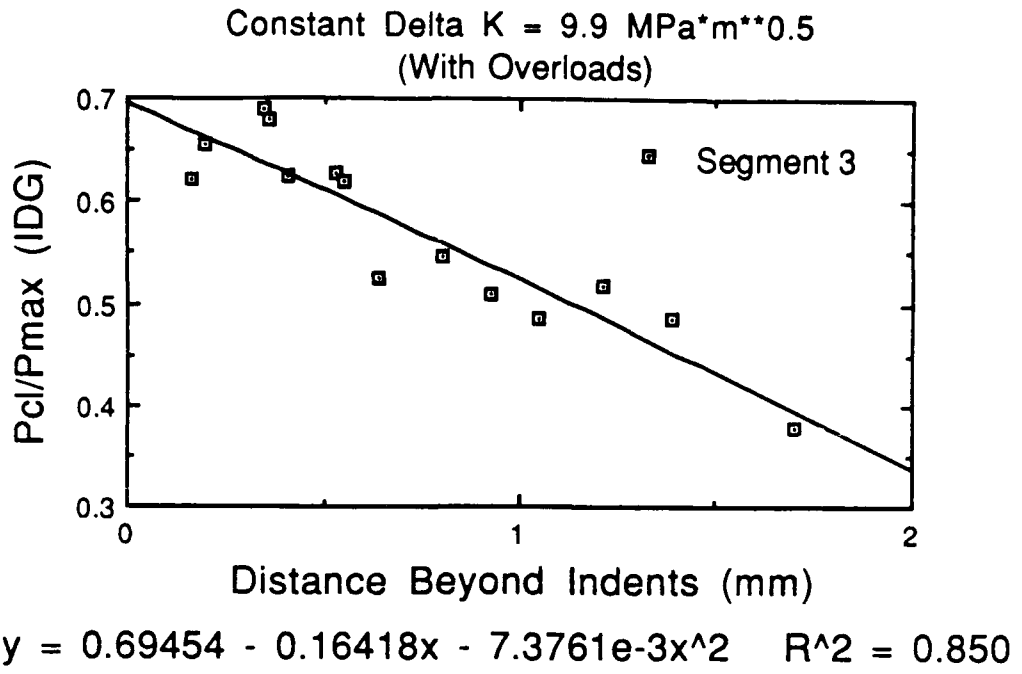

Figure E-33. Test #8, ΔK = 9.9 MPa$\sqrt{m}$, Crack Growth Segment 3

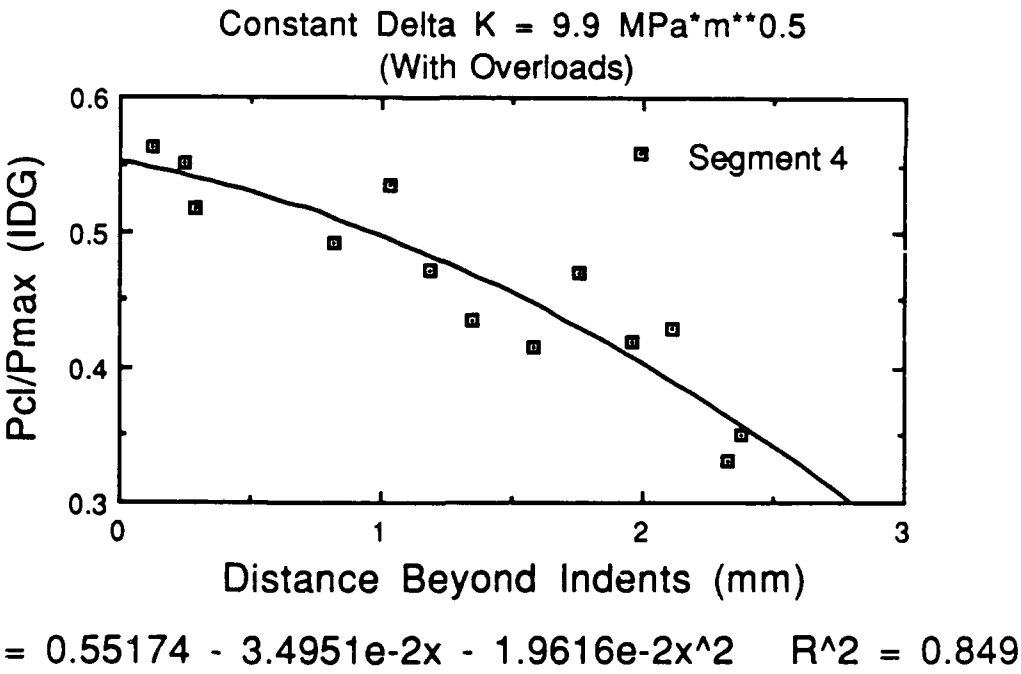

Figure E-34. Test #8, ΔK = 9.9 MPa$\sqrt{m}$, Crack Growth Segment 4

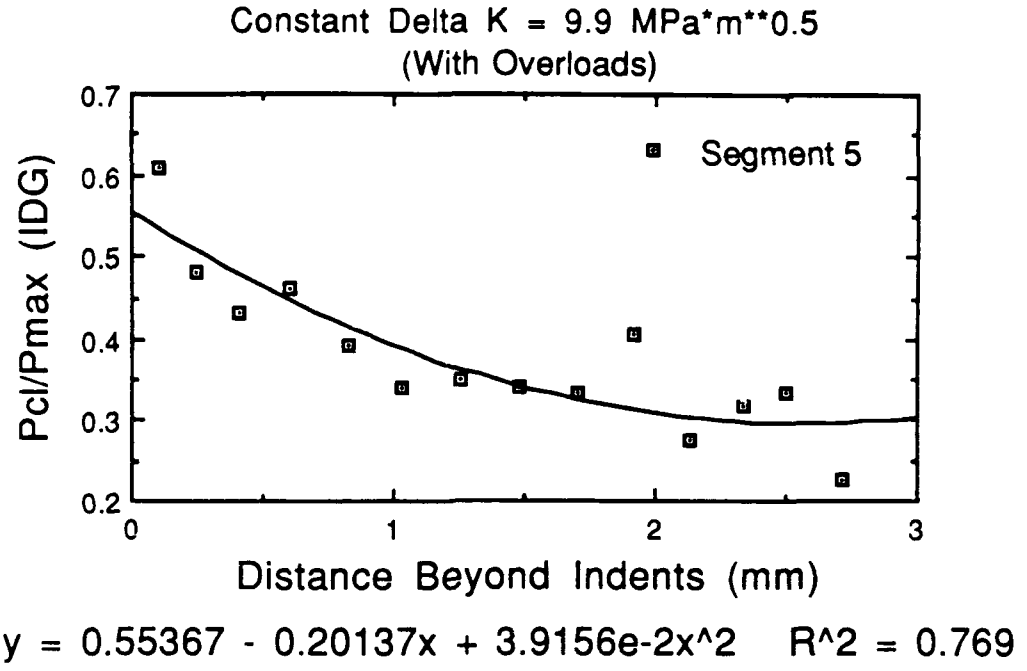

Figure E-35. Test #8, ΔK = 9.9 MPa$\sqrt{m}$, Crack Growth Segment 5

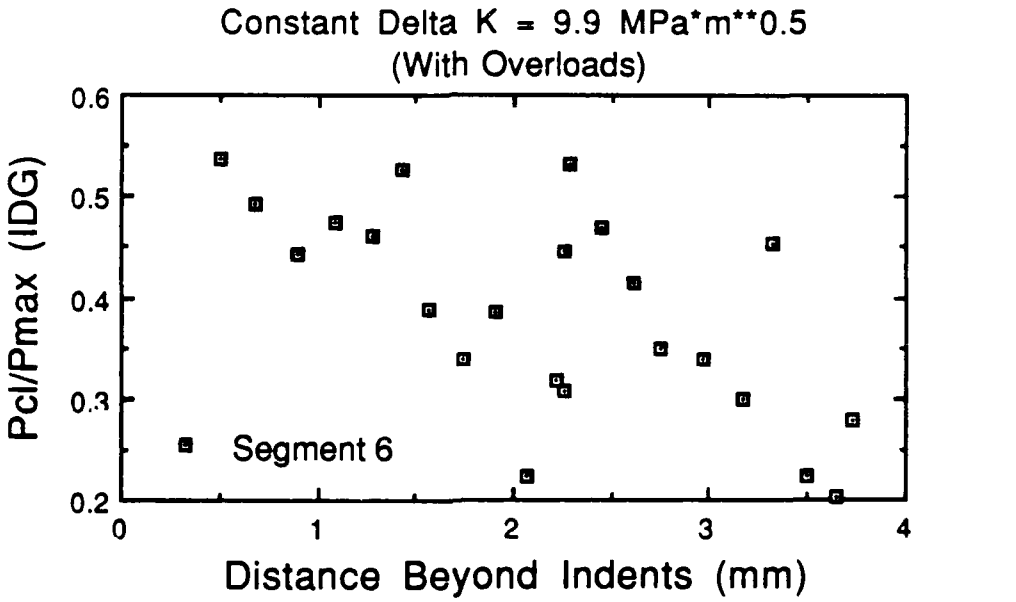

Figure E-36. Test #8, ΔK = 9.9 MPa$\sqrt{m}$, Crack Growth Segment 6

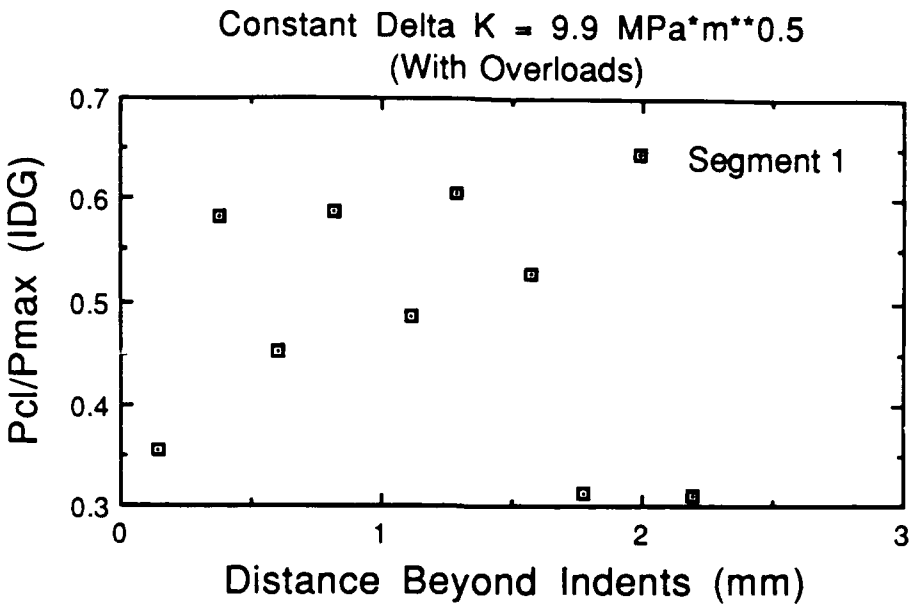

Figure E-37. Test #9, ΔK = 9.9 MPa$\sqrt{m}$, Crack Growth Segment 1

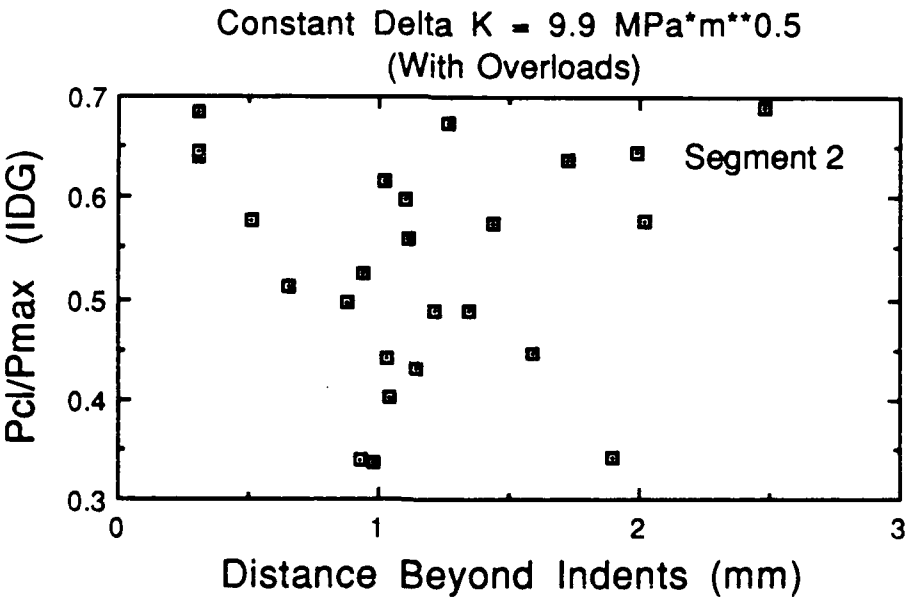

Figure E-38. Test #9, ΔK = 9.9 MPa$\sqrt{m}$, Crack Growth Segment 2

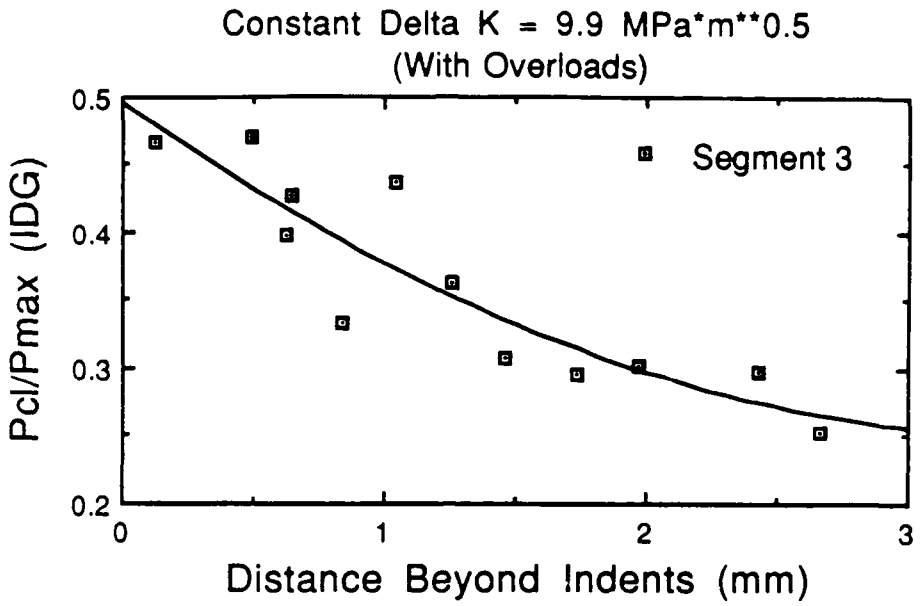

y = 0.49590 - 0.13858x + 1.9508e-2x^2 R^2 = 0.810

Figure E-39. Test #9, ΔK = 9.9 MPa$\sqrt{m}$, Crack Growth Segment 3

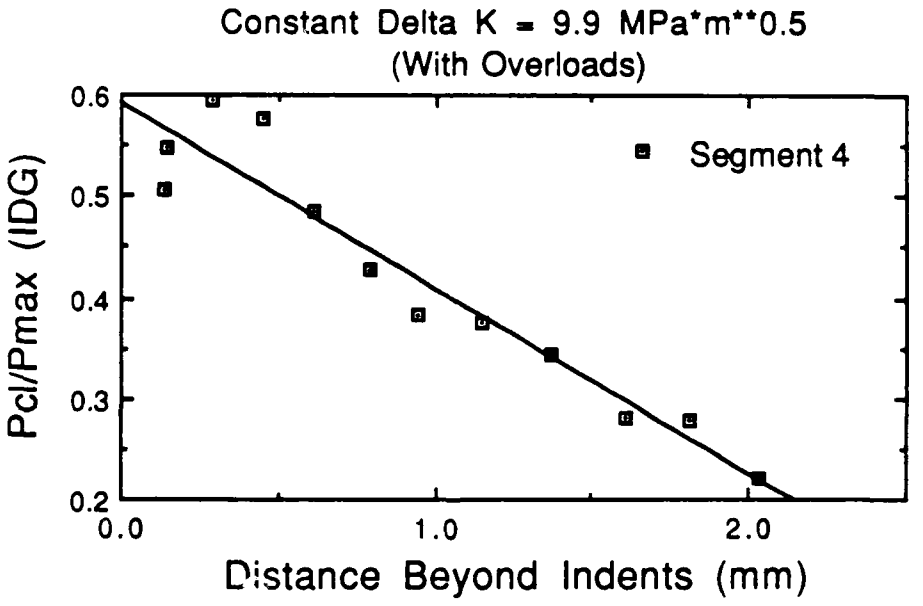

y = 0.59119 - 0.18280x - 1.6053e-4x^2 R^2 = 0.920

Figure E-40. Test #9, ΔK = 9.9 MPa$\sqrt{m}$, Crack Growth Segment 4

Appendix F: Raw Data Comparisons for Fatigue Tests Involving Overloads

The graphs in this appendix are presented in sets of three. The data presented are (from top to bottom): 1) crack growth rate, 2) P_{cl}/P_{max} as measured by the IDG, and 3) P_{cl}/P_{max} as measured by the clip gage. These data are presented as a function of crack length, which has been normalized such that the overload occurs at 0.0 mm.

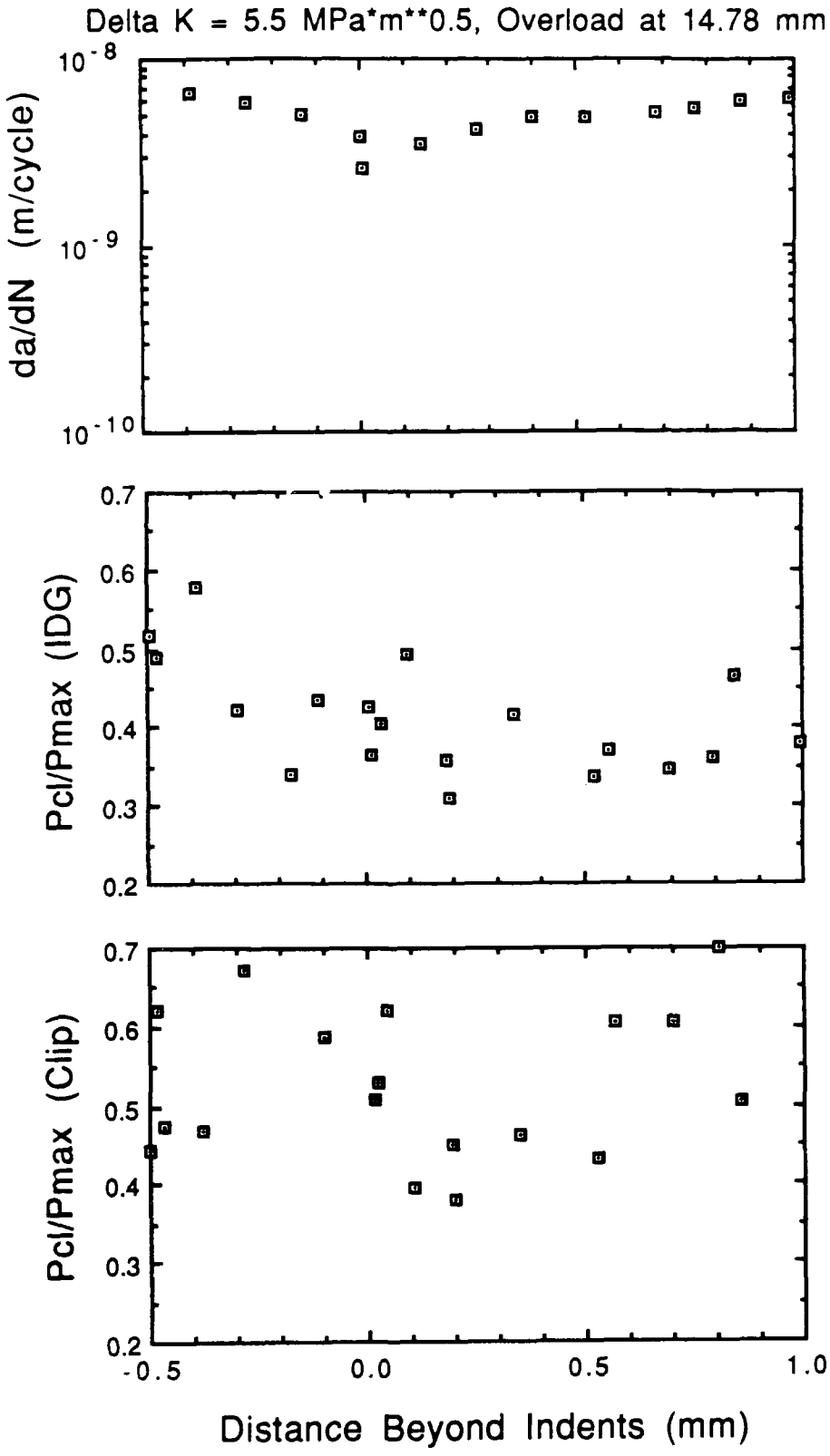

Figure F-1. Raw Data Comparison for Test #6, DK = 5.5 MPa$\sqrt{m}$ (Overload at 14.78 mm)

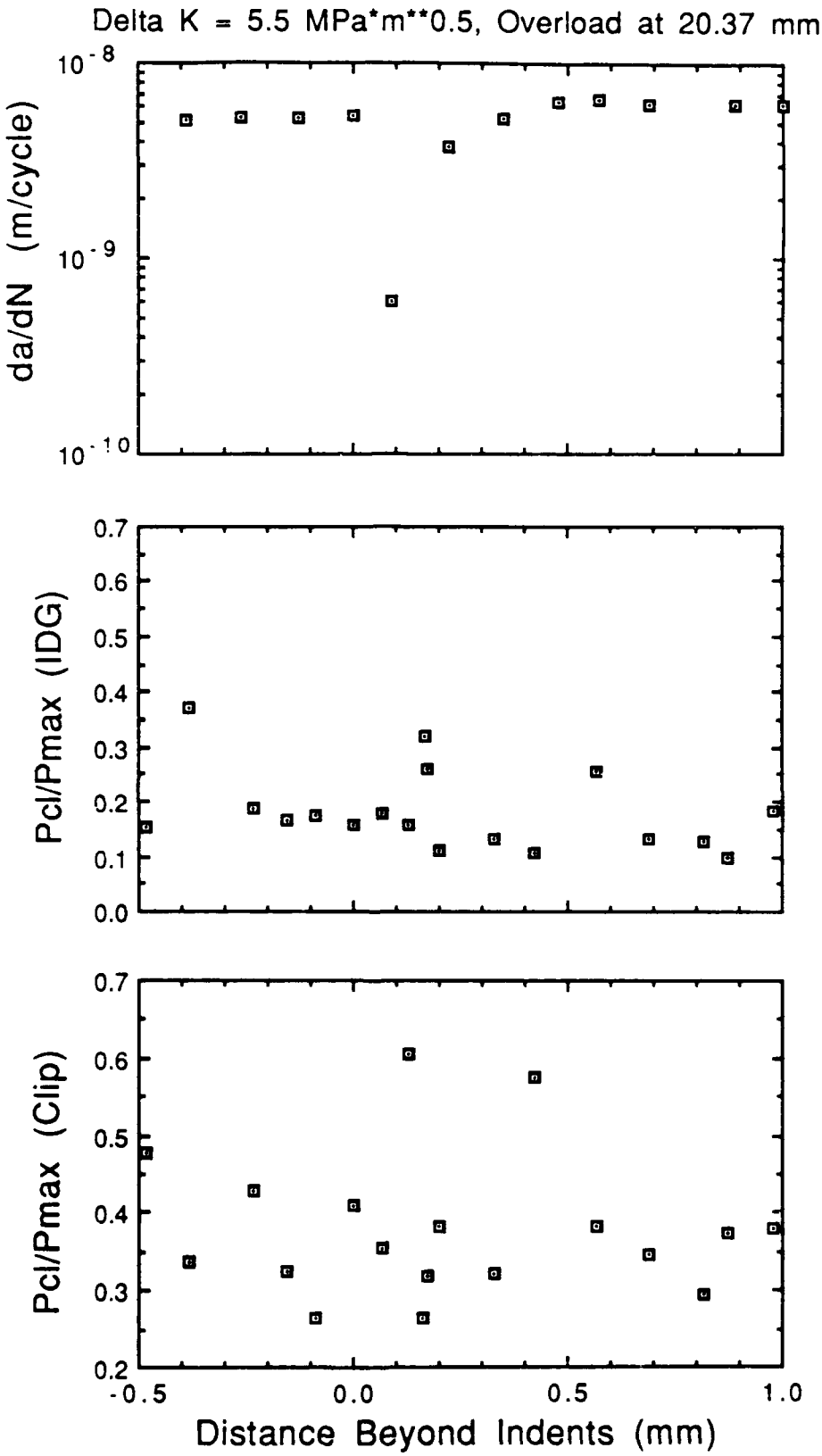

Figure F-2. Raw Data Comparison for Test #6, DK = 5.5 MPa$\sqrt{m}$ (Overload at 20.37 mm)

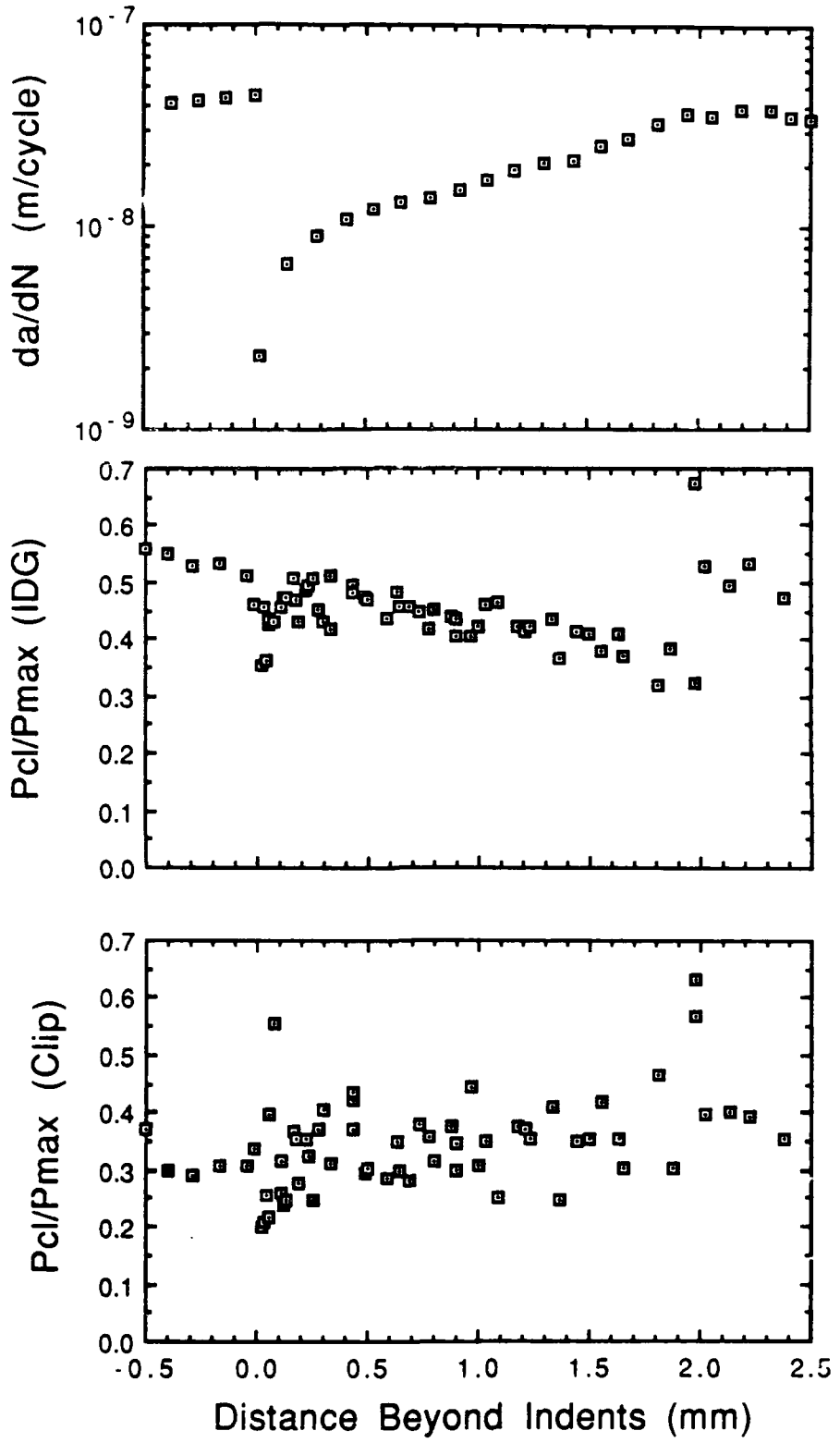

Figure F-3. Raw Data Comparison for Test #7, DK = 7.7 MPa$\sqrt{m}$ (Overload at 15.03 mm)

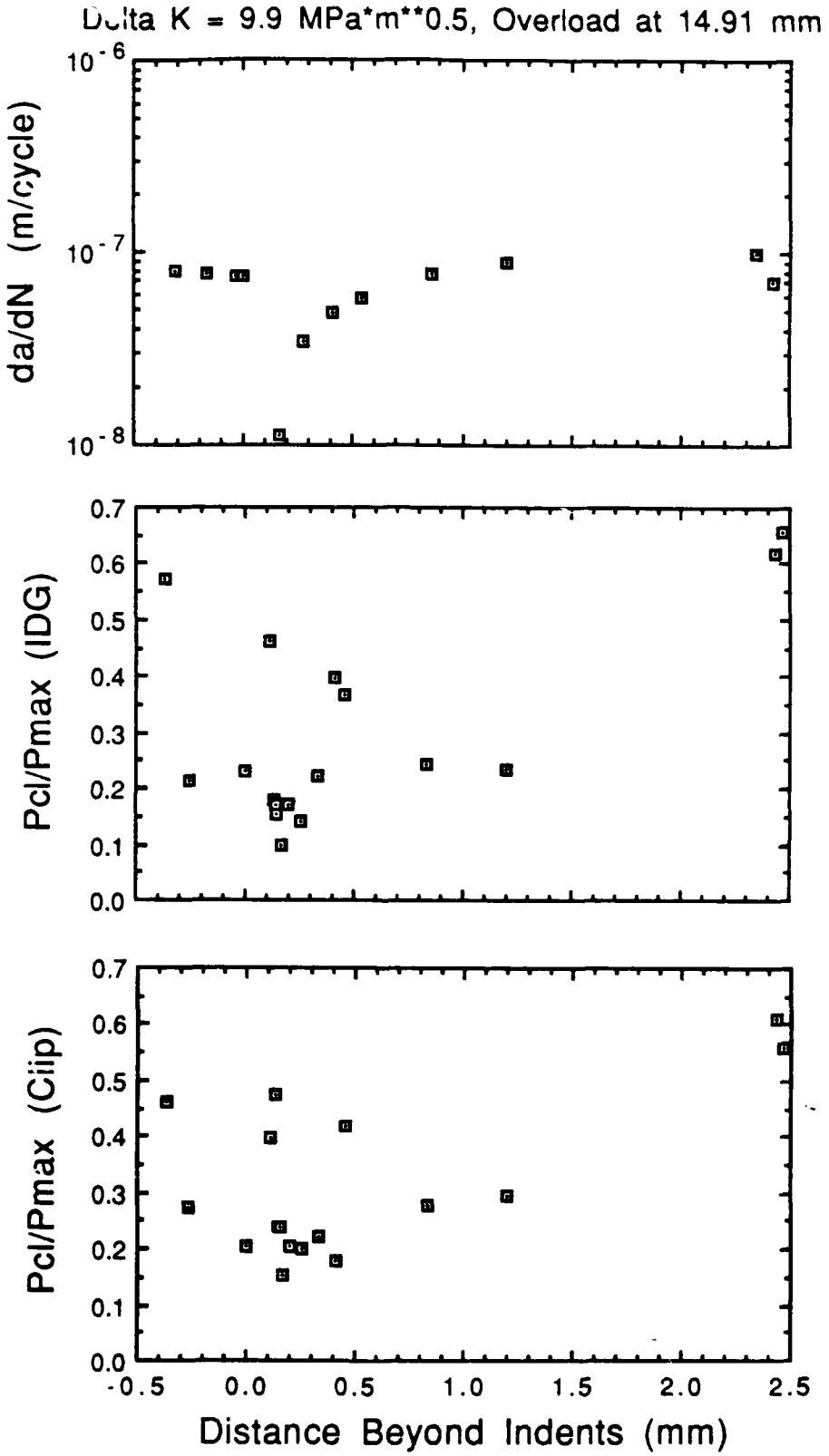

Figure F-4. Raw Data Comparison for Test #8, DK = 9.9 MPa$\sqrt{m}$ (Overload at 14.91 mm)

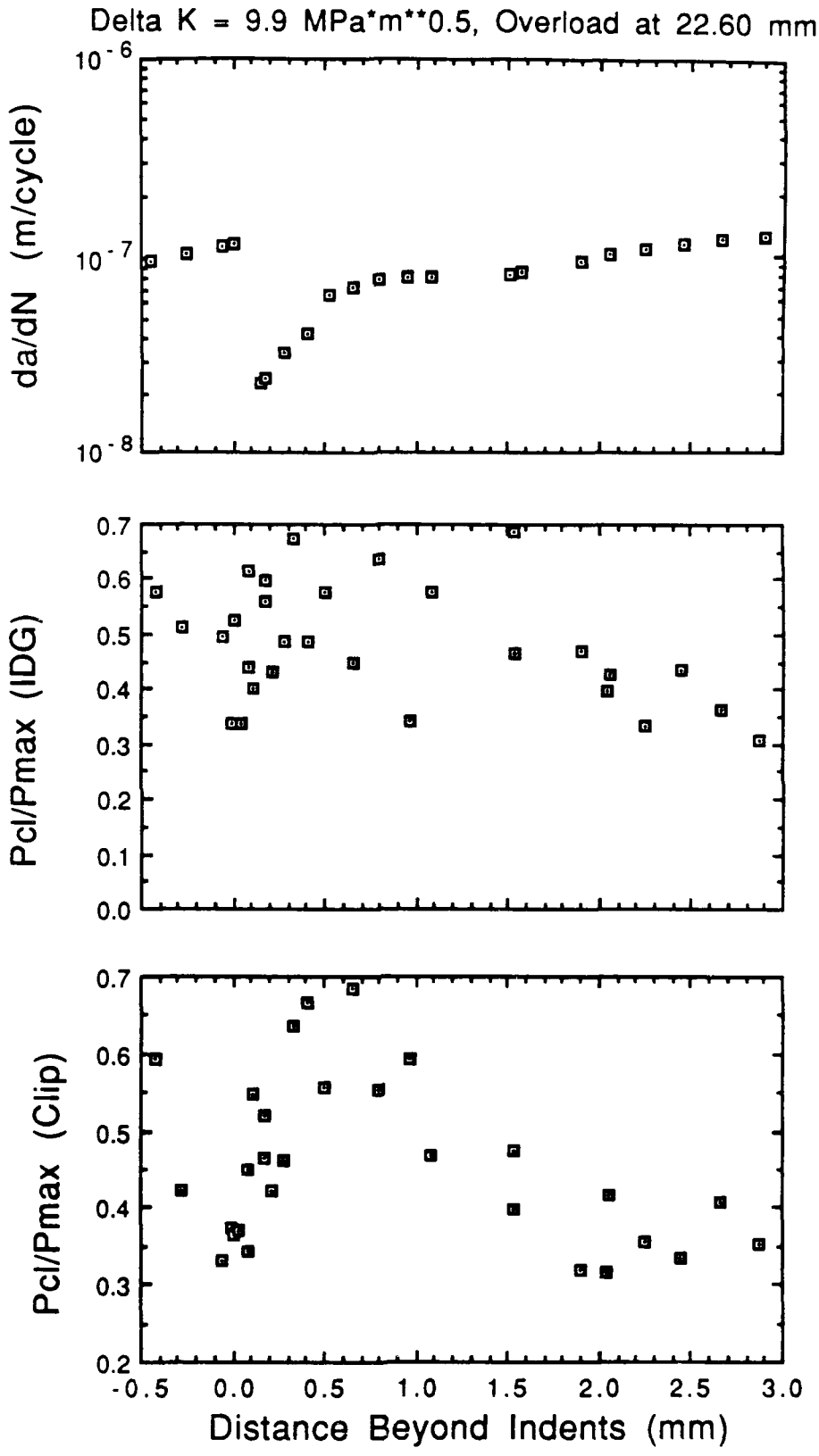

Figure F-5. Raw Data Comparison for Test #9, DK = 9.9 MPa$\sqrt{m}$ (Overload at 22.60 mm)

Appendix G: Delay Distances and Delay Cycles

The graphs in this appendix are reproductions of the crack growth histories presented in Appendix C. In some cases, the curves are presented in a slightly different manner in order to facilitate the calculation of delay distances and delay cycles.

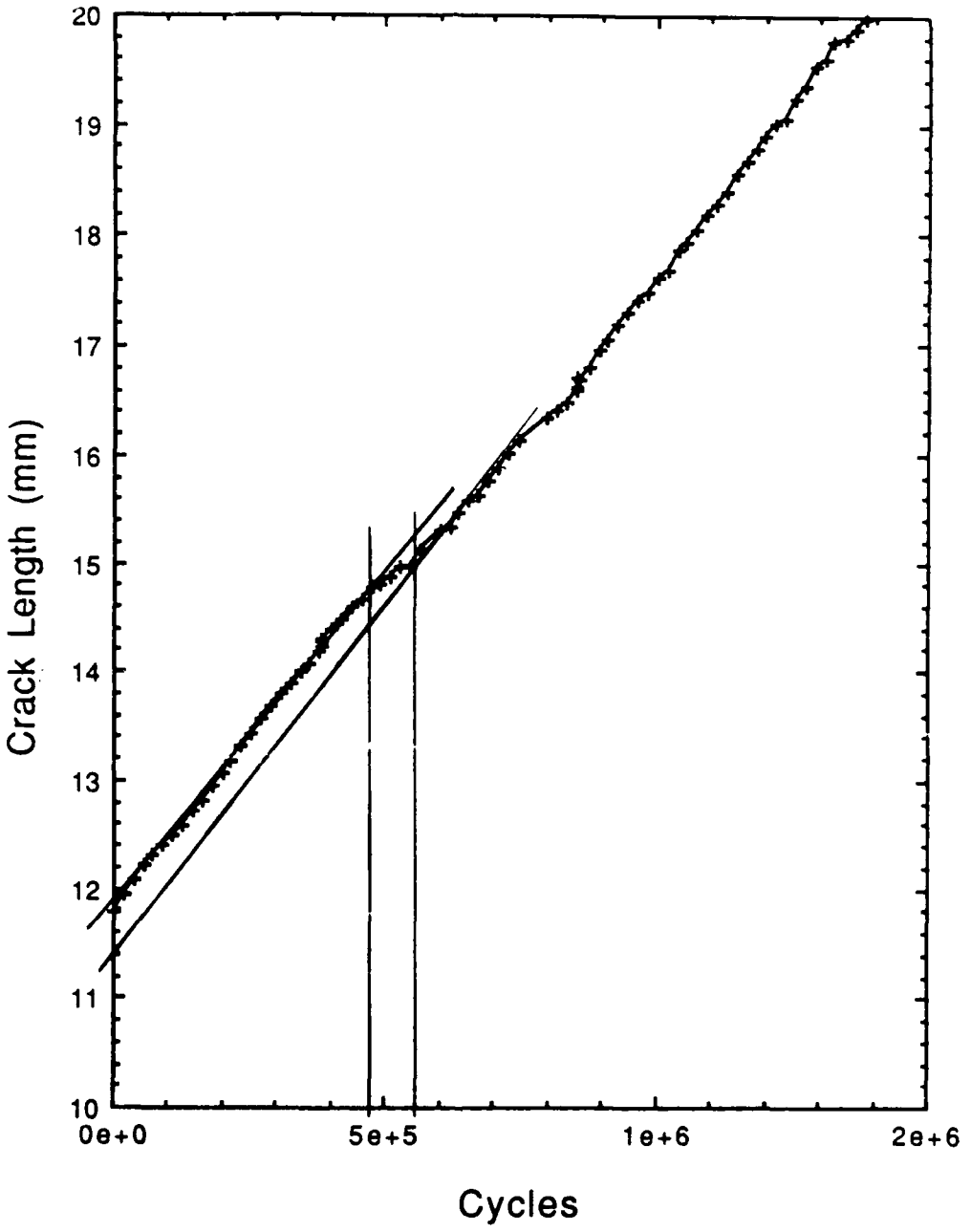

Figure G-1. Delay Cycles and Delay Distance from Test #6 (Overload at 14.78 mm)

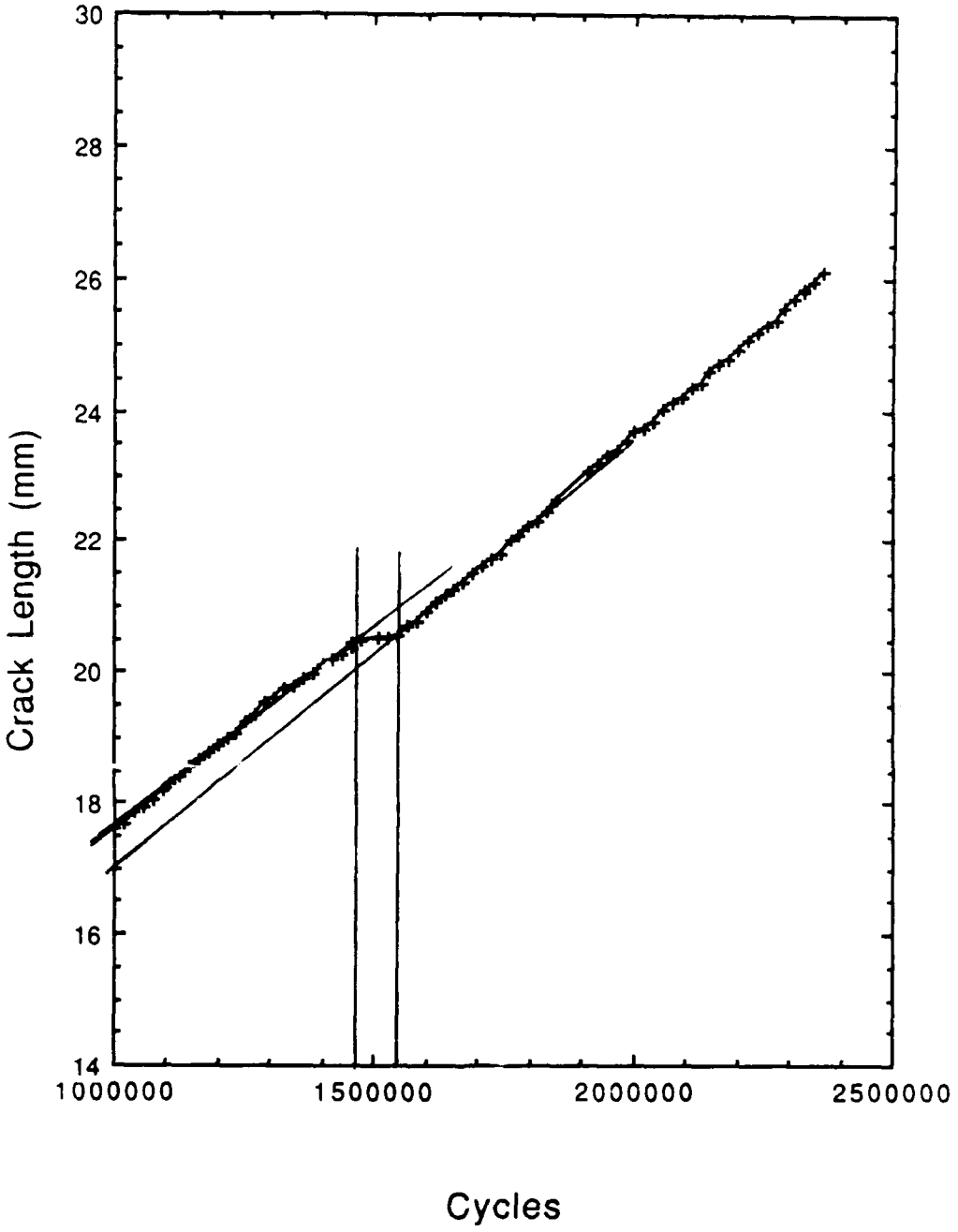

Figure G-2. Delay Cycles and Delay Distance from Test #6
(Overload at 20.37 mm)

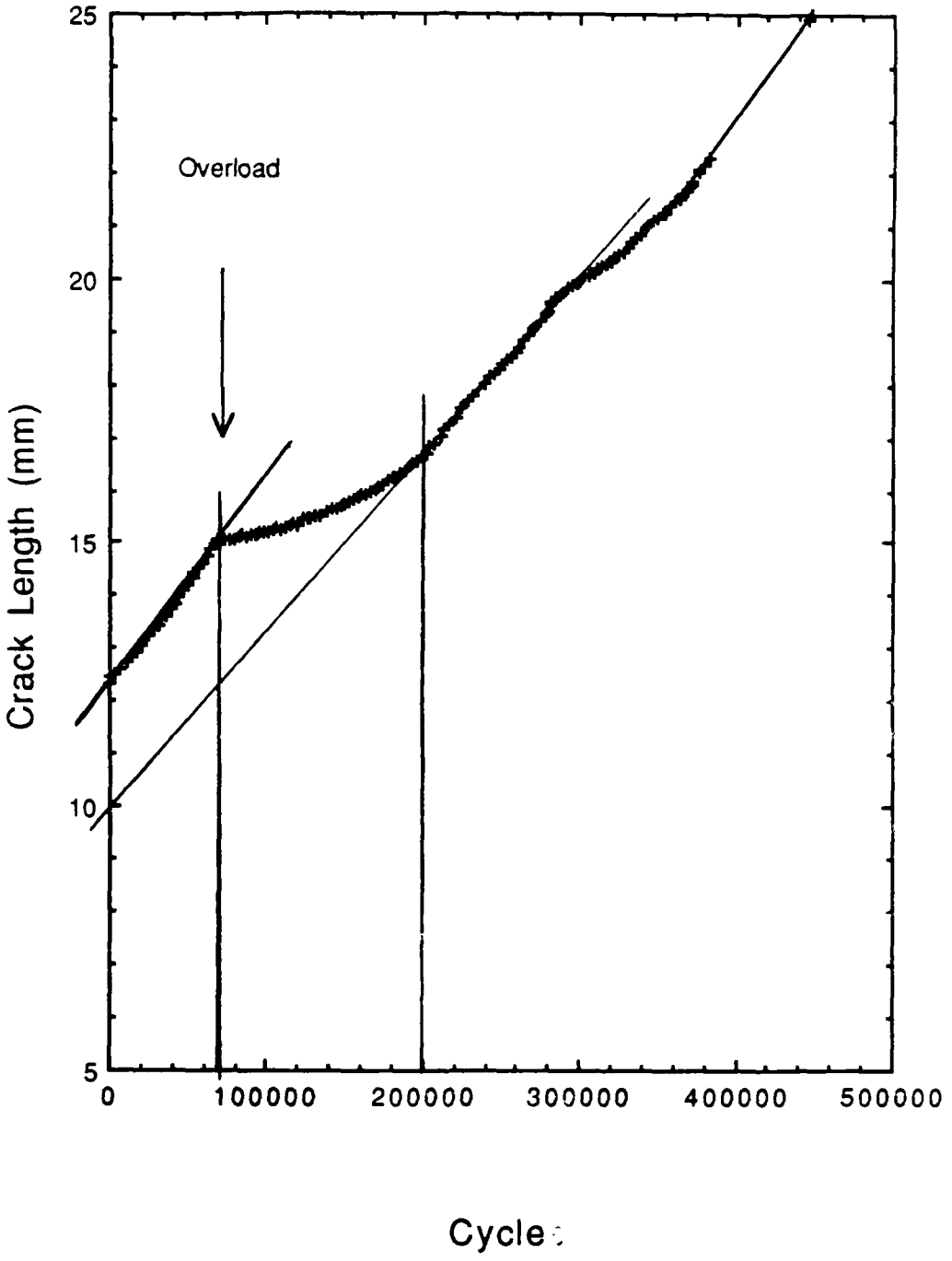

Figure G-3. Delay Cycles and Delay Distance from Test #7

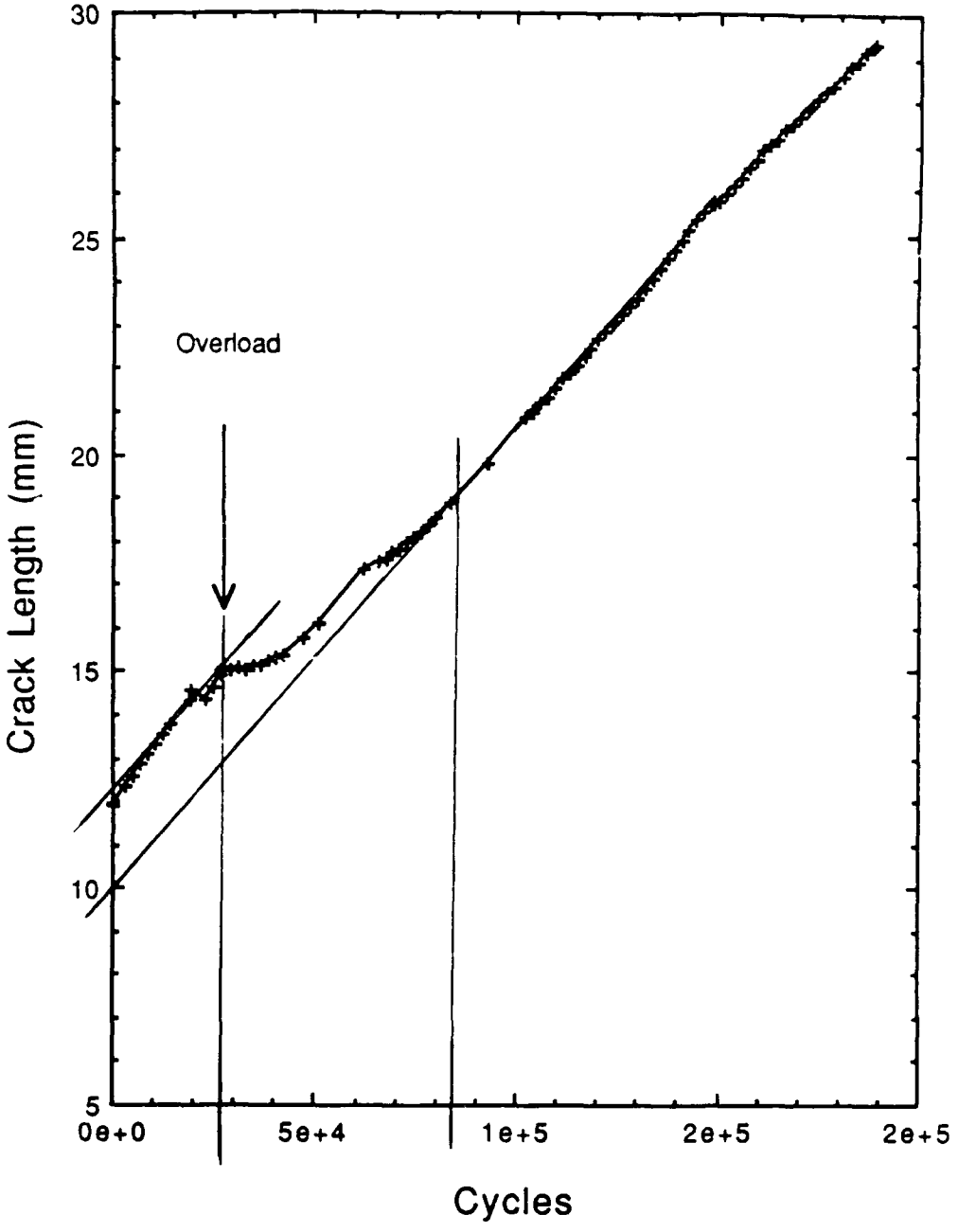

Figure G-4. Delay Cycles and Delay Distance for Test #8

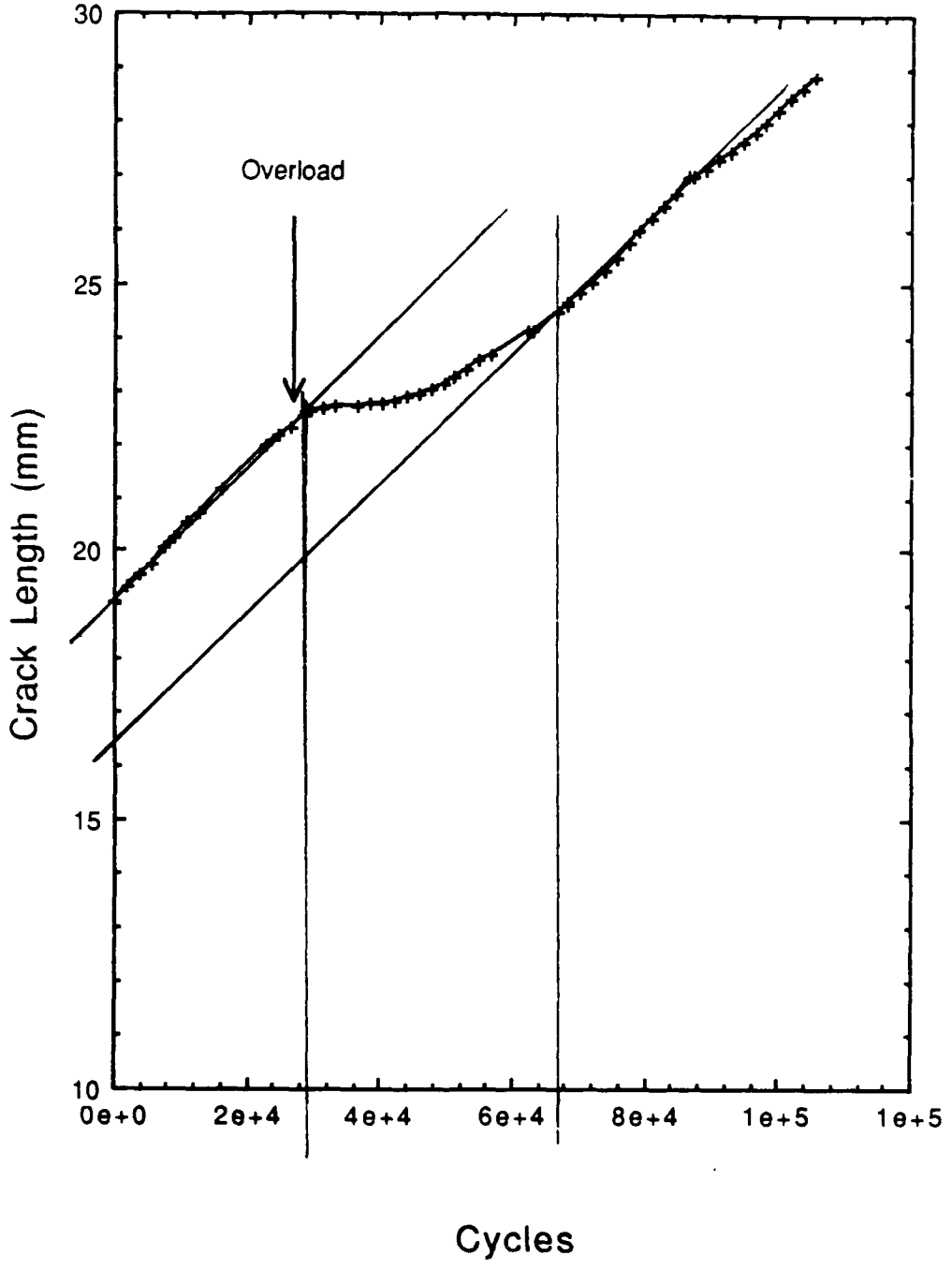

Figure G-5. Delay Cycles and Delay Distance for Test #9

Bibliography

1. Broek, David. Elementary Engineering Fracture Mechanics (Fourth Revised Edition). Dordrecht, The Netherlands: Martinus Nijhoff Publishers, 1986.

2. Paris, P. and Erdogan, F. "A Critical Analysis of Crack Propagation Laws," Journal of Basic Engineering, 85:528-534 (December 1963).

3. Elber, W. "Fatigue Crack Closure Under Cyclic Tension," Engineering Fracture Mechanics, Vol 2:37-45 (1970).

4. Elber, W. "The Significance of Fatigue Crack Closure", Damage Tolerance in Aircraft Structures, ASTM STP 486. 230-242. Philadelphia: American Society for Testing and Materials, 1971.

5. Carman, C. Davis, et al. "A Method for Determining Crack Opening Load from Load-Displacement Data," Mechanics Of Fatigue Crack Closure, ASTM STP 982. 214-221. Philadelphia: American Society for Testing and Materials, 1988.

6. Hudak, S.J., Jr, et al. Development of Standard Methods of Testing and Analyzing Fatigue Crack Growth Test Rate Data AFML TR-78-40. Air Force Material Laboratory, Air Force Systems Command, Wright-Patterson AFB OH, 1978

7. Liaw, Peter K. "Overview of Crack Closure at Near-Threshold Fatigue Crack Growth Levels," Mechanics Of Fatigue Crack Closure, ASTM STP 982. 62-92. Philadelphia: American Society for Testing and Materials, 1988.

8. Schijve, J. "Fatigue Crack Closure: Observations and Technical Significance," Mechanics Of Fatigue Crack Closure, ASTM STP 982. 5-34. Philadelphia: American Society for Testing and Materials, 1988.

9. Ritchie, R.O. "Environmental Effects on Near-Threshold Fatigue Crack Propagation in Steels: A Reassessment," Fatigue Thresholds: Fundamentals and Engineering Applications, Vol 1. 503-526. London: Engineering Materials Advisory Services Limited, 1982.

10. Freeman, B.L., et al. "The Influence of Corrosion Debris on Crack Closure at Near-Threshold Fatigue Crack Growth Rates," Fatigue Thresholds: Fundamentals and Engineering Applications, Vol 1. 547-561. London: Engineering Materials Advisory Services Limited, 1982.

11. Suresh, S., et al. "Crack Tip Oxide Formation and its Influence on Fatigue Thresholds," Fatigue Thresholds: Fundamentals and Engineering Applications, Vol 1. 391-408. London: Engineering Materials Advisory Services Limited, 1982.

12. Banerjee, S. A Review of Crack Closure, August 1983 - December 1983. AFWAL TR-84-4031. Dayton, Oh: University of Dayton, April 1984.

13. Johnson, H.H. "Calibrating the Electric Potential Method for Studying Slow Crack Growth," Materials Research and Standards, Vol 5, No 9:442-445 (September 1965)

14. Hartman, G.A., and Johnson, D.A. "D-C Electric-Potential Method Applied to Thermal/Mechanical Fatigue Crack Growth," Experimental Mechanics, March 1987, 106-112.

15. Gangloff, R.P. "Electrical Potential Monitoring of Crack Formation and Subcritical Crack Growth from Small Defects," Fatigue of Engineering Materials and Structures, Vol 4:15-33. (1981)

16. Wei, R.P. and Brazill, R.L. "An Assessment of A-C and D-C Potential Systems for Monitoring Fatigue Crack Growth," Fatigue Crack Growth Measurement and Data Analysis, ASTM STP 738. 103-119. Philadelphia: American Society for Testing and Materials, 1981.

17. Nicholas, T., et al. "An Analytical Investigation of Plasticity Induced Closure Involving Short Cracks," Mechanics Of Fatigue Crack Closure, ASTM STP 982. 361-379. Philadelphia: American Society for Testing and Materials, 1988.

18. Hartman, G. and Nicholas, T. "An Enhanced Laser Interferometer for Precise Displacement Measurements," Experimental Techniques, 11: 24-26 (February 1987)

19. Macha, D.E., et al. "On the Variation of Fatigue-crack-opening Load with Measurement Location," Experimental Mechanics, 207-213 (June 1979)

20. Ashbaugh, N. "Effects of Load History and Specimen Geometry on Fatigue Crack Closure Measurements", Mechanics of Fatigue Crack Closure, ASTM STP 982. 186-196. Philadelphia: American Society for Testing and Materials, 1988.

21. Clerivet, A. and Bathias, C. "Influence of Some Mechanical Parameters on the Crack Closure Effect in Fatigue Crack Propagation in Aluminum Alloys," Mechanics of Fatigue Crack Closure, ASTM STP 982. 583-597. Philadelphia: American Society for Testing and Materials, 1988.

22. Davidson, David L. "Plasticity Induced Fatigue Crack Closure," Mechanics of Fatigue Crack Closure, ASTM STP 982. 44-61. Philadelphia: American Society for Testing and Materials, 1988.

23. Zawada, Larry P. and Nicholas, Theodore "The Effect of Closure on the Near-Threshold Fatigue Crack Propagation Rates of a Nickel Base Superalloy," Mechanics of Fatigue Crack Closure, ASTM STP 982. 548-567. Philadelphia: American Society for Testing and Materials, 1988.

24. Allison, John E. "A Comparison of Measurement Methods and Numerical Procedures for the Experimental Characterization of Fatigue Crack Closure," Mechanics of Fatigue Crack Closure, ASTM STP 982. 171-185. Philadelphia: American Society for Testing and Materials, 1988.

25. Bowman, Randy et al. "A Demonstration of Problems Associated with Crack Closure Measurement Techniques," Engineering Fracture Mechanics, 31:703-712 (1988)

26. Ray, S.K. and Grandt, A.F.,Jr. "Comparison of Methods for Measuring Fatigue Crack Closure in a Thick Specimen," Mechanics of Fatigue Crack Closure, ASTM STP 982. 197-213. Philadelphia: American Society for Testing and Materials, 1988.

27. Ward-Close, C.M. and Ritchie, R.O. "On the Role of Crack Closure Mechanisms in Influencing Fatigue Crack Growth Following Tensile Overloads in a Titanium Alloy: Near-Threshold Versus Higher ΔK Behavior," Mechanics of Fatigue Crack Closure, ASTM STP 982. 93-111. Philadelphia: American Society for Testing and Materials, 1988.

28. Venkateswara Rao, K.T. and Ritchie, R.O. "Mechanisms for the Retardation of Fatigue Cracks Following Single Tensile Overloads: Behavior in Aluminum-Lithium Alloys," Acta Metallurgical, Vol 36, Number 10:2849-2862. (1988)

29. Larsen, J.M. et al. "Crack-Closure Effects on the Growth of Small Surface Cracks in Titanium-Aluminum Alloys," Mechanics of Fatigue Crack Closure, ASTM STP 982. 149-167. Philadelphia: American Society for Testing and Materials, 1988.

30. Jira, J.R. et al. "Effects of Closure on the Fatigue Crack Growth of Small Surface Cracks in a High-Strength Titanium Alloy," Mechanics of Fatigue Crack Closure, ASTM STP 982. 617-635. Philadelphia: American Society for Testing and Materials, 1988.

31. Mall, S., et al. "A Comparison of Different Test Techniques on Fatigue Threshold Behavior of Surface Flaws in a Titanium Alloy," Advances in Fracture Research: Proceedings of the Seventh International Conference on Fracture (ICF7), Vol 2. 1007-1014. Oxford: Pergamon Press, 1989

32. Turner, C.C., et al. "Fatigue Crack Closure Behavior at High Stress Ratios," Mechanics of Fatigue Crack Closure, ASTM STP 982. 528-535. Philadelphia: American Society for Testing and Materials, 1988.

33. Phillips, Mary Ann. Personal Interviews. WRDC/MLSE, Wright-Patterson AFB OH. May 1989, Nov 1989.

34. 1987 Annual Book of ASTM Standards, E647-86a. 899-926. Philadelphia: American Society for Testing and Materials, 1987.

35. 1987 Annual Book of ASTM Standards, E399-83. 680-715. Philadelphia: American Society for Testing and Materials, 1987.

36. Hartman, G.A. Personal Interviews. University of Dayton Research Institute, Dayton OH. April 1989 - December 1989.

Vita

Captain Albert S. Perkins [redacted] He graduated from high school in Covington, Tennessee, in 1976 and attended Christian Brothers College, from which he received the degree of Bachelor of Science in Natural Science in May 1980.

He received a commission in the United States Air Force through Officer Training School in May 1983, and received a Bachelor of Science in Aeronautical Engineering from the School of Engineering, Air Force Institute of Technology (AFIT), in March 1985.

Before returning to AFIT in May 1988 to pursue a Master's Degree, Captain Perkins served as Aircraft Structures Engineer and as Chief Engineer, Damage Tolerance Analysis for the Fighter/Tactical/Trainer System Program Management Division, San Antonio Air Logistics Center, Kelly Air Force Base, Texas.

UNCLASSIFIED

SECURITY CLASSIFICATION OF THIS PAGE

REPORT DOCUMENTATION PAGE

Form Approved
OMB No. 0704-0188

1a. REPORT SECURITY CLASSIFICATION UNCLASSIFIED	1b. RESTRICTIVE MARKINGS
2a. SECURITY CLASSIFICATION AUTHORITY	3. DISTRIBUTION / AVAILABILITY OF REPORT Approved for public release; distribution unlimited.
2b. DECLASSIFICATION / DOWNGRADING SCHEDULE	
4. PERFORMING ORGANIZATION REPORT NUMBER(S) AFIT/GAE/ENY/89D-27	5. MONITORING ORGANIZATION REPORT NUMBER(S)
6a. NAME OF PERFORMING ORGANIZATION School of Engineering 6b. OFFICE SYMBOL (*If applicable*) AFIT/ENG	7a. NAME OF MONITORING ORGANIZATION
6c. ADDRESS (*City, State, and ZIP Code*) Air Force Institute of Technology (AU) Wright-Patterson AFB OH 45433-6583	7b. ADDRESS (*City, State, and ZIP Code*)
8a. NAME OF FUNDING / SPONSORING ORGANIZATION Metals Behavior Materials Branch 8b. OFFICE SYMBOL (*If applicable*) WRDC/MLLN	9. PROCUREMENT INSTRUMENT IDENTIFICATION NUMBER
8c. ADDRESS (*City, State, and ZIP Code*) Materials Laboratory Wright-Patterson AFB OH 45433	10. SOURCE OF FUNDING NUMBERS PROGRAM ELEMENT NO. / PROJECT NO. / TASK NO / WORK UNIT ACCESSION NO

11. TITLE (*Include Security Classification*)
Effect of a Single Overload Upon Crack Growth in an Aluminum-lithium Alloy

12. PERSONAL AUTHOR(S)
Albert S. Perkins, B.S., Capt, USAF

13a. TYPE OF REPORT	13b. TIME COVERED	14. DATE OF REPORT (*Year, Month, Day*)	15. PAGE COUNT
MS Thesis	FROM _____ TO _____	1989 December	204

16. SUPPLEMENTARY NOTATION

17. COSATI CODES			18. SUBJECT TERMS (*Continue on reverse if necessary and identify by block number*)
FIELD	GROUP	SUB-GROUP	Fatigue, Crack Propagation, Crack Closure, Overload, Retardation, Aluminum-Lithium, Laser IDG
20	11		

19. ABSTRACT (*Continue on reverse if necessary and identify by block number*)

Thesis Advisor: Dr Shankar Mall
Professor of Mechanics
Department of Aeronautics and Astronautics

20. DISTRIBUTION / AVAILABILITY OF ABSTRACT ☒ UNCLASSIFIED/UNLIMITED ☐ SAME AS RPT. ☐ DTIC USERS	21. ABSTRACT SECURITY CLASSIFICATION UNCLASSIFIED
22a. NAME OF RESPONSIBLE INDIVIDUAL Shankar Mall, Professor of Mechanics	22b. TELEPHONE (*Include Area Code*) 513-255-3517 / 22c. OFFICE SYMBOL AFIT/ENY

DD Form 1473, JUN 86 *Previous editions are obsolete.* SECURITY CLASSIFICATION OF THIS PAGE

This study investigated the effect of a single overload upon the crack growth in an aluminum-lithium alloy 2091. Compact tension specimens were tested; fatigue crack growth was induced by a 30 Hertz cyclic loading of a constant load ratio (0.1) and a constant stress intensity range. Baseline (non-overload) tests and tests involving overloads were performed.

Crack length was tracked using electric potential method. Closure measurements were made in the far field by a non-conducting clip gage at the specimen mouth; closure measurements were made in the region near the crack tip by a laser interferometric displacement gage (IDG).

A method of normalizing the closure data measured by the IDG to a point 0.2 mm behind the crack tip was developed. The closure load measured by the IDG, when adjusted to 0.2 mm behind the crack tip, was found to be higher than the closure load measured by the clip gage for all crack lengths where a direct comparison between the two measurements could be made. The closure load measured by the IDG was found to be a function of crack length and applied stress intensity range.

Changes in load history were found to have an effect upon crack growth behavior. An 80% level of overload caused significant retardation for all stress intensity ranges studied. The overload also caused secondary cracking, which introduced Mode II behavior in the region of the overload. The Mode II behavior introduced large amounts of scatter in the closure data; this scatter was observed by measurements in both the near field and the far field.